

Adolf-Butenandt-Institut  
Lehrstuhl: Molekularbiologie  
im Biomedizinischem Centrum  
der Ludwig-Maximilians-Universität München  
Vorstand: Prof. Dr. rer. nat. Peter B. Becker

# **Interplay of nucleosome positioning and transcription initiation in *Schizosaccharomyces pombe***

Dissertation  
zum Erwerb des Doktorgrades der Naturwissenschaften  
an der Medizinischen Fakultät  
der Ludwig-Maximilians-Universität München

vorgelegt von

Maria Walker

aus Put Kommunismu

2018

**Gedruckt mit Genehmigung der Medizinischen Fakultät  
der Ludwig-Maximilians-Universität München**

Betreuer: PD Dr. rer. nat. Philipp Korber

Zweitgutachterin: Prof. Michaela Smolle, PhD

Dekan: Prof. Dr. med. dent. Reinhard Hickel

Tag der mündlichen Prüfung: 18.01.2019

## Eidesstattliche Versicherung

Walker, Maria

Ich erkläre hiermit an Eides statt,  
dass ich die vorliegende Dissertation mit dem Thema

**“Interplay of nucleosome positioning  
and transcription initiation  
in *Schizosaccharomyces pombe*“**

selbständig verfasst, mich außer der angegebenen keiner weiteren Hilfsmittel bedient und alle Erkenntnisse, die aus dem Schrifttum ganz oder annähernd übernommen sind, als solche kenntlich gemacht und nach ihrer Herkunft unter Bezeichnung der Fundstelle einzeln nachgewiesen habe.

Ich erkläre des Weiteren, dass die hier vorgelegte Dissertation nicht in gleicher oder in ähnlicher Form bei einer anderen Stelle zur Erlangung eines akademischen Grades eingereicht wurde.

---

München, den 11.02.2019

Ort, Datum

---

Maria Walker



---

# Table of Contents

Preface.....	I
Summary.....	III
Zusammenfassung.....	V
<b>1 Introduction .....</b>	<b>1</b>
<b>1.1 <i>Schizosaccharomyces pombe</i> as a model organism .....</b>	<b>2</b>
<b>1.2 Structure of chromatin - from nucleosomes to higher order structures.....</b>	<b>3</b>
1.2.1 The nucleosome .....	3
1.2.2 The higher order structure .....	5
<b>1.3 Nucleosome positioning mechanisms.....</b>	<b>7</b>
1.3.1 Mapping of nucleosome positions .....	7
1.3.2 Terminology of nucleosome positioning.....	9
1.3.3 Factor-independent/ <i>cis</i> -factor nucleosome positioning mechanism .....	10
1.3.4 Statistical nucleosome positioning mechanism .....	11
1.3.5 Factor-dependent nucleosome positioning mechanism.....	12
1.3.5.1 Classes and functions of chromatin remodelers.....	12
1.3.5.2 Role of chromatin remodelers in the nucleosome positioning mechanism .....	14
1.3.5.3 Role of GRFs in the nucleosome positioning mechanism .....	15
<b>1.4 Chromatin and transcription regulation.....</b>	<b>16</b>
1.4.1 Promoter architecture.....	16
1.4.2 Chromatin structure at promoters.....	18
1.4.3 Chromatin factors and transcription elongation.....	19
1.4.4 Cryptic transcription.....	21
<b>1.5 Aims of this thesis.....</b>	<b>23</b>
<b>2 Results .....</b>	<b>25</b>
<b>2.1 Chromatin and sequence features of promoters in <i>S. pombe</i> .....</b>	<b>26</b>
2.1.1 Classification and quality control of TSSs annotated by CAGE-seq .....	27
2.1.2 Chromatin structure at the TSSs as a further quality criterion .....	29
2.1.2.1 Chromatin structure at promoters with sharp or broader TSS peak distribution .....	31
2.1.2.2 Chromatin structure at the TSSs for different conditions and mutants .....	31
2.1.3 Definition and annotation of newly characterized CSCTs in chromatin factor mutants and additional transcripts in wild type cells grown in minimal medium (EMM) .....	34
2.1.4 Features of CSCTs in the chromatin factor mutants .....	36
2.1.4.1 CSCT-TSSs localize to the very 5' flank of a corresponding +1 nucleosome .....	36
2.1.4.2 CSCT-TSSs are located in regions with more than average expression levels .....	37
2.1.4.3 CSCT-TSSs share distinctive DNA shape features with canonical TSSs .....	38
2.1.4.4 Some CSCT-TSSs are enriched for a GC skew signal.....	39
2.1.5 Annotation and characterization of Tbp1 binding by ChIP-seq .....	41
<b>2.2 CHD1-dependent NDR-array pattern in <i>S. pombe</i>.....</b>	<b>43</b>
2.2.1 Effect of MNase digestion degree on the NDR-array pattern.....	43
2.2.2 Role of CHD1 chromatin remodelers in the generation of NDR-array patterns assessed by <i>in vivo</i> complementation assay in the <i>hrp1Δ hrp3Δ</i> mutant.....	46
2.2.3 Effectiveness of Chd1/Hrp3 hybrid constructs in the rescue of NDR-array pattern in the <i>hrp1Δ hrp3Δ</i> mutant .....	47
2.2.4 Supplementary materials .....	50

---

---

<b>2.3</b>	<b><i>In vitro</i> reconstitution systems for genome-wide <i>in vivo</i>-like nucleosome positioning ..</b>	<b>52</b>
2.3.1	<i>In vitro</i> reconstitution using whole cell extract from <i>S. pombe</i> .....	52
2.3.2	<i>In vitro</i> reconstitution using purified chromatin remodelers Hrp1 and Hrp3 .....	55
2.3.3	<i>In vitro</i> reconstitution using purified chromatin remodelers Hrp1 and Hrp3 and the GRF Sap1 as barrier .....	57
2.3.4	Cooperativity between nucleosomes during SGD chromatin assembly .....	62
2.3.4.1	Nucleosome cluster formation is independent of assembly degree and histone-tails during SGD chromatin assembly .....	63
2.3.4.2	Simulation of nucleosome assembly revealed that the observed cluster frequency can hardly be explained without cooperativity .....	66
2.3.4.3	Supplementary materials .....	68
<b>3</b>	<b>Discussion .....</b>	<b>69</b>
<b>3.1</b>	<b>Promoter organization in <i>S. pombe</i> .....</b>	<b>70</b>
3.1.1	TSS annotation by CAGE-seq revealed a close overlap with other high-resolution TSS annotations.....	70
3.1.2	Promoters with sharp or broader TSS peak distribution harbored both similar chromatin structure in <i>S. pombe</i> .....	71
3.1.3	Minimal criteria to define a promoter region in <i>S. pombe</i> .....	72
3.1.4	Characterization of TATA box motif containing promoters in <i>S. pombe</i> .....	75
<b>3.2</b>	<b>Nucleosome pattern at promoter regions in <i>S. pombe</i> .....</b>	<b>77</b>
<b>3.3</b>	<b>NDR-array pattern formation in <i>S. pombe</i> .....</b>	<b>79</b>
3.3.1	NDR-array pattern formation by CHD1 chromatin remodelers <i>in vivo</i> .....	79
3.3.2	NDR-array pattern formation investigated by <i>in vitro</i> reconstitution approach .....	81
<b>3.4</b>	<b>Cooperativity between nucleosomes during SGD chromatin assembly .....</b>	<b>84</b>
<b>4</b>	<b>Materials and Methods .....</b>	<b>87</b>
<b>4.1</b>	<b>Molecular Biology.....</b>	<b>88</b>
4.1.1	Generation of chemically competent <i>E. coli</i> cells.....	88
4.1.2	Transformation of <i>E. coli</i> .....	88
4.1.3	Plasmid isolation from <i>E. coli</i> .....	88
4.1.4	Polymerase chain reaction (PCR), restriction enzyme digestion, DNA ligation and cloning .....	88
4.1.5	Cultivation of <i>S. pombe</i> cells.....	89
4.1.6	Transformation of <i>S. pombe</i> .....	89
4.1.7	Chromatin Immunoprecipitation (ChIP) of Flag-tagged Tbp1 and DNA preparation for ChIP-seq .....	89
4.1.8	Mononucleosomal DNA preparation for MNase-seq.....	90
4.1.9	DNA preparation for MNase-anti-H3-ChIP-seq .....	91
4.1.10	RNA extraction for CAGE-seq .....	92
<b>4.2</b>	<b>Biochemistry .....</b>	<b>92</b>
4.2.1	Preparation of embryonic <i>Drosophila</i> histone octamers .....	92
4.2.2	Recombinant histone octamers .....	93
4.2.3	Preparation of yeast whole cell extract.....	93
4.2.4	TAP-tag purification of endogenous Hrp3.....	94
4.2.5	FLAG-tag purification of endogenous Hrp1 .....	94
4.2.6	<i>In vitro</i> reconstitution of chromatin by salt gradient dialysis (SGD) .....	95

---

---

4.2.7	<i>In vitro</i> reconstitution remodeling reaction and MNase digestion.....	95
4.2.8	MNase digestion for SGD chromatin.....	96
4.2.9	Restriction enzyme accessibility assay.....	96
4.2.10	Sequencing library preparation.....	96
4.2.11	Sequencing.....	97
4.2.12	Southern blot analysis.....	97
<b>4.3</b>	<b>Bioinformatics.....</b>	<b>98</b>
4.3.1	Data sets and genomic coordinates for TSS annotation.....	98
4.3.1.1	TSS annotation and statistical analysis.....	98
4.3.1.2	DNA feature analysis.....	99
4.3.2	MNase-seq analysis.....	99
4.3.3	ChIP-seq analysis.....	99
4.3.4	Simulation of nucleosome assembly.....	99
	<b>References.....</b>	<b>100</b>
	<b>Abbreviations.....</b>	<b>113</b>
	<b>Acknowledgements.....</b>	<b>115</b>

---





## Preface

This PhD thesis on “Interplay of nucleosome positioning and transcription initiation in *Schizosaccharomyces pombe*” includes results from collaborative work of the laboratories of PD Dr. Philipp Korber, Prof. Dr. Jürg Bähler, Dr. Samuel Marguerat, Prof. Dr. Karl Ekwall and Prof. Dr. Ulrich Gerland.

The results of this PhD thesis are divided in four projects:

- I. Chromatin and sequence features of promoters in *S. pombe* (chapter 2.1)
- II. CHD1-dependent NDR-array pattern in *S. pombe* (chapter 2.2)
- III. *In vitro* reconstitution systems for genome-wide nucleosome positioning (chapter 2.3)
- IV. Cooperativity between nucleosomes during SGD chromatin assembly (chapter 2.3.4)

The corresponding contributions to the results of the projects I to IV are summarized in the following:

- I. For TSS annotation by CAGE-seq RNA was prepared in the laboratory of Prof. Dr. Jürg Bähler, University College, London and Dr. Samuel Marguerat, Imperial College, London and send for sequencing to DNAFORM (SourceBioScience). I performed MNase-seq and Tbp1-ChIP-seq experiments. Sequencing was done at the laboratory of Functional Genome Analysis (LAFUGA), LMU Munich. The bioinformatical analyses of data sets derived from CAGE-, MNase- and Tbp1-ChIP-seq experiments were done by Dr. Pawel Smialowski.
- II. Cloning and MNase-seq for the *in vivo* complementation approach were done by me (cloning and MNase-seq) with the help of Dr. Corinna Lieleg (cloning) and Andrea Schmid (cloning and MNase-seq). I performed MNase-anti-H3-ChIP-seq experiment and contributed to the bioinformatical analyses of MNase-seq and MNase-anti-H3-ChIP-seq data sets.
- III. Purification of the chromatin remodelers, Hrp1 and Hrp3, was done by me with the help of Dr. Punit Prasad and Wenbo Dong, PhD student, in the laboratory of Prof. Dr. Karl Ekwall in the Department of Biosciences and Nutrition, Karolinska Institut, Stockholm. Purification of Sap1 was done by Dr. Julia Pointner. I performed the *in vitro* reconstitution assays, library sequencing preparation and bioinformatical analyses. PWM mapping was done by Dr. Tobias Straub.
- IV. I performed the Southern blot analyses. Dr. Johannes Nuebler performed simulation analysis of nucleosome cluster.

---

## Summary

The compaction of DNA into chromatin with the nucleosome as basic unit restricts the accessibility for DNA binding factors. DNA binding factors regulate fundamental cellular processes, for example, transcription. Transcription initiation occurs at promoters. To characterize promoter regions it is crucial to know where the transcription start sites (TSSs) are. Some promoters comprise DNA elements such as the TATA box or Initiator motif. In addition, some promoter regions harbor a specific chromatin organization, the NDR-array pattern. The NDR-array pattern is characterized by a nucleosome depleted region (NDR) upstream to the TSS, well-positioned +1 and -1 nucleosomes down- and upstream to the NDR, respectively, and nucleosome arrays over the gene coding region. This NDR-array pattern is disturbed if specific chromatin factors are mutated such as histone chaperones or chromatin remodelers. The latter are ATP-dependent enzymes that mobilize or restructure nucleosomes. General regulatory factors (GRFs), which are sequence-specific DNA binding factors, are also implicated to contribute to the NDR-array pattern. Importantly, cryptic transcripts arise in these chromatin factor mutants, indicating an interplay of nucleosome positioning mechanisms and transcription initiation.

To understand this interplay, following aspects are crucial and in the focus of this thesis: (1) where are the TSSs, in particular, TSSs of cryptic transcripts in chromatin factor mutants; (2) which features characterize TSSs; (3) specifically, how does the nucleosome pattern look like around TSSs; and (4) how is this nucleosome pattern generated.

In this thesis, *S. pombe* yeast was used as model organism since it is easy to manipulate, similar to the well-studied, but far-diverged *S. cerevisiae* yeast. *S. pombe* shares many aspects with higher eukaryotes such as cell cycle regulation, heterochromatin maintenance or other chromatin-related aspects. Studying these aspects in *S. pombe* facilitates to understand the underlying mechanism in higher eukaryotes.

Using CAGE-seq, as a method to specifically capture the start site of transcripts, showed that *S. pombe* promoter regions mostly harbor a single dominant but sometimes also multiple TSSs. Aspects of the promoter nucleosome pattern such as NDR width and +1 nucleosome fuzziness were quite similar for both promoter classes. Additionally, “fragile” nucleosomes seemed to be part of some *S. pombe* promoter regions.

We focused on a specific subset of transcripts, which are not detected in wild type cells but exclusively present in the chromatin factor mutants *spt6-1 ts* and *hrp1Δ hrp3Δ*. These are called “chromatin suppressed cryptic transcripts” (CSCTs) by us and enabled us to identify minimal criteria that define a promoter region in *S. pombe*. The minimal criteria comprise a specific relative location of +1 nucleosome and TSS, permissive chromatin as indicated by a neighborhood with higher than genomic average expression level, a peak of the DNA roll shape parameter for all, and a characteristic GC skew distribution for

some TSSs. The DNA roll shape feature and the +1 nucleosome location are conserved between the yeasts *S. pombe* and *S. cerevisiae*. To understand which further features may characterize promoter regions, we annotated TATA box binding protein (Tbp1) binding sites and analyzed the underlying sequence, the TATA box motif. Only a minority of *S. pombe* TSSs is in the vicinity of a TATA box, but usually at a canonical distance of about 30-35 base pairs. This distance is similar to the analogous distance in higher eukaryotes.

In *S. pombe*, it was shown previously that the chromatin remodeler mutant *hrp1Δ hrp3Δ* harbors a disrupted nucleosome pattern suggesting that the two CHD1-class chromatin remodelers Hrp1 and Hrp3 are important for generating this pattern. By using two strategies, an *in vivo* complementation approach and an *in vitro* reconstitution approach, we asked how these remodelers contribute to the NDR-array pattern.

In the *in vivo* complementation approach, we focused on the conserved or diverged function of the orthologous *S. cerevisiae* Chd1 and *S. pombe* Hrp3 remodelers. Chd1 and all Chd1/Hrp3 hybrid constructs could rescue the NDR-array pattern in the *S. pombe hrp1Δ hrp3Δ* mutant. Previous work showed differences for the analogous approach in *S. cerevisiae*, i.e., Hrp3 as well as a particular Chd1/Hrp3 hybrid construct could not rescue the NDR-array pattern there. This difference might be due to differences in the recruitment mechanism for CHD1-class chromatin remodelers or in the environment regarding competing remodelers.

Using an *in vitro* reconstitution system for *S. pombe* would enable to elucidate if a factor is necessary, sufficient and plays a direct role in the nucleosome positioning mechanism. The *in vitro* reconstitution approach is based on: (a) salt gradient dialysis (SGD) of plasmids with genomic inserts and histones to generate genome-wide “SGD chromatin”, (b) incubation of the SGD chromatin with cell extracts and/or purified factors, and (c) MNase-seq nucleosome mapping to study the ATP-dependent impact on nucleosome positioning by these factors. In *S. cerevisiae*, such previously published *in vitro* reconstitution approach showed successfully that the incubation of *S. cerevisiae* SGD chromatin with whole cell extract leads to a proper *in vivo*-like nucleosome pattern. Moreover, chromatin remodelers and GRFs contribute to the NDR-array pattern. Here, for *S. pombe*, the whole cell extract did not establish a proper *in vivo*-like nucleosome pattern. Preliminary results indicated that the chromatin remodeler Hrp1 together with the GRF Sap1 seems to be involved in a barrier-dependent nucleosome positioning mechanism.

In the context of SGD chromatin assembly, clusters of closely packed nucleosomes are observed, even at reduced nucleosome density. Theoretical modeling showed that these clusters occurred more often than expected by chance. Cooperativity between nucleosomes during SGD is assumed to explain this high frequency of closely packed nucleosomes.

## Zusammenfassung

Die Kompaktierung von der DNA ins Chromatin, wobei das Nukleosom die kleinste Einheit darstellt, schränkt die Zugänglichkeit für DNA-bindende Faktoren ein. DNA-bindende Faktoren steuern fundamentale zelluläre Prozesse, wie zum Beispiel die Transkription. Die Transkriptionsinitiation findet in Promotoren statt. Um die Promotorenregion zu beschreiben, ist es entscheidend zu wissen, wo sich die Transkriptionsstartpunkte (*TSSs*) befinden. Manche Promotoren beinhalten Elemente wie zum Beispiel das TATA-Box- oder Initiator-Motiv. Zusätzlich weisen manche Promotoren eine spezifische Chromatinorganisation auf, das sogenannte *NDR-array* Muster. Das *NDR-array* Muster ist durch eine nukleosomenarme Region (*NDR*) stromaufwärts der *TSS*, gut-positionierte +1 und -1 Nukleosomen jeweils stromabwärts und stromaufwärts zur *NDR* und eine regelmäßige Nukleosomen-Anordnung (*array*) über der kodierenden Region charakterisiert. Dieses *NDR-array* Muster wird durcheinander gebracht, wenn spezielle Chromatinfaktoren, wie zum Beispiel Histon-Chaperone oder Chromatin-Remodeler, mutiert sind. Die Letztgenannten sind ATP-abhängige Enzyme, die Nukleosome mobilisieren oder umstrukturieren. Die generellen regulatorische Faktoren (*GRFs*), welche sequenzspezifische DNA-bindenden Faktoren sind, stehen ebenfalls im Zusammenhang an dem *NDR-array* Muster beteiligt zu sein. Wichtig ist noch, dass kryptische Transkripte in diesen Chromatinfaktor-Mutanten auftreten, was auf ein Zusammenspiel zwischen dem Nukleosomen-Positionierungsmechanismus und der Transkriptionsinitiation hinweist.

Um dieses Zusammenspiel zu verstehen, sind folgende Aspekte entscheidend und sind Schwerpunkt dieser Arbeit: (1) Wo befinden sich die *TSSs*, insbesondere die *TSSs* der kryptischen Transkripte in den Chromatinfaktor-Mutanten; (2) welche Eigenschaften charakterisieren die *TSSs*; (3) im Speziellen wie sieht das Nukleosomenmuster um die *TSSs* herum aus; und (4) wie wird dieses Nukleosomenmuster gebildet.

In dieser Arbeit wurde die Hefe *S. pombe* als Modellorganismus verwendet, da sie einfach zu manipulieren ist vergleichbar zur gut-untersuchte und evolutionär-weitentfernten Hefe *S. cerevisiae*. *S. pombe* teilt viele Aspekte mit höheren Eukaryoten wie zum Beispiel Zellzyklusregulierung, Erhaltung des Heterochromatins und andere Chromatin-bezogene Aspekte. Die Untersuchung dieser Aspekte ermöglicht es die grundlegenden Mechanismen in höheren Eukaryoten zu verstehen.

Die Verwendung von CAGE-seq, als eine spezifische Methode um die Startpunkte der Transkripte zu erfassen, zeigte, dass in *S. pombe* Promotorregionen meistens eine einzelne dominante *TSS*, manchmal aber auch viele *TSSs* auftreten. Aspekte des Promoter-Nukleosomenmusters, wie zum Beispiel die *NDR*-Weite und die +1 Nukleosomen-Verteilung, waren ziemlich ähnlich in beiden Promotorklassen. Zusätzlich schienen die „fragile“ Nukleosome Teil mancher *S. pombe* Promotorregionen zu sein.

Wir legten unser Augenmerk auf eine spezifische Gruppe von Transkripten, welche nicht in Wildtyp-Zellen detektiert werden, sondern ausschließlich in den Chromatinfaktor-Mutanten, *spt6-1 ts* und *hrp1Δ hrp3Δ*, vorkommen. Diese werden von uns „Chromatin-unterdrückte, kryptische Transkripte“ (CSCTs) genannt und ermöglichten es uns die Mindestmerkmale zu identifizieren, welche eine Promotorregion in *S. pombe* definiert. Die Mindestmerkmale beinhalten eine spezifische relative Position des +1 Nukleosoms und der TSS, permissives Chromatin, angedeutet durch eine Umgebung mit einem höheren Expressionslevel als dem Genomdurchschnitt, einem Peak für die DNA-„roll“-Form-Parameter für alle TSSs und eine charakteristische GC skew Verteilung für einige TSSs. Die Eigenschaften, DNA-„roll“-Form, und die +1 Nukleosomposition sind zwischen den Hefen, *S. pombe* und *S. cerevisiae*, konserviert. Um weitere Eigenschaften in Promotorregionen zu charakterisieren, haben wir die Bindungsstellen des TATA-box-bindenden Proteins (Tbp1) und die zugehörige Sequenz, das TATA-Box-Motiv, analysiert. Nur eine Minderheit der TSSs in *S. pombe* befindet sich in der Nähe einer TATA-Box, aber für gewöhnlich innerhalb einer kanonischen Distanz von 30-35 Basenpaaren. Diese Distanz ist ähnlich zu der analogen Distanz in höheren Eukaryoten.

In *S. pombe* wurde zuvor gezeigt, dass die Chromatin-Remodeler Mutante *hrp1Δ hrp3Δ* ein zerstörtes Nukleosomenmuster aufweist, dies weist darauf hin, dass zwei Chromatin-Remodeler der CHD1-Klasse, Hrp1 und Hrp3, wichtig für die Bildung dieses Musters sind. Durch Anwendung zweier unterschiedlichen Strategien, den *in-vivo* Komplementationsversuch und den *in-vitro* Rekonstitutionsversuch, fragten wir uns wie die Remodeler zum NDR-array Muster beitragen.

Wir konzentrieren uns beim *in-vivo* Komplementationsversuch auf die konservierte oder abweichende Funktion vom orthologen *S. cerevisiae* Chd1 und *S. pombe* Hrp3 Remodeler. Chd1 und alle Chd1/Hrp3 Hybrid-Konstrukte konnten das NDR-array Muster in der *S. pombe* Mutante *hrp1Δ hrp3Δ* wiederherstellen. Vorherige Arbeit zeigten Unterschiede für den analogen Ansatz in *S. cerevisiae* auf, da konnten Hrp3 sowie ein bestimmtes Chd1/Hrp3 Hybrid-Konstrukt nicht das NDR-array Muster wiederherstellen. Dieser Unterschied kann durch Unterschiede im Rekrutierungsmechanismus der CHD1-Chromatin-Remodeler-Klasse oder im Umfeld bezogen auf konkurrierende Remodeler begründet werden.

Die Verwendung eines *in-vitro* Rekonstitutionssystems für *S. pombe* würde es ermöglichen zu klären, ob ein Faktor notwendig, ausreichend ist und eine direkte Rolle im Nukleosomen-Positionierungsmechanismus spielt. Der *in-vitro* Rekonstitutionsansatz basiert auf: (a) einer Salzgradientendialyse (SGD) von Plasmiden, die genomische DNA enthält, und Histonen, um das genomweite „Chromatin-SGD“ zu erhalten; (b) Inkubation des Chromatin-SGD mit Zellextrakten und/oder gereinigten Faktoren, und (c) MNase-seq-Nukleosomen-Kartierung, um den ATP-abhängigen Einfluss dieser Faktoren auf die Nukleosomenpositionierung zu untersuchen. In *S. cerevisiae* zeigte dieser vorher veröffentlichte *in-vitro* Rekonstitutionsansatz erfolgreich, dass der Gesamtzellextrakt zu

ordnungsgemäßen *in vivo*-ähnlichen Nukleosomenmuster führt. Außerdem tragen die Chromatin-Remodeler und die GRFs zu dem ordnungsgemäßen *in vivo*-ähnlichen Nukleosomenmuster bei. Hier gezeigt für *S. pombe*, trug der Gesamtzellextrakt nicht zu dem ordnungsgemäßen *in vivo*-ähnlichen Nukleosomenmuster bei. Die vorläufigen Ergebnisse deuteten aber darauf hin, dass der Chromatin-Remodeler Hrp1 zusammen mit dem GRF Sap1 an einem Barriere-abhängigen Nukleosomen-Positionierungsmechanismus beteiligt zu sein scheint.

In Zusammenhang von *SGD*-Chromatin-Assemblierung werden Cluster von enganeinander gepackte Nukleosome beobachtet, sogar bei verringerter Nukleosomendichte. Theoretische Modellierungen zeigten, dass Cluster öfters auftraten als durch Zufall erwartet. Kooperativität zwischen Nukleosomen wird angenommen, um die hohe Anhäufung von enganeinander gepackten Nukleosomen zu erklären.





---

# 1 Introduction

## 1.1 *Schizosaccharomyces pombe* as a model organism

In addition to its far-diverged cousin, *Saccharomyces cerevisiae*, *Schizosaccharomyces pombe* is an important and widely used unicellular model organism for studying fundamental aspects of eukaryotic cell biology. The general advantage of working with these unicellular organisms is that they are fast growing cells, easy to cultivate, and genetically easy to manipulate through the homologous recombination system (Hoffman *et al.*, 2015). Thus, it is comparably easy in yeast cells to modulate gene expression or even establish gene deletion mutants and to study the resulting phenotypic effects.

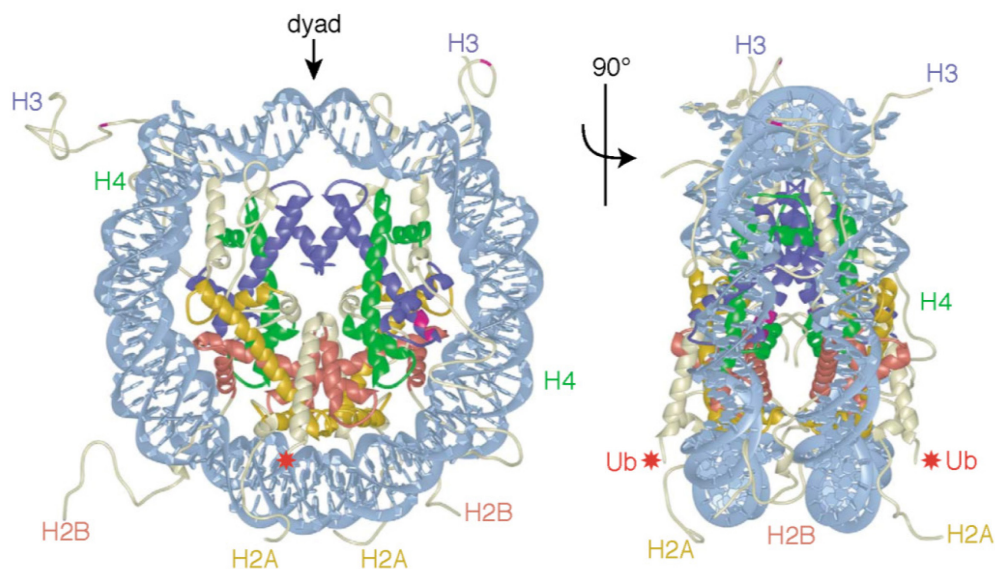
In 1996, the *S. cerevisiae* genome was fully sequenced and shortly after that the full genome sequence of *S. pombe* became available as well (Goffeau *et al.*, 1996; Wood *et al.*, 2002). This enables not only genome-wide studies in *S. pombe* and *S. cerevisiae*, but also revealed similarities and differences between both yeasts in more detail: Both yeasts have a similar genome size, i.e. around 13.6 Mb in case of *S. pombe* and around 12.5 Mb in case of *S. cerevisiae*. Interestingly, the genome of *S. pombe* is distributed over only three large chromosomes, chromosomes I (5.7 Mb), II (4.6 Mb), and III (3.5 Mb). In contrast, *S. cerevisiae* has in total 16 chromosomes and the maximal size of a single chromosome is only 1.5 Mb (Wood *et al.*, 2002). The GC content is also similar for both yeasts and lies at 36% and 38% in *S. pombe* and *S. cerevisiae*, respectively. Although *S. cerevisiae* has a smaller genome size, also the number of genes compares well with around 5000 genes in *S. pombe* and 5500 genes in *S. cerevisiae*. Interestingly, *S. pombe* and *S. cerevisiae* have diverged approximately 350 million years ago, and *S. pombe* is indeed more similar to higher eukaryotes than to *S. cerevisiae*, which is also reflected in gene composition: the genes in *S. pombe* contain introns, whereas the genes in *S. cerevisiae* have almost no introns (Kaufer and Potashkin 2000). In context of genome organization, one further major difference between both yeasts is found at the centromeres. *S. cerevisiae* has a small, 125 bp sequence element that is sufficient for full centromere function, whereas *S. pombe* comprises several kilo base pairs long centromere regions. Besides the actual centromere size, also the factors and molecular mechanism involved in centromere establishment in *S. pombe*, especially the constitutive heterochromatin, are similar to higher eukaryotes, while some of them are even completely absent in *S. cerevisiae* (Allshire and Ekwall 2015). Thus, the centromeres in *S. pombe* represent a good model for studying heterochromatin and to investigate factors such as HP1 (= Swi6 in *S. pombe*), etc., and the RNAi machinery that contribute to heterochromatin assembly and maintenance. In addition to the discussed differences in heterochromatin formation, there are more chromatin-related aspects that make *S. pombe* a valuable model organism. These chromatin-related aspects will be discussed in proceeding sections in this thesis and will be compared to features of *S. cerevisiae* as well as of higher eukaryotes.

In summary, *S. pombe* shares many features such as centromere formation, cell cycle regulation, cytokinesis and the splicing machinery with higher eukaryotes (Kaufer and Potashkin 2000; Sipiczki 2000). This makes *S. pombe* a particularly powerful model organism and tool to provide insights into the molecular functions of higher eukaryotes.

## 1.2 Structure of chromatin - from nucleosomes to higher order structures

### 1.2.1 The nucleosome

In eukaryotic cells, DNA is packaged in form of chromatin to fit into the nucleus. This compaction restricts the accessibility to DNA for various factors. These factors are involved in cellular processes such as DNA replication, repair and transcription. The most basic unit of chromatin is named nucleosome. Here, DNA is wrapped around an octamer of highly conserved histone proteins building the canonical nucleosome core particle (NCP). More precisely, the NCP consists of 147 bp of DNA and four different histone proteins, H2A, H2B, H3 and H4, that form two H2A-H2B dimers and one (H3-H4)<sub>2</sub> tetramer. Histones are small, positively-charged proteins, ranging from 11 to 15 kDa, and contain two functional domains, the “histone-fold” and “histone-tail” domains. These domains are crucial for histone-histone/histone-DNA interactions. The “histone-fold” domain is mainly composed of alpha-helical secondary structure and is well conserved among the histones. The “histone-fold” domain facilitates heterodimerization of histones in a “handshake”-like manner. This arrangement contributes to the stability of the histone octamer. The “histone-tail” domains are mostly unstructured and therefore very flexible and are located at the N-terminus of all four histones and at the C-terminus of the H2A and H2B histones. Although the “histone-tail” domains are predominately unstructured, they nevertheless contribute to the stability of the NCP (Luger *et al.*, 1997).



**Figure 1.1 High resolution structure of nucleosome core particle.** Top and a by 90° rotated view of the nucleosome core particle, where DNA (light blue) is wrapped around canonical histones (H2A (yellow), H2B (red), H3 (violet), H4 (green)) with histone tails and extensions (white). High resolution nucleosome structure as published by (Luger *et al.*, 1997). {Adapted and reprinted with permission from Elsevier (Luger 2003)}

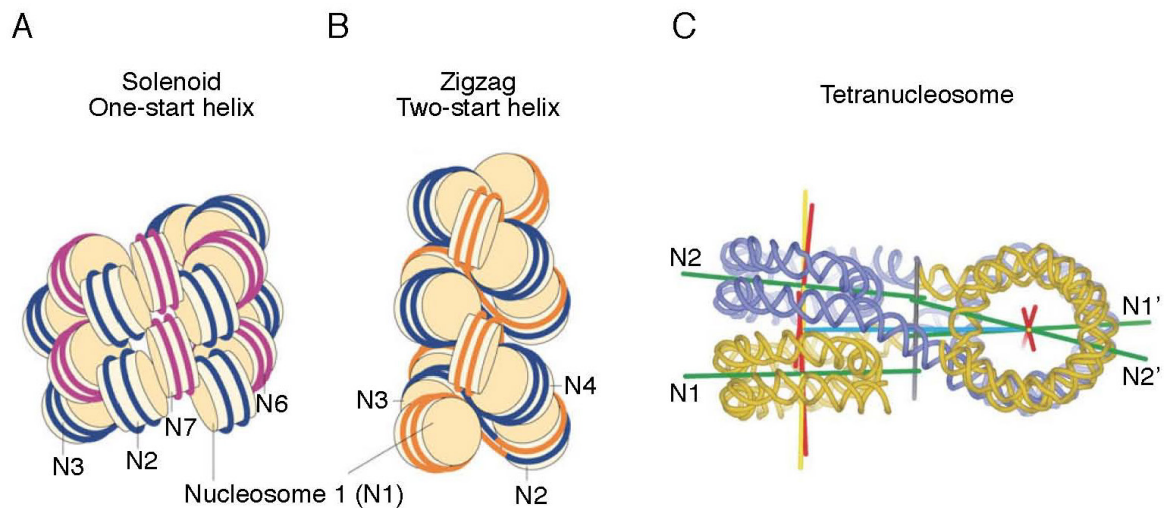
The high-resolution X-ray structure of the NCP revealed that the 147 bp long DNA is wrapped 1.65 times around the histone octamer in a left-handed superhelix, that builds a disc-/spool-like structure (Figure 1.1) (Luger *et al.*, 1997; Luger 2003). The positions of the DNA around the histone octamer are marked by superhelical locations (SHL): SHL0 represents the dyad, and goes from SHL7 to SHL-7 depending on the exit/entry site of the DNA. The NCPs are connected by free linker DNA and form nucleosomes. The length of the linker DNA varies among species. The model organism of this study, *S. pombe*, has a DNA linker length of only 7 bp (Lantermann *et al.*, 2010). In contrast, the DNA linker length adopts the length of 18 bp in *S. cerevisiae* or even of 90 bp in sea urchin sperm (Spadafora *et al.*, 1976; Jiang and Pugh 2009). Notably an additional histone, i.e. the linker histone H1, is present in almost all species, but not in *S. pombe* (Godde and Widom 1992).

In addition to canonical histones, the NCPs can incorporate histone variants which differ in their amino acid sequence and expression pattern (Henikoff and Ahmad 2005; Weber and Henikoff 2014). Almost no histone variants are known for H4 and H2B, but several histone variants exist for H2A and H3 that are involved in diverse cellular processes. The yeast model organisms *S. cerevisiae* and *S. pombe* harbor only two histone variants, the H2A.Z variant of H2A and the CENP-A variant of H3. H2A.Z is the most frequent variant among the many H2A variants and is highly conserved among species ( $\approx 90\%$ ). The sequence identity between H2A and H2A.Z is only 60% (Suto *et al.*, 2000). H2A.Z plays an important role in diverse cellular processes such as DNA repair, cell cycle progression and transcription (chapter 1.4.3). CENP-A is part of centromeres in all eukaryotes and is involved in chromosome segregation. CENP-A is the most diverged H3 variant sharing only 50% sequence identity with H3 (Tachiwana *et al.*, 2011; Tachiwana *et al.*, 2012).

Moreover, histones can be post-translationally modified (PTM), whereby mainly the H3 and H4 histones are targeted by modifications such as acetylation, phosphorylation, methylation, ubiquitination, and sumoylation. These modifications are found at amino acid residues of serine, lysine, arginine and threonine (Bannister and Kouzarides 2011). The PTMs of histones occur predominantly on N-terminal histone tails but are also found on globular histone domains (Jack and Hake 2014). The effect of PTMs on chromatin structure can be either direct through modulation of histone/DNA interactions or indirect through recruitment of factors to the chromatin. The enzymes, adding or removing PTMs, are termed "writers" or "erasers", respectively. "Readers" are chromatin factors, which recognize PTMs and are recruited to chromatin. One group of these factors are the so-called chromatin remodeling enzymes (chapter 1.3.5.1). The exact site and type of modification determine the function of PTMs for cellular processes such as transcriptional regulation, DNA repair and chromatin structure maintenance (Zentner and Henikoff 2013). Taken together, nucleosomes exist either as canonical NCP which includes the canonical histone proteins H3, H4, H2A and H2B or can come in different flavors where the nucleosome incorporates histone variants and/or post-translationally modified histones.

### 1.2.2 The higher order structure

Nucleosomes are organized into a 10 nm fiber, where nucleosomes are arranged like beads-on-a-string. This “beads-on-a-string” structure was originally visualized by electron microscopy (Olins *et al.*, 1975). Whereas the structure of the nucleosome is well characterized, higher order structures of chromatin beyond the 10 nm fiber are still under investigation. Introduction of artifacts during isolation of native chromatin hamper the elucidation of the higher order structure. For a long time, the next level of compaction was thought to be a folded, helical 30 nm fiber (Finch and Klug 1976). The solenoid and zigzag model are discussed for the underlying structure of the 30 nm fiber (Figure 1.2) (Finch and Klug 1976; Woodcock *et al.*, 1984). In the solenoid model, the nucleosomes are organized in an adjacent manner along a helical turn, thus this model is also alternatively called “one-start-helix” model. In the second model, the nucleosomes are arranged in a zigzag manner, hence this model is called zigzag or “two-start-helix” model. The crystal structure of an *in vitro* reconstituted tetranucleosome and the fact that such a tetranucleosome can be modeled into the 30 nm fiber support the “two-start helix” model (Schalch *et al.*, 2005). The tetranucleosome is composed of 2x2 stacked nucleosomes and each stack is connected by linker DNA. A hypothesis alternative to the 30 nm fiber emphasizes that chromatin is loosely and dynamically organized and folded into irregular fibers. The recently developed technique Micro-C enables mapping of contacts at the single nucleosome level (Hsieh *et al.*, 2015). Briefly, cross-linked chromatin DNA is fragmented by MNase, and then labeled nucleotides are incorporated into the generated DNA ends followed by ligation of the DNA ends. Ultimately, paired-end deep sequencing is used to characterize the ligation products thus enabling the identification of nearby DNA locations. Micro-C identified nucleosomes to be arranged in “gene-crumple”, where nucleosomes interact within genes (Hsieh *et al.*, 2015). This finding does not agree with the findings of the 30 nm fiber structure. The next state of chromatin arrangement is the building of mitotic and meiotic chromosomes, which were originally observed by Walther Flemming, who also coined the term chromatin for the first time (Flemming 1878). The underlying mechanism of chromosome compaction is still unclear and needs further investigation.



**Figure 1.2 Models of higher order structure of nucleosomes. A-B** Two models for the 30 nm fiber, solenoid model (one-start helix) **(A)** and zigzag model (two-start helix) **(B)**. **C** The tetranucleosome structure with two nucleosomes which are stacked on top of each other and connected by the linker DNA to other two stacked nucleosomes. {Adapted and reprinted with permission from Nature Publishing Group ((Luger *et al.*, 2012) **(A+B)**, (Schalch *et al.*, 2005) **(C)**)}

## 1.3 Nucleosome positioning mechanisms

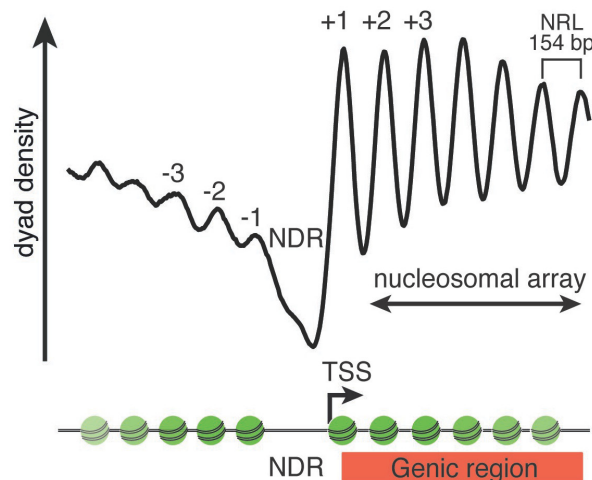
The accessibility of DNA for DNA binding and regulatory factors is determined by nucleosomes, i.e. the presence of nucleosomes can restrict the binding of regulatory factors. This way, nucleosomes can influence cellular processes that depend on DNA access such as transcription. Thus, important questions are which genomic regions are occupied by nucleosomes (chapter 1.3.1) and how these nucleosome positions are established (chapters 1.3.3, 1.3.4 and 1.3.5). Therefore, different methods to determine nucleosome positions will be introduced in this chapter followed by a discussion of factor-independent (*cis*-factor) and factor-dependent (*trans*-factor) nucleosome positioning mechanisms.

### 1.3.1 Mapping of nucleosome positions

The incorporation of DNA into the NCP protects nucleosomal DNA from digestion by nucleases. This feature is often exploited in nuclease-based techniques to map the positions of nucleosomes. One genome-wide approach to determine the nucleosome positions is MNase-seq (Lieleg *et al.*, 2015; Lai and Pugh 2017). Here, chromatin is digested by micrococcal nuclease (MNase) to obtain mononucleosomal DNA, which is then sequenced after library generation. One discussed issue for this approach is that the MNase technique suffers from sequence bias of the MNase, especially if one aims for a limited digest of DNA by MNase. The MNase has indeed a higher probability to cut at dA:dT base pairs than at dG:dC. This might lead to enrichment of distinct fragments and might cause that MNase cuts in the intranucleosomal region if high MNase concentration is used (Horz and Altenburger 1981). Another issue is that MNase could also produce DNA fragments with a length of a nucleosome although this DNA fragment was completely free of histones or protected by non-histone containing complexes (Chung *et al.*, 2010; Lorch *et al.*, 2014). To ensure that a DNA fragment originates indeed from a nucleosome, the strategy is to combine MNase-seq with an additional chromatin immunoprecipitation (ChIP) step targeted against histone proteins (Albert *et al.*, 2007). Here, chromatin is first digested by MNase and then pulled down using an antibody against a histone protein, e.g. H3. Another alternative way to map elegantly nucleosomes is hydroxyl-radical-seq (Brogaard *et al.*, 2012). The hydroxyl-radical based approach is nuclease-independent and therefore also circumvents the potential sequence biases produced by MNase. For hydroxyl-radical-seq, a special strain is used that harbors a mutation in the gene encoding histone H4 that generates a cysteine at position 47 (H4S47C) close to the dyad of nucleosomal DNA. Phenanthroline binds covalently to this cysteine, which enables copper chelation. Hydroxyl radicals, generated by addition of copper ions, mercaptopropionic acid and hydrogen peroxide induce DNA cleavage at a defined distance from the nucleosome dyad. This way, DNA fragments are produced that span from one dyad to the dyad positions of a neighboring nucleosome (Brogaard *et al.*, 2012). Sequencing of these DNA fragments and mapping back to the genome enables the determination of the exact

positions of nucleosome dyads with single-base pair resolution. The recently published method, called the H3Q85C cleavage method, is also based on the hydroxyl-radical approach, but uses a different strain that harbors a mutation in the gene encoding histone H3 generating a cysteine at position 85 (H3Q85C) (Chereji *et al.*, 2018). Using the hydroxyl-radical approach with this strain enables the detection of a DNA fragment, which originates from one single nucleosome. Overall, the nucleosome positions mapped by both hydroxyl-radical approaches are in good agreement with the nucleosome positions mapped by the MNase-dependent approach. Thus, the discussed problems of MNase such as the MNase bias for dA:dT-rich DNA regions seem not to be a major problem for MNase-generated nucleosome maps. Therefore, the MNase-dependent approach is still a good way to determine nucleosome position.

Nucleosomes *in vivo* are highly organized and show a stereotypical nucleosome pattern at promoters of most genes in yeasts (chapter 1.4.2). This stereotypical nucleosome pattern, also known as NDR-array pattern, harbors a nucleosome-depleted region (NDR, or alternatively called nucleosome free region (NFR)) right upstream of the TSS (Lee *et al.*, 2007). The NDR is flanked by two well-positioned nucleosomes, the +1 and -1 nucleosomes (Jiang and Pugh 2009; Hughes and Rando 2014). Nucleosome arrays are aligned at these well-positioned +1 and -1 nucleosomes. To visualize this nucleosome pattern from genome-wide nucleosome mapping data, a composite plot is often used: The composite plot represents an average of all nucleosome dyad positions over all genes, which are aligned to a reference point (Figure 1.3). The dyad of a nucleosome is a unique base pair and is used to represent the nucleosome positions. The transcription start site (TSS) is a commonly used reference point for the alignment of nucleosome dyad positions to visualize the NDR-array pattern at promoters (Lee *et al.*, 2007). In TSS aligned composite plots the nucleosome arrays appear more pronounced downstream to the +1 nucleosome than upstream to the -1 nucleosome.

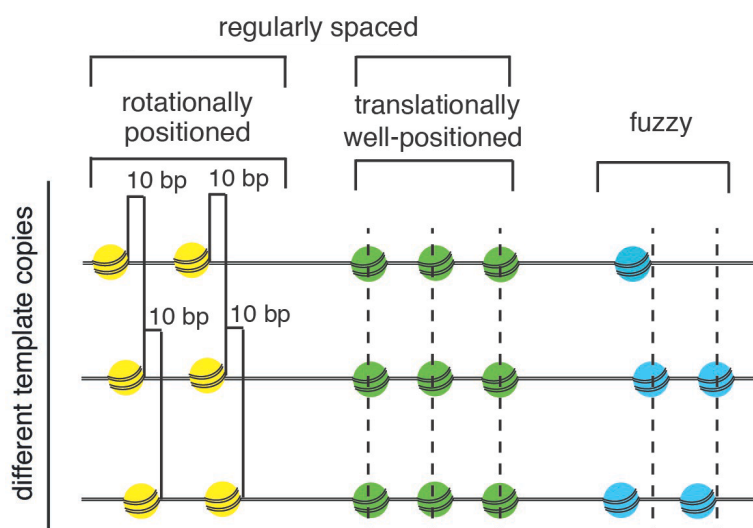


**Figure 1.3 Nucleosome positioning pattern.** The stereotypical nucleosome promoter pattern shown here for *S. pombe* as a composite plot derived from MNase-seq. The composite plot is an average of all nucleosome dyad positions over all genes aligned to the TSSs. The stereotypical nucleosome pattern harbors the NDR, the well-positioned +1/-1 nucleosomes and nucleosome arrays up- and downstream to the NDR.



### 1.3.2 Terminology of nucleosome positioning

To describe nucleosome organization, different terms are reported in the literature: rotational positioning, translational positioning, nucleosome occupancy, nucleosome repeat length (NRL) and spacing (Lieleg *et al.*, 2015; Lai and Pugh 2017). Rotational positioning describes the relative orientation of the DNA helix to the histone octamer. The DNA helix-structure (one turn per 10 bp) is also reflected in the nucleosome. Here, the DNA binds to the histone octamer in a  $\sim 10$  bp-periodical manner. Thus, the major groove, for example, faces towards the histone core every helical turn of 10 bp. The major groove is potentially less accessible when facing the histone core compared to when the major groove is facing away from the histone core, i.e. depends on the rotational positioning. Translational positioning specifies the genomic position of the unique dyad position of the NCP. Additionally, nucleosomes can be further distinguished into translationally well-positioned and fuzzy nucleosomes if the nucleosome position is described for a population or cells or DNA template copies (Figure 1.4). Translationally well-positioned nucleosomes are nucleosomes, which occupy the same positions in the genome in a cell population. Fuzzy nucleosomes are nucleosomes, which are distributed more broadly over corresponding genome regions in a cell population. The NRL, or spacing, is defined as an average of the dyad-to-dyad distances between two neighboring nucleosomes within a regularly spaced array. This NRL varies between species, for example, with sizes of 154, 165 and 197 bp in *S. pombe*, *S. cerevisiae* and *Drosophila*, respectively (Becker and Wu 1992; Jiang and Pugh 2009; Lantermann *et al.*, 2010). The nucleosome occupancy is often misleadingly used to describe the nucleosome positions. Nucleosome occupancy, however, deals with the probability of how often a given base pair is occupied by any or by a particularly positioned nucleosome in a cell population.



**Figure 1.4 Terminology in context of nucleosome positioning.** The illustration shows rotationally positioned, translationally well-positioned, regularly spaced and fuzzy nucleosomes. {Adapted and reprinted with permission from Springer Nature (Lieleg *et al.*, 2015)}

### 1.3.3 Factor-independent/*cis*-factor nucleosome positioning mechanism

The factor-independent/*cis*-factor nucleosome positioning mechanism is based on a DNA-sequence-driven mechanism involving exclusively DNA and histones. This mechanism is intrinsically driven by the binding properties of histones to DNA and no further factors (*trans*-factors) are involved (chapter 1.3.5). The histone octamer could be interpreted as a DNA binding factor with a very long 147 bp DNA footprint. The “genomic code” model for nucleosome positioning postulates that DNA sequences guide the histone octamer to their position and that the nucleosome pattern as observed *in vivo* is solely or mainly generated this way (Segal *et al.*, 2006; Kaplan *et al.*, 2009; Kaplan *et al.*, 2010). This model is based on the observation that different DNA sequences vary in their binding affinity to histone octamers *in vitro*. One example for a DNA sequence with high histone binding affinity is the artificially selected Widom 601 sequence (Lowary and Widom 1998). Consequently, this sequence is often used to assemble nucleosomes for *in vitro* studies, which require precisely positioned nucleosomes. To assemble such nucleosomes, histones and DNA are first combined at high salt concentrations and then assembled on the Widom 601 sequence during a salt gradient dialysis, which reconstitutes chromatin by slowly reducing the salt concentration in the DNA/histone mix (Krietenstein *et al.*, 2012; Wippo and Korber 2012). Nevertheless, the high *in vitro* histone binding affinity of the 601 Widom sequence does not lead to corresponding nucleosome positioning *in vivo* (Perales *et al.*, 2011). One example for DNA sequences with low histone binding affinity are poly(dA:dT)-rich sequences. *In vitro* reconstitution of chromatin showed that poly(dA:dT) sequences have anti-nucleosomal properties presumably because they are intrinsically stiff (Lowary and Widom 1998; Kaplan *et al.*, 2009; Zhang *et al.*, 2009; Zhang *et al.*, 2011). Interestingly, poly(dA:dT) sequences are enriched in the promoter NDRs of *S. cerevisiae* (Lee *et al.*, 2007). Thus, the NDRs at promoters in *S. cerevisiae* can be partially reconstituted *in vitro* as the poly(dA:dT) sequences exclude nucleosomes. However, other aspects of the stereotypical nucleosome organization, such as +1 nucleosomes or nucleosome arrays, could not be reconstituted *in vitro* using DNA and histones only (Zhang *et al.*, 2011). Additionally, comparison of promoter/NDR-array regions of 13 yeasts revealed that poly(dA:dT) sequences or other nucleosome excluding sequences are neither evolutionarily conserved nor essential to build NDRs at promoter regions (Tsankov *et al.*, 2010; Tsankov *et al.*, 2011). For example, in *S. pombe*, the poly(dA:dT) sequences are not enriched at promoter NDRs and are mostly occupied by nucleosomes (Lantermann *et al.*, 2010; Tsankov *et al.*, 2011; Moyle-Heyrman *et al.*, 2013). This argues that the DNA sequence rules for NDR formation are not universal and most likely not the only driving force.

Further evidence that DNA-histone interactions are not sufficient to properly position nucleosomes comes from cross-species studies. In one study, long DNA stretches from *Kluyveromyces lactis* were introduced in the form of yeast artificial chromosomes into *S. cerevisiae*. Since histones are highly conserved, the “genomic code” model would predict that the nucleosome spacing formed on *K. lactis* DNA in the recipient *S. cerevisiae*

would reflect the spacing normally observed in the donor yeast (*K. lactis*). However, the observed nucleosome spacing resembled that of the host yeast (*S. cerevisiae*) and not the nucleosome spacing of the donor yeast (*K. lactis*) (Hughes and Rando 2015). Similar observations were made in another cross-species study, where DNA of *S. pombe* was introduced into mouse cells. Here, the spacing of the mouse host cells was adapted on the *S. pombe* DNA (McManus *et al.*, 1994). The results of both cross-species studies rather imply a factor-specific involvement of the host organism to generate the nucleosome pattern.

Taken together, DNA sequences and histones are not sufficient to explain the observed stereotypical nucleosome pattern *in vivo*. Hence, other mechanisms are involved in forming the stereotypical nucleosome pattern.

#### **1.3.4 Statistical nucleosome positioning mechanism**

Statistical nucleosome positioning describes a model where nucleosomes behave randomly on DNA, but where resulting nucleosome positions are nonetheless non-random on average if a boundary element is introduced. The nucleosomes become ordered relative to the boundary but the regularity decreases with the distance to the boundary (Kornberg and Stryer 1988; Mobius and Gerland 2010). Such a boundary could be represented, for example, by the NDR/+1 nucleosome or a poly(dA:dT) sequence. Additionally, this model implies that nucleosome spacing depends only on the density of nucleosomes; as a consequence the spacing would be wider if the nucleosome density were reduced. Studies, where nucleosome density were reduced either *in vitro* or *in vivo*, were not in agreement with the statistical positioning model as the spacing remained constant despite lower nucleosome density (Celona *et al.*, 2011; Zhang *et al.*, 2011). Moreover, it was observed that the deletion of components for the histone chaperone complex FACT in yeast, decrease in histone expression levels, and cell aging, all led to reduced nucleosome density, but the spacing was not altered (Celona *et al.*, 2011; Gossett and Lieb 2012; Hennig *et al.*, 2012; van Bakel *et al.*, 2013; Hu *et al.*, 2014). So the original statistical positioning mechanism cannot account for the generation of boundary-aligned nucleosome arrays *in vivo*.

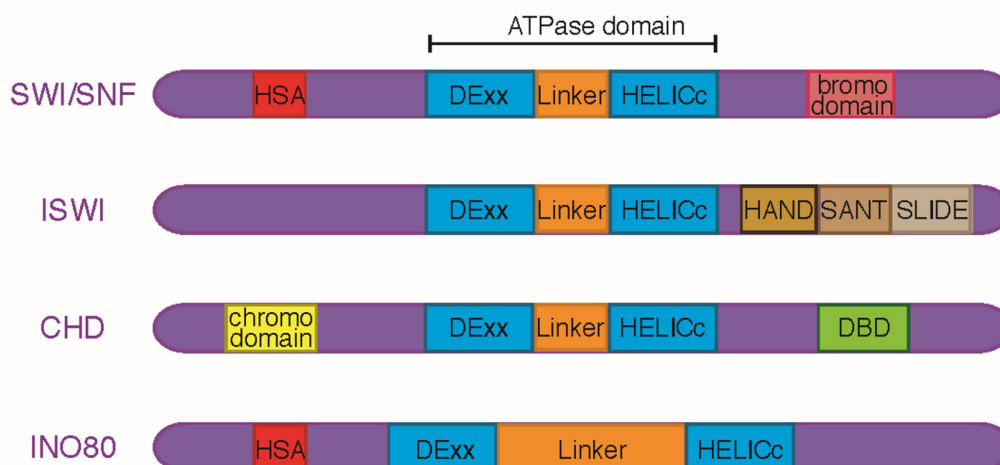
### 1.3.5 Factor-dependent nucleosome positioning mechanism

The factor-dependent/*trans*-factor nucleosome positioning mechanism considers the contribution of additional factors, besides DNA and histones, to generate the *in vivo* nucleosome pattern. Chromatin remodelers and general regulatory factors (GRFs) belong to such *trans*-factors.

#### 1.3.5.1 Classes and functions of chromatin remodelers

Chromatin remodelers are ATP-dependent enzymes that translocate along the DNA and belong to the Snf2-type subfamily of ATP-dependent DNA/RNA helicases (Ryan and Owen-Hughes 2011; Narlikar *et al.*, 2013; Bartholomew 2014). The major classes of chromatin remodelers are SWI/SNF, CHD, ISWI, and INO80 (Figure 1.5) (Flaus *et al.*, 2006). However, the exact number of classes and the number of chromatin remodeler per class varies from species to species. For example, *S. pombe* does not have the ISWI class at all. *S. cerevisiae* has only one member of the CHD class, namely Chd1, whereas *S. pombe* has three, Hrp1, Hrp3 and Mit1, and humans have even nine different CHD chromatin remodelers. So far more than 100 chromatin remodeling complexes were described in humans (Bartholomew 2014). The majority of chromatin remodelers exists as multiprotein complexes where the ATPase associates with several other subunits. Sometimes, remodeler complexes even utilize the same ATPase subunit, but are then composed of different associated subunits. Importantly, the CHD chromatin remodelers predominantly exist as monomers, with some exceptions found in higher eukaryotes, such as in vertebrates.

The common feature of all chromatin remodeler classes is the conserved core ATPase domain that is composed of the DExx and HELICc subdomains. Each chromatin remodeler class (see above) is defined by sequence homology within their ATPase domain and by the presence of functional domains, such as bromo-, chromo-, linker, DNA binding domain (DBD), helicase SANT (HSA) and HAND-SANT-SLIDE (HSS) domain (Figure 1.5). ISWI remodelers for example have a unique HSS domain at the C-terminus (Grune *et al.*, 2003). This HSS domain combines three subdomains, the HAND, the SANT and the SLIDE subdomain. The subdomains SANT and SLIDE are not only present in the ISWI class, but also in the CHD class. Another common feature of the CHD class (Clapier and Cairns 2009) is the chromodomain which is located at the N-terminus. Furthermore, a linker domain is located between the DExx and HELICc domains within the ATPase domain. In most remodeler classes, such as SWI/SNF, ISWI, and CHD, this linker insertion in the ATPase domain is rather short compared to the long linker subdomain characteristic for the INO80 class.



**Figure 1.5 Domain structure of Snf2-type chromatin remodeler ATPase classes.** The SWI/SNF, ISWI, CHD and INO80 represent the major ATP-dependent chromatin remodeler classes. All chromatin remodelers share the ATPase domain with DExx and HELICc domains. The ATPase domains differ in their linker lengths, especially for the INO80 class. Chromatin remodelers include functional domains such as the bromo-, chromo-, linker, DBD, HSA and HSS domain and are classified according to their domains into the corresponding classes.

The chromatin remodelers can act in various ways on nucleosomes using ATP-hydrolysis. For example, chromatin remodelers can move nucleosomes along the DNA, also referred to as sliding or, more specifically, spacing. Additionally, they can assemble histones onto the DNA or disassemble histones from DNA, and they can exchange histones from the nucleosome core particles for histone variants and vice versa.

Nucleosome sliding is the translocation of nucleosomes along the DNA, as a consequence the translational position of the nucleosomes is changed. The sliding activity is one main function of the CHD class. Chd1 acts in a linker-length-dependent manner and cannot move nucleosomes closer than 15 bp to DNA ends (Stockdale *et al.*, 2006). The DBD contributes to the directionality of Chd1 sliding activity (Patel *et al.*, 2013).

The spacing activity describes a mechanism to set regularly spaced nucleosomes in nucleosome arrays. This spacing activity is typical for the ISWI and CHD classes, e.g. ISW2, Chd1, and ISW1a in *S. cerevisiae*. Interestingly, ISW1b, a complex that utilizes the same ATPase as ISW1a, lacks spacing activity, underlining that the chromatin remodeler subunit-composition can modulate remodeling activity (Tsukiyama *et al.*, 1999; Vary *et al.*, 2003).

The disassembly or eviction activity of nucleosomes is one of the main functions of the SWI/SNF class. The mechanism probably involves that a nucleosome is pushed towards a neighboring nucleosome and afterwards the H3/H4 histones of the neighboring nucleosome are removed, followed by complete nucleosome disassembly (Dechassa *et al.*, 2010).

Lastly, the exchange of canonical histones for histone variants and vice versa is one main function of INO80 and SWR1, that both belong to the INO80 class. For example, the SWR1 chromatin remodeler is predominantly localized in the NDRs and the +1 nucleosome regions, and exchanges histone H2A for the histone variant H2A.Z. The INO80 chromatin remodeler is involved in the reverse reaction (Yen *et al.*, 2013). In more detail, H2A.Z removal depends on Arp5, a subunit of the INO80 complex. Replacement of H2A.Z is more

efficient in the dimeric stage of H2A.Z/H2B to H2A/H2B (Papamichos-Chronakis *et al.*, 2011; Watanabe and Peterson 2016).

### 1.3.5.2 Role of chromatin remodelers in the nucleosome positioning mechanism

As mentioned before, chromatin remodelers belong to the *trans*-factors and contribute to the establishment of nucleosome patterns as shown in various *in vivo* studies. For example, RSC, a remodeling complex of the SWI/SNF class, is known to be involved in the NDR formation. The depletion of the Sth1 ATPase of RSC leads to increased nucleosome occupancy at NDRs (Hartley and Madhani 2009). The ablation of the RSC subunit Rsc3 causes increased nucleosome occupancy at promoters with Rsc3 binding sites (Badis *et al.*, 2008). Chromatin remodelers of the ISWI and CHD class are rather involved in array formation. Interestingly, the single deletion of genes encoding for chromatin remodelers such as *Isw1*, *Isw2* or *Chd1* shows only mild effect on the nucleosome pattern in *S. cerevisiae*. For example, the deletion of *Isw2*, the ATPase of the ISW2 chromatin remodeler, leads to a shift of +1 nucleosome positions for some genes (Whitehouse *et al.*, 2007). Other studies on the single mutants, *chd1Δ* or *isw1Δ*, revealed that the *Chd1* chromatin remodeler sets a tighter nucleosome spacing than the *Isw1* chromatin remodeler (Ocampo *et al.*, 2016). In this context, these chromatin remodelers compete with each other to set their preferred nucleosome spacing. To see a more severe genome-wide effect on NDR-array pattern, the simultaneous deletion of several chromatin remodelers is necessary. The triple deletion of *isw1Δ isw2Δ chd1Δ* in *S. cerevisiae* or the double deletion of *hrp1Δ hrp3Δ* in *S. pombe* leads to substantial loss of nucleosome array peaks over the gene coding regions in TSS or +1 nucleosome aligned composite plots (Gkikopoulos *et al.*, 2011; Hennig *et al.*, 2012; Pointner *et al.*, 2012; Ocampo *et al.*, 2016). Importantly, NDRs and the +1 nucleosomes are almost unaffected in these deletion mutants. Notably, the deletion mutants still have regularly spaced nucleosomes, as visualized by MNase ladders of bulk chromatin. Hence, regular nucleosome spacing is still maintained in these deletion mutants, but the nucleosome arrays are out of register, i.e., not aligned to the TSSs/NDRs (Pointner *et al.*, 2012), which highlights their importance for linking nucleosome arrays to the TSS/NDR.

As explained above, many *in vivo* studies showed that chromatin remodelers contribute to the nucleosome pattern, but as they act redundantly and in the context of other factors *in vivo*, it is difficult to infer direct or indirect, specific, or sufficient contributions of the chromatin factors to the nucleosome pattern from these *in vivo* experiments. As an alternative approach, genome-wide *in vitro* reconstitution that uses purified histone octamers, a plasmid library that covers the whole yeast genome, and a whole cell extract from *S. cerevisiae* (YEX) is able to recapitulate the physiological NDR-array nucleosome pattern and elegantly showed that the nucleosome positioning mechanism is indeed ATP-dependent (Zhang *et al.*, 2011). Previous single loci studies using a similar *in vitro* approach were able to demonstrate a direct, specific and necessary contribution of RSC to the NDR formation at, for example, the *PHO8* promoter (Wippo *et al.*, 2011). Thus, this

*in vitro* reconstitution approach is an effective way to test the individual contributions of *trans*-factors on nucleosome positioning pattern. Indeed, this *in vitro* reconstitution approach was recently further refined and elucidated the mechanistic contribution of the individual components to the stereotypical nucleosome positioning pattern by using either purified chromatin remodelers alone or in combination with purified GRFs (Krietenstein *et al.*, 2016). This study demonstrated that the generation of the NDR-array pattern can be divided into four different stages. (1) RSC removes nucleosomes from promoter regions in a poly(dA:dT) dependent manner, where the poly(dA:dT) sequences are readout by RSC. (2) INO80 alone or ISW2 in combination with Abf1/Reb1 (at their binding sites) positions the +1 nucleosome. (3) INO80 and ISW2 generate nucleosome arrays with wider spacing than observed *in vivo*. (4) ISW1a sets spacing to physiological repeat lengths.

### **1.3.5.3 Role of GRFs in the nucleosome positioning mechanism**

General regulatory factors (GRFs) are involved in transcription regulation and are mostly essential for cell viability. GRFs have sequence-specific DNA binding sites, which are enriched in promoter regions (Tsankov *et al.*, 2010). Multiple *in vivo* studies demonstrate that GRFs contribute to the establishment of nucleosome pattern. Different mechanisms are possible how GRFs could contribute to nucleosome positioning: GRFs could either compete with histone octamers for DNA binding, they could recruit other factors to chromatin, such as chromatin remodeling enzymes, or they could act as barrier for other factors. GRFs of *S. cerevisiae*, such as Rap1, Abf1, and Reb1, have their binding sites enriched in promoter regions (Badis *et al.*, 2008; Parnell *et al.*, 2008; van Bakel *et al.*, 2013) and their depletion leads to increased nucleosome occupancy at their DNA binding sites (Hartley and Madhani 2009; Morse 2009; Tsankov *et al.*, 2010; Tsankov *et al.*, 2011). In addition, the engineering of a Reb1 binding site in combination with a poly(dA:dT) sequence into a nucleosome-rich region, the *SNT1* gene coding region, caused nucleosome depletion (Hartley and Madhani 2009). In *S. pombe*, Sap1 is the only major potential GRF identified so far (Tsankov *et al.*, 2011). Similar to GRF depletions in *S. cerevisiae*, inactivation of Sap1 in *S. pombe* leads to higher nucleosome occupancy around the Sap1 binding sites that are enriched at promoter regions, indicating its involvement in NDR formation.

Taken together, all these experiments highlight the role of GRFs in NDR formation and this function seems to be conserved throughout evolution, but the factors, which act as GRFs, can vary from species to species (Tsankov *et al.*, 2011). Another observation regarding the GRFs is that these factors are essential for the organism. As GRFs have a major role in NDR formation at promoters this implicates that NDR formation seems to be a vital mechanism for the organism.

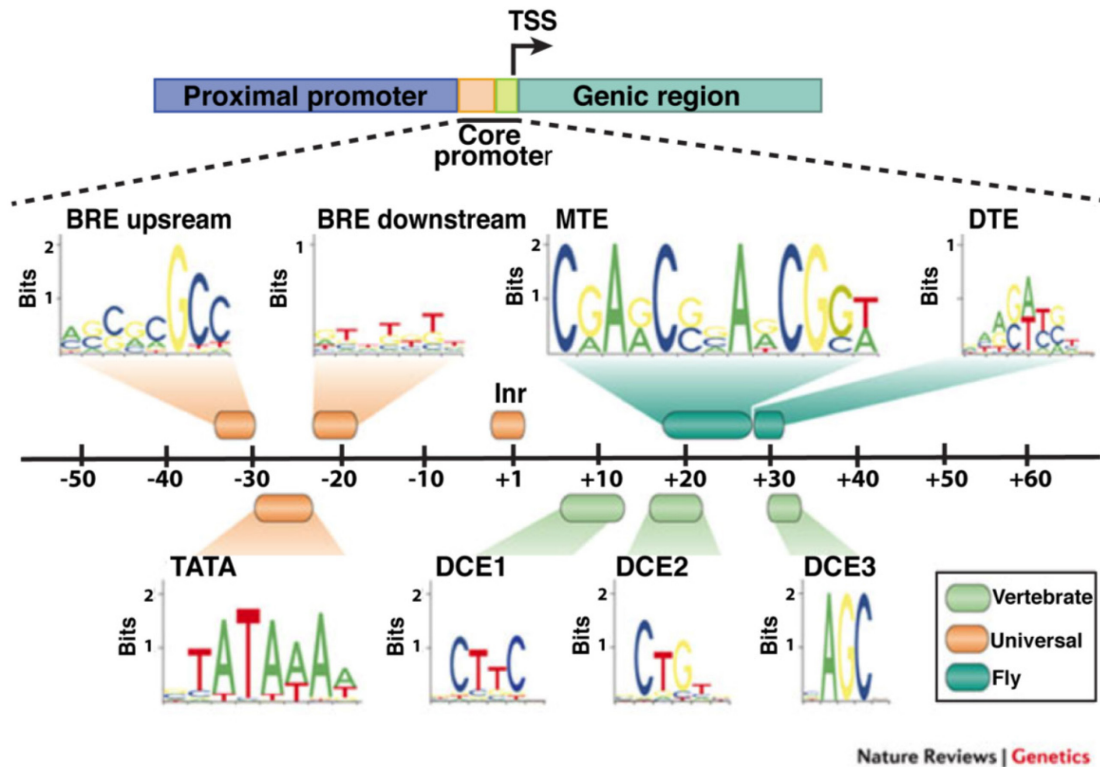
## 1.4 Chromatin and transcription regulation

### 1.4.1 Promoter architecture

Transcription is highly regulated. The basic mechanism of transcription initiation is the binding of general transcription factors (GTFs) to their DNA binding sites and the subsequent assembly of the pre-initiation complex (PIC) machinery there. The PIC machinery is a multi-subunit complex and consists of the RNA PolII and the GTFs, which comprise the TATA box binding protein (TBP) and TBP-associated factors (Kadonaga 2004; Thomas and Chiang 2006). Promoters are genomic regions where transcription initiation and regulation take place and promoters can be classified in core promoter (ca. -35 to +35 bp relative to the TSS) and proximal promoter (ca. -100 and -200 bp upstream of the TSS) (Butler and Kadonaga 2002; Lenhard *et al.*, 2012). The core promoter represents the DNA region where the PIC assembles and transcription starts.

To map the start sites of transcripts high-throughput sequencing approaches are used such as RNA-seq, Pro-cap-seq and CAGE (cap analysis of gene expression)-seq (Nagalakshmi *et al.*, 2008; Takahashi *et al.*, 2012; Mahat *et al.*, 2016). Conventional RNA-seq approaches monitor the mRNA pool and library preparation for RNA-seq suffers from incomplete cDNA reverse transcription. These shorter incomplete fragments are nevertheless sequenced in RNA-Seq, which is especially problematic for the accurate annotation of transcription start sites. The 5'-cap RNA structure dependent approaches such as CAGE-seq or Pro-cap-seq use an additional selection step to overcome the problem of partial cDNA sequences: here a specific chemistry is used to capture the 5'-cap mRNA structure, which can be biotinylated. After reverse transcription, RNase is added to remove RNA of incomplete cDNA/RNA products. In the next step, biotinylation tag is used to pull down the full-length cDNA (Carninci *et al.*, 1998). Therefore, the main advantage of 5'-cap-dependent mRNA-seq approaches in comparison to conventional RNA-seq is the specific capture of the 5'-cap mRNA structure and consequently the accurate annotation of start sites of transcripts. The TSS annotation derived from CAGE-seq reveals either sharp or broad distributions of TSSs at promoters, which was first described for mouse, followed by human, *Drosophila* and recently for *S. pombe*. (Hoskins *et al.*, 2011; Forrest *et al.*, 2014; Li *et al.*, 2015). The sharp promoters harbor TATA box elements, whereas broad promoters harbor CpG islands in higher eukaryotes (Carninci *et al.*, 2006). In zebrafish the TSS positions during the developmental transition from maternal to zygotic transcription reveal a dynamic change of TSS positions (Haberle *et al.*, 2014). The TSSs of the maternal transcripts are associated with an A/T-rich motif (W-box element), whereas TSSs of the zygotic transcripts harbor a broader dinucleotide composition. This hints towards alternative TSS selection in the same promoter region. Furthermore, transcription starting from one promoter can go in both directions. This bidirectionality is observed from yeasts to humans (Trinklein *et al.*, 2004; Chen and Zhang 2016). The transcripts from such bidirectional promoters are either two protein-coding RNAs, or one protein-coding RNA and one noncoding RNA (ncRNA). The latter is more frequent.





**Figure 1.6 Core promoter structure in higher eukaryotes.** The core promoter elements are presented with their most abundant underlying DNA consensus sequence and are arranged in close vicinity to the TSSs. The core promoter harbors the regulatory core promoter elements such as TATA box element, BRE, Inr, and the more specific core promoter elements such as MTE and DTE, found in *Drosophila* and DCE, found in vertebrates. {Adapted and reprinted with permission from Springer Nature ((Lenhard *et al.*, 2012))}

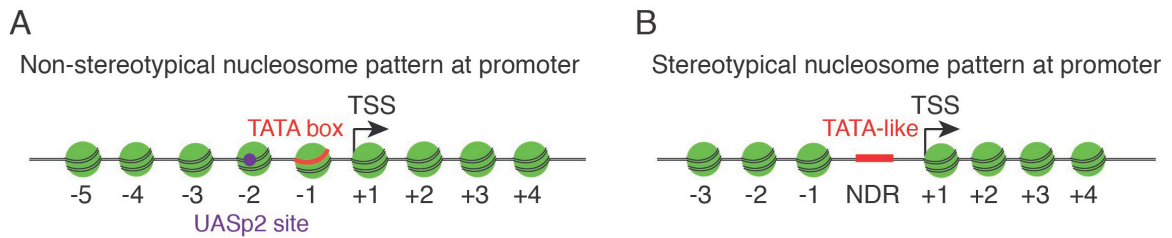
Promoter regions can be defined by core promoter elements (Figure 1.6). Core promoter elements can harbor well-defined and universal elements, which can be bound by their corresponding DNA binding factors to enhance transcription initiation. The ChIP-seq approach is used to map factors, which bind to these promoter regions (Johnson *et al.*, 2007). Specific antibodies are used to pull down DNA binding factors. The DNA attached to the DNA binding factors is sequenced such that the position of the binding sites can be identified. Furthermore, by doing so, the underlying DNA consensus sequence and the binding motif of the corresponding DNA binding factor can be annotated. Such binding motifs or promoter elements are for example the TATA box element, B recognition element (BRE) or Initiator (Inr) elements. Additional elements, such as motif ten element (MTE) and downstream promoter element (DPE) are found in *Drosophila* and the downstream core element (DCE) is found in vertebrates (Lenhard *et al.*, 2012). Notably, most of the mentioned core promoter elements are present only in higher eukaryotes. The well-annotated and well-studied TATA box element however is present in all eukaryotes reaching from yeast to human. This element is located -25 to -30 bp upstream to TSSs for metazoan, -40 to -120 bp for *S. cerevisiae* and -25 to -37 bp for *S. pombe* (Struhl 1989; Smale and Kadonaga 2003; Li *et al.*, 2015). TATA box elements are present in around 10-20% of potential promoters in *S. cerevisiae* (Rhee and Pugh 2012) and up to 43% of potential promoters in *Drosophila* (Kutach and Kadonaga 2000). They contain an

AT-rich consensus sequence and are mainly bound by TBP, Tbp1 in *S. pombe*. TATA-like elements have mismatches in the consensus sequence of the TATA box elements and they are assigned to most genes, especially in *S. cerevisiae* (Basehoar *et al.*, 2004; Rhee and Pugh 2012). In general, the core promoter elements comprise a rather degenerate DNA consensus sequence and it seems that there is no universal core promoter element, which is present in all promoters. It is still necessary to better define what is sufficient to build a core promoter. Not all core promoter elements occur simultaneously and hence different versions exist for the core promoter structure. They vary from species to species and are not readily exchangeable.

### 1.4.2 Chromatin structure at promoters

Besides specific sequence features, also specific chromatin structures are found at promoter regions which contribute to transcription regulation. These very well-defined chromatin structures of promoters are grouped into non-stereotypical (closed promoter) and stereotypical (open promoter, NDR-array pattern) nucleosome patterns at promoters (Figure 1.7) (Tirosch and Barkai 2008).

Interestingly, chromatin structures at inducible promoters, which display a non-stereotypical nucleosome pattern, were early in the focus of studies. This was due the fact, that the interplay of chromatin and transcription regulation at these promoters is well tractable after induction of the gene expression. In *S. cerevisiae*, these inducible genes are referred to as stress or environmentally regulated genes (Cairns 2009; Hughes and Rando 2014). A very important and well-studied example is the *PHO* regulon in *S. cerevisiae*. Lack of phosphate induces the transcriptional activation of genes such as *PHO5*, *PHO8* and *PHO84* (Almer *et al.*, 1986; Korber and Barbaric 2014). The *PHO5* promoter region is occupied by five translationally well-positioned nucleosomes in its repressed state such that important transcription factor binding sites are occluded: The -1 nucleosome occupies the TATA box and TSS and the -2 nucleosome occupies the UASp2 site (Figure 1.7 A). The UASp2 site is the upstream activating sequence and can be bound by the transcription factor Pho4. Under phosphate-limited conditions, Pho4 binds to its target promoter via the UASp2 site and allows recruitment of additional chromatin factors that are needed to remove the nucleosomes and facilitate the binding of other factors to the sites that leads ultimately to transcriptional activation. Chromatin remodelers, histone chaperones and histone modifying factors participate in this transition process (Korber and Barbaric 2014). Other cases, where such a dynamic chromatin structure transition is observed, are *CUP1*, *GAL1-10*, *RNR3* or heat shock genes (Shen *et al.*, 2001; Sharma *et al.*, 2003; Zhao *et al.*, 2005; Floer *et al.*, 2010). Besides this switch between transcriptional repression and activation, additional features of such promoters are the enrichment for TATA box binding sites and a high nucleosome turnover (Basehoar *et al.*, 2004; Dion *et al.*, 2007).



**Figure 1.7 Two distinct chromatin structures at promoter regions.** **A** The non-stereotypical nucleosome pattern at promoters features nucleosome-occluded regions. The removal of nucleosomes leads to transcriptional induction of genes. Mostly, promoters with the non-stereotypical nucleosome pattern harbor a TATA box element. **B** The stereotypical nucleosome pattern at promoters features an NDR and well-positioned nucleosomes up-/downstream of the NDR. Mostly, promoters with the stereotypical nucleosome pattern harbor a TATA-like element.

The stereotypical NDR-array pattern is conserved in eukaryotes, from yeast to human (Schones *et al.*, 2008; Tsankov *et al.*, 2011). Basic features such as the NDR, the well-positioned +1 and -1 nucleosome are similar (Figure 1.7 B); however variations of these features can be found between and within species. These features are NDR width, +1 nucleosome position relative to TSS and the spacing of nucleosome array. The promoters with stereotypical nucleosome pattern are mostly located at constitutively expressed genes and contain transcription factor binding sites and TATA-like elements in the NDR region (Basehoar *et al.*, 2004; Lee *et al.*, 2007; Rhee and Pugh 2012).

In the context of sharp and broad promoters and their chromatin structure in vertebrates, the sharp promoters are described to be occluded by nucleosomes whereas the broad promoters are excluded by nucleosomes, i.e. harbor a NDR (Sandelin *et al.*, 2007; Forrest *et al.*, 2014). The TSSs in *S. cerevisiae* and *S. pombe* are located within the +1 nucleosome. The distance between the TSS and the border of the +1 nucleosome varies by a few base pairs between *S. cerevisiae* and *S. pombe* (Tsankov *et al.*, 2010; Tsankov *et al.*, 2011; Soriano *et al.*, 2013). Interestingly, the TSS is located in the promoter NDR upstream of the +1 nucleosome in higher eukaryotes (Schones *et al.*, 2008). When the TSS position changes during the developmental transition of the zebrafish, the nucleosomes are organized accordingly to their positions relative to the TSSs before the transcription initiates at the newly selected TSSs (Haberle *et al.*, 2014). This argues that nucleosome positioning is prior and not consequence of transcription initiation.

### 1.4.3 Chromatin factors and transcription elongation

The nucleosomes are major obstacles for the transcription machinery (Kornberg and Lorch 1999). Both position and composition of nucleosomes (PTMs or histone variants) must be highly regulated during transcription and chromatin factors play a major role here.

For example, the histone variant H2A.Z is enriched at practically all +1 nucleosome positions, and especially in yeasts at all actively transcribed genes (Albert *et al.*, 2007; Buchanan *et al.*, 2009). In *Drosophila*, the H2A.Z (named H2A.V in *Drosophila*) containing nucleosomes occur downstream of the NDR, whereas in humans the H2A.Z containing nucleosomes appear in both directions, up- and downstream of the NDR (Mavrich *et al.*,

2008; Schones *et al.*, 2008). In addition to histone variants, PTMs of histones correlate with transcription (Smolle and Workman 2013). PTMs such as trimethylation of H3K4 and acetylation of H3K56 are associated with active promoters (Sobel *et al.*, 1995; Pokholok *et al.*, 2005).

Further major players in the regulation of transcription are the histone chaperones. In yeasts, the essential histone chaperones are Spt6 and FACT, and both factors are highly conserved from yeast to humans. The Spt6 chaperone interacts mainly with H3 and assembles histones onto DNA, especially during transcription elongation (Bortvin and Winston 1996; Ivanovska *et al.*, 2011). The Spt6 binding sites correlate well with the binding site of RNA PolII and Spt6 directly interacts with the RNA PolII. The inactivation of Spt6 in yeasts leads to severe loss of the stereotypical nucleosome pattern, as described for *S. cerevisiae* and *S. pombe* (Kaplan *et al.*, 2003; DeGennaro *et al.*, 2013). This pattern loss can be explained by the missing nucleosome reassembly after RNA PolII passage. Additionally, H3K4me3 and H3K36me3 levels are reduced over transcribed regions in *spt6* mutants of *S. pombe* (DeGennaro *et al.*, 2013). These two histone modifications are hallmarks of active promoters and gene transcription, respectively. The histone chaperone FACT has diverse functions linked to chromatin structure establishment, also particularly during transcription elongation. FACT interacts mainly with H2A/H2B dimers, disassembling the nucleosomes in front of RNA PolII and assembling the nucleosomes after RNA PolII passage (Belotserkovskaya *et al.*, 2003). The interaction of FACT with the chromatin remodeler Chd1 implicates an involvement of Chd1 in transcriptional elongation (Krogan *et al.*, 2002).

Other major players of transcription regulation by changing chromatin structure are the chromatin remodelers. Chd1 co-localizes with RNA PolII and can be recruited to H3K36me3 (Simic *et al.*, 2003; Park *et al.*, 2014). In this context, Chd1 probably removes nucleosomes in the wake of RNA PolII passage, and a similar function has been seen for the chromatin remodeler Isw1b (Lee *et al.*, 2012; Smolle *et al.*, 2012).

Taken together, on the one hand nucleosomes must be repositioned during transcription to allow for passage of RNA PolII but on the other hand the NDR-array pattern must be properly restored indicating a close interplay of chromatin and transcription. This is not only true at promoter regions, where transcription starts, but also for gene bodies where transcription elongation takes place. Chromatin factors are critically involved in all these steps. The maintenance of the chromatin structure during transcription is important to maintain genome integrity. Disturbed chromatin structure leads to cryptic transcription (chapter 1.4.4). The increased transcription events might cause higher collision rate between RNA PolII and replication fork, the replication fork collapses and this might lead to DNA double-strand breaks. Chromosome strand breaks and rearrangements impair genome stability and genome integrity (Svejstrup 2010; Papamichos-Chronakis and Peterson 2013; Gaillard and Aguilera 2016).

#### 1.4.4 Cryptic transcription

The genome is vastly transcribed; this process is known as pervasive transcription (Birney *et al.*, 2007). However, not all transcripts encode proteins. Additional non-coding RNAs can be grouped into functional not translated RNAs, like tRNAs or rRNAs, and RNAs of unknown function. Many of them are “cryptic” as they are not observed in wild type cells due to their rapid degradation. The cryptic transcripts are subdivided into cryptic unstable transcripts (CUTs), and Xrn1-sensitive transcripts (XUTs) (Smolle and Workman 2013). These groups are not mutually exclusive as there is a certain overlap between these groups and they might not be complete (Wyers *et al.*, 2005; Neil *et al.*, 2009; Xu *et al.*, 2009). CUTs and XUTs can be examined and hence annotated in cells, which are defective in RNA degradation pathways. CUTs are identified in a *rrp6Δ* mutant and XUTs in a *xrn1Δ* mutant. Rrp6, an exonuclease subunit of the nuclear exosome complex, is involved in the nuclear RNA degradation, whereas the exonuclease Xrn1 is involved in cytoplasmic RNA degradation. The cryptic transcripts share similar structural aspects with regular mRNAs such as the 5′-cap structure as well as the polyA tail (Carninci 2009). Most of the cryptic transcripts are not well-characterized in terms of their functions and might be, with few exceptions, just non-functional RNAs.

Several *in vivo* studies showed that disturbed chromatin structure correlates with additional transcriptional start events, these transcripts are also referred as cryptic transcripts. The difference to the previously mentioned cryptic transcripts is that they arise in chromatin factor mutants. Examples for chromatin factors, which contribute to proper chromatin structure and hence prevent cryptic transcription, are histone chaperones, chromatin remodelers, etc. Cryptic transcription in chromatin factor mutants was observed for the first time in *S. cerevisiae* if genes encoding for the histone chaperones Spt6 or Spt16, a subunit of FACT, were deleted (Bortvin and Winston 1996; Kaplan *et al.*, 2003). As these histone chaperones are known to play a role in nucleosome reassembly during transcription elongation (chapter 1.4.3), it is plausible that cryptic transcription arises if the chromatin structure is not properly restored in the wake of RNA PolII passage.

The chromatin remodeler mutants, *isw1Δ isw2Δ chd1Δ* in *S. cerevisiae* or *hrp1Δ hrp3Δ* in *S. pombe*, are characterized by a disrupted nucleosome organization over the gene coding regions (Gkikopoulos *et al.*, 2011; Hennig *et al.*, 2012; Pointner *et al.*, 2012). Additionally, these mutants suffer from increased cryptic antisense transcription (Gkikopoulos *et al.*, 2011; Pointner *et al.*, 2012). Moreover, the chromatin remodeler mutant *isw1Δ isw2Δ chd1Δ* in *S. cerevisiae* shows a higher histone turnover over gene coding regions. In contrast, wild type cells usually have a high histone turnover at promoter regions and a low nucleosome turnover over gene coding regions. Hence, it is conceivable that the increased histone turnover contributes to increased accessibility of cryptic promoters in these chromatin remodeler mutants. Finally, acetylation of histones seems to play a role in cryptic transcription, too. Cryptic starts of transcripts are blocked if the incorporation of acetylated histones is prevented, in particular for actively transcribed

genes (Smolle and Workman 2013). H3K36 methylation normally prevents the incorporation of newly acetylated histones over transcribed regions. Chromatin over gene bodies becomes predominantly hyperacetylated if components of the histone acetylation and methylation pathways such as Set2/Rpd3S or Set2/Set3C are mutated. As a consequence, the chromatin structure is less compact which favors intragenic transcription initiation (Smolle and Workman 2013).

Functions and features are described for some cryptic transcripts in chromatin factor mutants. For example, some cryptic transcripts present in the *spt6* mutant of *S. cerevisiae* can potentially be translated into proteins (Cheung *et al.*, 2008). Some cryptic promoters depend on a TATA box element, for example the cryptic promoter within the *S. cerevisiae* *FLO8* gene. Other cryptic promoters do not harbor a TATA box element such as the cryptic promoter within the *STE11* gene. Both cryptic promoters were identified in *S. cerevisiae* (Kaplan *et al.*, 2003; Pattenden *et al.*, 2010). The cryptic promoters seem to harbor NDRs, but further functions and features of cryptic promoters remain ill-defined.

Taken together, the maintenance of the chromatin structure through chromatin factors such as histone chaperones and chromatin remodelers is important to prevent additional cryptic transcripts. The functions and features of such transcripts are ill-defined and need further investigations.

## 1.5 Aims of this thesis

- (1) Nucleosomes are organized in a stereotypical manner at promoters (chapter 1.4.2). The promoter comprises the TSS. A proper annotation of the TSSs positions is required to characterize a promoter region. One main aim of this thesis was to annotate TSSs by CAGE-seq for the model organism *S. pombe*.
- (2) Furthermore, disrupted nucleosome patterns correlate with cryptic transcripts (chapter 1.4.4) (Gkikopoulos *et al.*, 2011; Pointner *et al.*, 2012; Shim *et al.*, 2012; DeGennaro *et al.*, 2013). These cryptic promoter regions are less characterized compared to their counterparts, the canonical promoters. So the TSSs of cryptic transcripts in chromatin mutants, such as *spt6-1 ts* and *hrp1Δ hrp3Δ*, were to be determined by CAGE-seq. We sought for further features of transcription initiation at these sites, using bioinformatical analyses. Furthermore, the chromatin structure was determined by MNase-seq to analyze if the nucleosome-free regions are the reason why cryptic transcripts arise in the chromatin mutants.
- (3) The third main aim was to examine the nucleosome positioning mechanism in *S. pombe*. The *trans*-factors, such as chromatin remodelers or GRFs, play an important role in the nucleosomes positioning mechanism such as nucleosome array and NDR formation (chapter 1.3.5). The CHD1 remodelers in *S. pombe*, Hrp1 and Hrp3, contribute to the maintenance of aligned nucleosome arrays over genes (Pointner *et al.*, 2012). An equivalent mechanism was observed for the remodelers Isw1, Isw2 and Chd1 in *S. cerevisiae*. The orthologous Chd1 in *S. cerevisiae* and Hrp3 in *S. pombe* exhibited the strongest contribution (Gkikopoulos *et al.*, 2011; Pointner *et al.*, 2012). We used an *in vivo* complementation approach to reveal what kind of function they have in NDR-array formation in *S. pombe*, and we investigated in particular the conserved or diverged functions of the domains of Chd1 and Hrp3 in *S. pombe*.
- (4) As only a combined deletion of chromatin remodelers led to a major disruption of nucleosome array organizations, it is complicated to distinguish the individual factor contributions *in vivo*. Additionally, some factors such as the GRFs are essential, which hampers *in vivo* studies. To overcome these problems, we used an *in vitro* reconstitution approach to dissect the individual contribution of chromatin factors to the NDR-array formation. Such an *in vitro* reconstitution approach was already successfully used for the model organism *S. cerevisiae* showing that chromatin remodelers and GRFs contribute individually to the NDR-array pattern (Zhang *et al.*, 2011; Krietenstein *et al.*, 2012; Krietenstein *et al.*, 2016). We intended to establish the *in vitro* reconstitution system for *S. pombe* and tested several candidates such as whole cell extract, CHD1 chromatin remodelers, Hrp1 and Hrp3, and the GRF Sap1. In the context of SGD chromatin assembly, we asked in addition if the assembly of nucleosomes during salt gradient dialysis is cooperative.





---

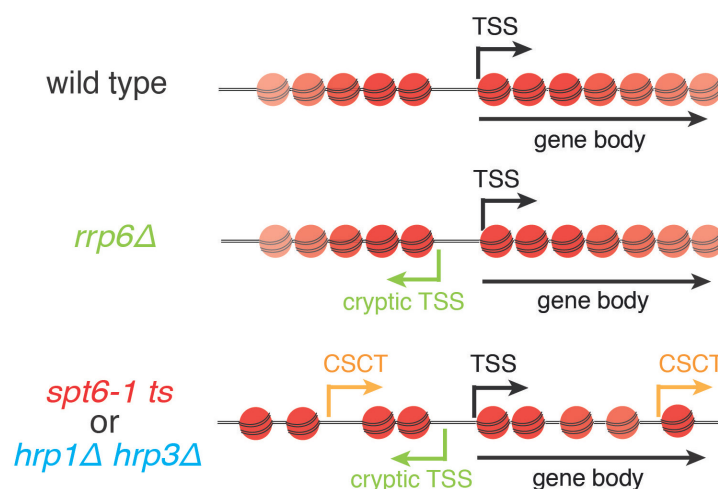
## 2 Results

## 2.1 Chromatin and sequence features of promoters in *S. pombe*

The promoter region represents the initiation region of transcription. Some promoter regions have defined sequence elements, which are arranged around the TSS, others have not. It is still poorly understood how promoters are defined. It is crucial to know, first, where the exact location of the TSSs is, and second, what characteristics the TSSs and their promoter regions harbor.

Different methods were used to annotate TSSs in *S. pombe* such as RNA-hyb-chip, RNA-seq or CAGE-seq (Dutrow *et al.*, 2008; Lantermann *et al.*, 2010; Rhind *et al.*, 2011; Li *et al.*, 2015; Eser *et al.*, 2016). A wild type TSS annotation that was widely used for many years in the *S. pombe* field was derived from RNA-hyb-chip and annotated manually (Dutrow *et al.*, 2008; Lantermann *et al.*, 2010). Recently, a wild type TSS annotation of higher resolution was reported using CAGE-seq (Li *et al.*, 2015). This technique has the advantage of capturing directly the 5'-cap structure, which represents the exact start site of the transcripts.

Therefore, also we used CAGE-seq to get the exact locations of TSSs in *S. pombe*. In addition to wild type *S. pombe* cells at two different growth conditions (full (YES) and minimal (EMM) medium), we also mapped TSSs for three mutants affecting either the exosome (*rrp6Δ*) or chromatin factors (*spt6-1 ts* and *hrp1Δ hrp3Δ*). The latter two chromatin factor mutants were known to generate additional transcripts compared to wild type (Hennig *et al.*, 2012; Pointner *et al.*, 2012; Shim *et al.*, 2012; DeGennaro *et al.*, 2013). We defined these transcripts as chromatin suppressed cryptic transcripts (CSCTs, Figure 2.1). This distinguishes these additional transcripts from those seen in the exosome mutant *rrp6Δ*, where transcripts are detected, which are transcribed in wild type cells, but not detected there due to fast RNA degradation by the exosome. As the additional transcripts detected in the *rrp6Δ* mutant are likely also produced in the wild type and as we are interested in the initiation of transcription and not in downstream processes, we used all transcripts of the *rrp6Δ* mutant as our reference.



**Figure 2.1 Schematic representation of the CSCTs definition:** CSCTs are defined as transcripts present only in the chromatin factor mutants, *hrp1Δ hrp3Δ* and *spt6-1 ts*. The transcripts detected in exosome mutant *rrp6Δ* are used as reference.

Here, we examined where the TSSs were located for two different conditions and three different mutants (Table 2.1). We specifically mapped the nucleosome organization at these TSSs (chapter 2.1.2.2 and 2.1.4.1). Additionally, we examined features such as expression levels of the regions, where the transcripts are located (chapter 2.1.4.2), DNA shape (chapter 2.1.4.3) and DNA composition (chapter 2.1.4.4).

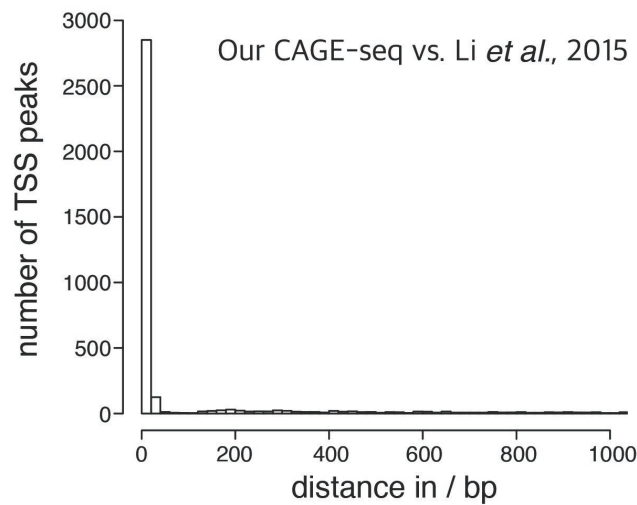
**Table 2.1 Strains and conditions used for CAGE-seq and MNase-seq.** (Replicate number given by “n”.)

Strain	Genotype	Source	Conditions	Data sets
wild type	<i>h- 972</i>	Ekwall group	YES, 32°C	CAGEscan-seq (n = 2) MNase-seq (n = 2)
			EMM, 32°C	CAGEscan-seq (n = 2) MNase-seq (n = 2)
<i>rrp6Δ</i>	<i>h- rrp6::ura4+ ura4-D18 leu1-32 ade6-m210</i>	Bähler group	YES, 32°C	nanoCAGE-seq (n = 2) MNase-seq (n = 3)
<i>spt6-1 ts</i>	<i>h- spt6-1::NatMX ura4-D18 leu1-32 ade6-m210</i>	Winston group	YES, 32°C	nanoCAGE-seq (n = 2) MNase-seq (n = 2)
			YES, 37°C	MNase-seq (n = 3)
<i>hrp1Δ hrp3Δ</i>	<i>h- hrp1::ura4+ hrp3::leu+ ura4-D18 leu1-32 ade6-m210</i>	Ekwall group	YES, 32°C	nanoCAGE-seq (n = 2) MNase-seq (n = 2)

### 2.1.1 Classification and quality control of TSSs annotated by CAGE-seq

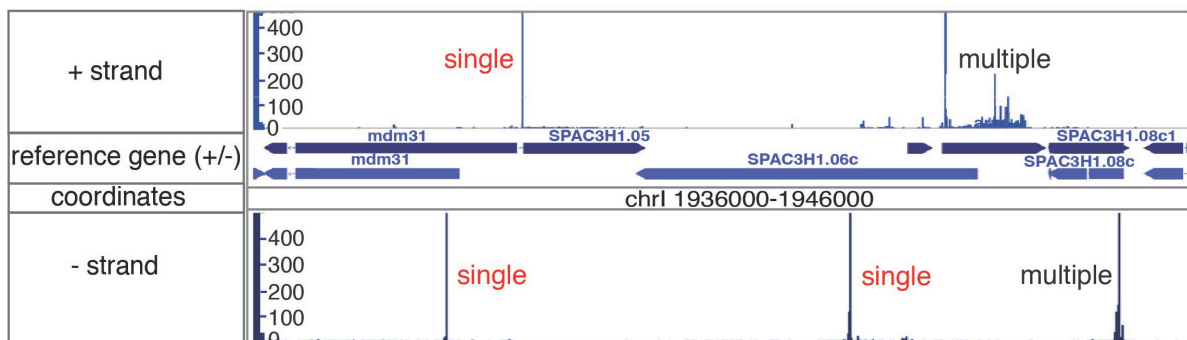
We compared the recently published CAGE-seq TSS data set (Li *et al.*, 2015) with our own CAGE-seq data set. We used the same bioinformatical pipeline to call the TSSs for all data sets. In total we could identify 7525 and 12623 TSSs in our data set for wild type cells grown in YES medium or for the *rrp6Δ* mutant, respectively. We identified 4819 TSSs for the data set by Li *et al.*, 2015, for wild type cells grown in YES medium. We identified more TSSs in our CAGE-seq data set compared to CAGE-seq data set by Li *et al.*, 2015, although the total read number in our data set was lower compared to the published data set (total read number: ca. 12.3 million (our CAGE-seq for wild type cells grown in YES medium) vs. ca. 16.6 million (Li *et al.*, 2015 for wild type cells grown in YES medium)). The lower number of annotated TSSs for the published compared to our data set might be due to lower signal-to-noise ratio in the published data set. In addition, we correlated both raw data sets with regard to TSS positions using the Jaccard method (Favorov *et al.*, 2012) and identified 1644 overlapping TSSs, overlapping within a 30 bp window, and a generally low correlation overlap (coefficient = 0.1815). As the direct correlation of raw data sets was difficult due to different noise levels, but this remains speculative, since there were no standardized methods to compare this kind of data, we chose another approach. Relative distance analysis (Favorov *et al.*, 2012) compares the pattern of signals, rather than direct overlap of signals in the data sets. This relative distance analysis revealed a good agreement of both data sets (Figure 2.2). Additionally, the calculation of the distance between TSSs peaks in both data sets revealed that most corresponding TSSs were located closely to each other (Figure 2.2). Taken together, our TSS analysis by CAGE-seq yielded

similar results as in the published data set. But already here we realized how difficult it is to compare this kind of data sets across different samples, platforms and labs.



**Figure 2.2 Comparison of our CAGE-seq data set with CAGE-seq from Li *et al.*, 2015 revealed a good overlap.** Relative distance analysis for our CAGE-seq data set compared to the CAGE-seq data by Li.*et al.*, 2015. One bin has a size of 30 bp.

Among the TSSs identified in our CAGE-seq data set, we classified three different promoter classes according to their TSS distributions (Figure 2.3). The first promoter class harbored a sharp TSS distribution (or a single TSS peak) within a 30 bp window. The second promoter class harbored a broader TSS peak distribution (or multiple TSS peaks) within a window from 30 to 100 bp, and the third class had multiple peaks distributed over a region larger than 100 bp. The majority of TSSs were characterized as sharp TSSs, 84.6% in wild type cells grown in YES, 70.6% in *rrp6Δ* mutant and 90.4% in Li *et al.*, 2015 (Table 2.2). For most analyses in the following only these sharply defined TSSs were used as only for these a high resolution genomic location can be annotated.



**Figure 2.3 Promoters with sharp TSS peak distribution are more frequent than promoters with broader TSS peak distribution.** Genome browser shot showing single and multiple TSS peaks.

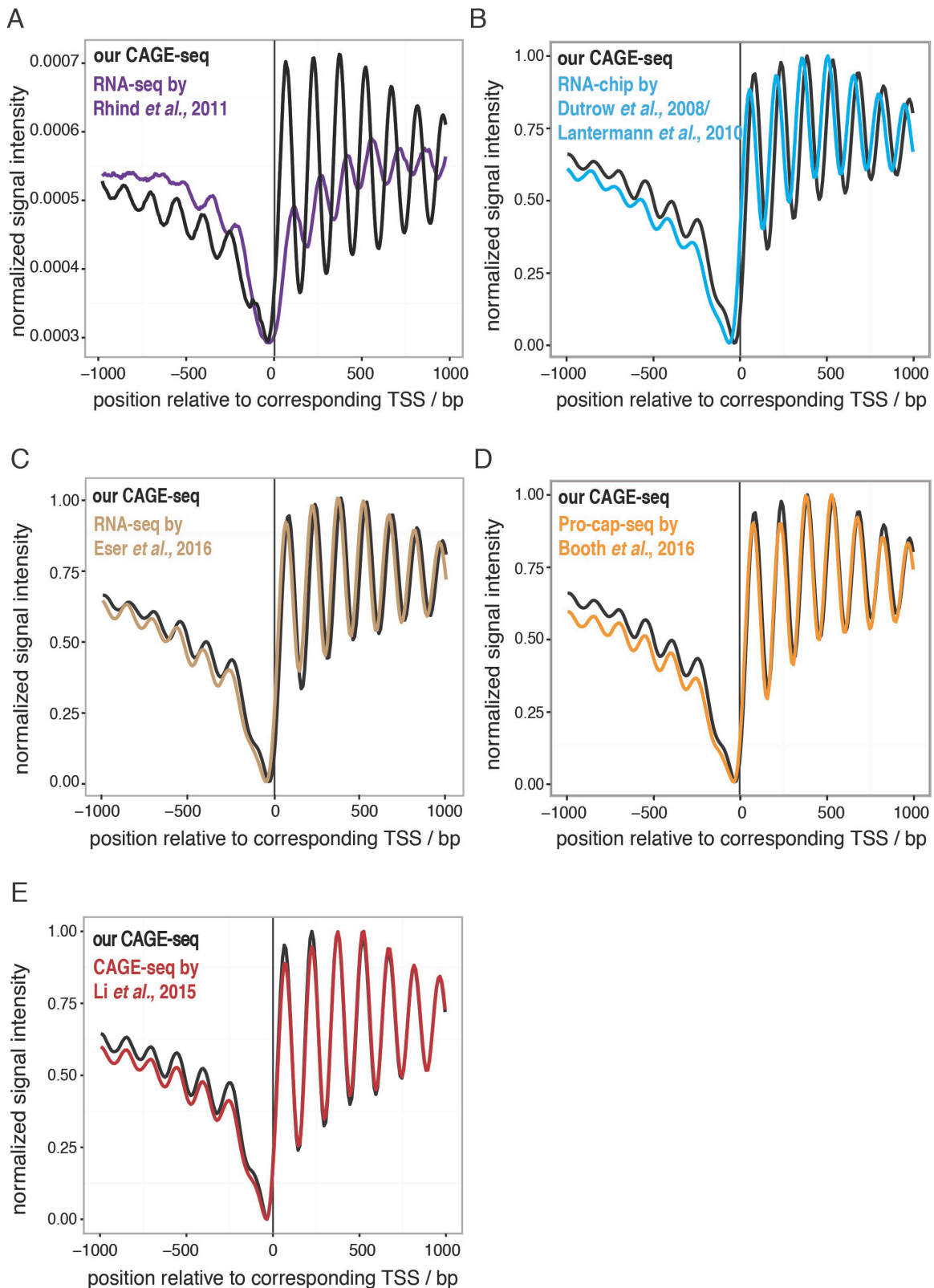
**Table 2.2 Three promoter classes and their frequency in different CAGE-seq data sets for *S. pombe***

Data set	Sharp TSS [%]	Multiple TSSs [%]	Multiple TSSs [%]	Total number
	≤ 30 bp	> 30 bp	> 100 bp	≤ 100 bp
wild type grown in YES medium	6364 [84,6%]	1161 [15,4%]	729 [9,7%]	7525
<i>rrp6Δ</i> grown in YES medium	8934 [70,6%]	3689 [29,2%]	2773 [22%]	12623
wild type grown in YES medium by Li <i>et al.</i> , 2015	4357 [90,4%]	462 [9,6%]		4741

### 2.1.2 Chromatin structure at the TSSs as a further quality criterion

We used our MNase-seq nucleosome data as a further quality criterion for the TSS annotations. We aligned always the same nucleosome data for the *S. pombe* wild type strain grown in YES medium to the TSSs according to the different annotations and compared the resulting peak-to-trough ratios (amplitude) and peak positions of the nucleosome patterns. We assumed that a more accurate TSS annotation would lead to higher amplitude regularity of the nucleosome patterns. For the peak positions relative to the TSSs we do not have an independent reference but assume that the positions of the more regular pattern are more true.

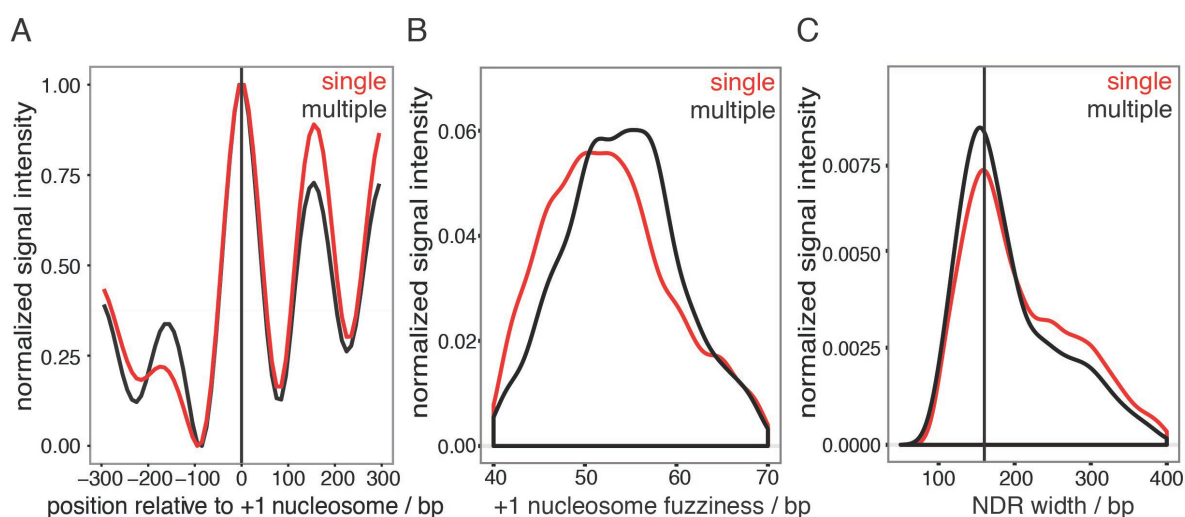
In this way, we compared the TSS annotations derived from approaches that capture whole RNA such as RNA-hyb-chip, RNA-seq, and from approaches that specifically capture the 5'-cap structure such as Pro-cap-seq and CAGE-seq (Figure 2.4). The amplitude and also the peak positions were strikingly different comparing the TSS annotation derived from RNA-seq (Rhind *et al.*, 2011) and from our CAGE-seq data (Figure 2.4 A). The TSS annotation by Rhind *et al.*, 2011 shifted the nucleosomes more downstream of the TSS so that the TSSs did not seem to be located within the +1 nucleosome, and the amplitude was dramatically reduced. Peak positions were also shifted, but upstream compared to our CAGE-seq TSS annotation, if nucleosome data were aligned to the TSSs annotated by Lantermann *et al.*, 2010 (Figure 2.4 B). In the case of the TSS annotations by Eser *et al.*, 2016, Booth *et al.*, 2016, and Li *et al.*, 2015 the peak positions overlapped very well with those according to our CAGE-seq annotation and showed almost no difference in the composite plot and the amplitudes were very similar (Figure 2.4 C, D and E). This argues that these data sets, which utilized directly or indirectly methods that directly capture the 5'-cap structure (Eser *et al.*, 2016 rely on data from Li *et al.*, 2015 for the annotation of their RNA-seq data), generate the more true TSS annotations. This also means that the TSS is, on average, located more upstream in the flank of the +1 nucleosome than described previously (Lantermann *et al.*, 2010).



**Figure 2.4 Alignment of the same MNase-seq nucleosome data to TSSs derived from different approaches revealed the more accurate TSS annotation.** A-E The same MNase-seq data of wild type cells grown in YES were aligned to TSSs derived from our CAGE-seq data or from RNA-seq data by Rhind *et al.*, 2011 (A), RNA-hyp-chip data by Dutrow *et al.*, 2008/Lantermann *et al.*, 2010 (B), RNA-seq data by Eser *et al.*, 2016, (C), Pro-cap-seq data by Booth *et al.*, 2016, (D) and CAGE-seq data by Li *et al.*, 2015 (E) (Dutrow *et al.*, 2008; Lantermann *et al.*, 2010; Rhind *et al.*, 2011; Li *et al.*, 2015; Booth *et al.*, 2016; Eser *et al.*, 2016).

### 2.1.2.1 Chromatin structure at promoters with sharp or broader TSS peak distribution

For the wild type grown in YES medium, we looked at the nucleosome organization of the promoter classes with sharp or broader TSS distribution. The canonical distance between TSSs and +1 nucleosomes may suggest a causal relationship between both features in one way or the other. If the position of the +1 nucleosome were a direct result of the TSS position, then promoters with multiple TSSs should show fuzzier +1 nucleosome positions and possibly wider NDRs compared to promoters with sharp TSS distribution. First, we called the +1 nucleosome position as the first MNase-seq peak downstream of the TSS or TSS clusters for those with sharp and broader distributions, respectively, and then aligned the MNase-seq nucleosome data to these +1 nucleosome positions. There was no clear difference in the overall nucleosome organizations, especially no broader (= more fuzzy) +1 nucleosome peak for promoters with multiple TSSs (Figure 2.5 A). Additionally, we calculated “fuzziness” as defined through the DANPOS algorithm for the +1 nucleosomes as well as NDR width for both promoter classes, but no major difference was observable (Figure 2.5 B and C) (Chen *et al.*, 2012). This argues against a direct causal role of TSS positions in +1 nucleosome positioning.

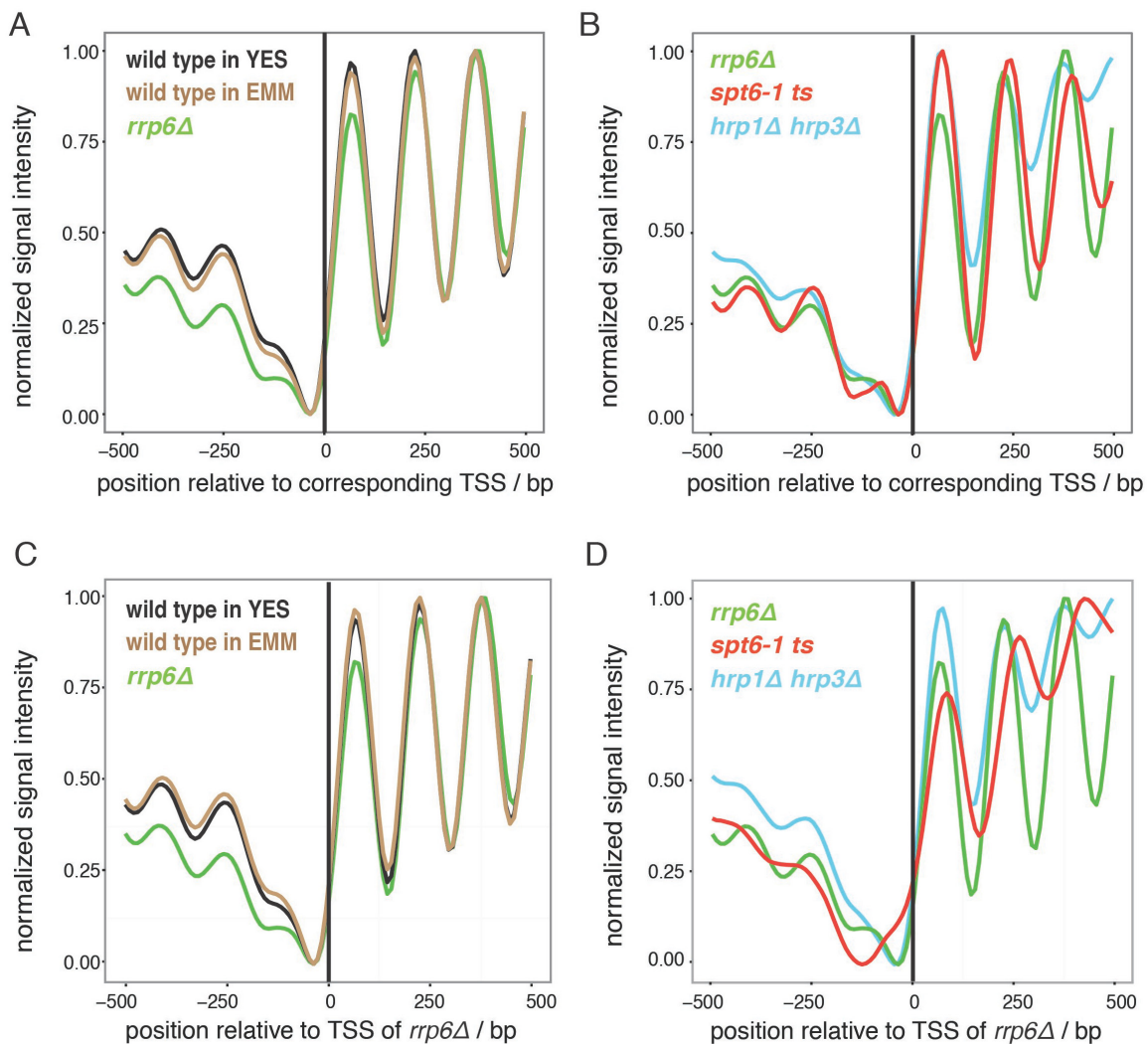


**Figure 2.5 Chromatin organization at promoter regions with sharp or broader TSS peak distribution showed no major difference.** A Nucleosome organization at single and multiple TSSs aligned to the +1 nucleosome positions. B-C +1 nucleosome fuzziness (B) or NDR width (C) for promoters with sharp or broader TSS distributions (at single or multiple TSSs, respectively).

### 2.1.2.2 Chromatin structure at the TSSs for different conditions and mutants

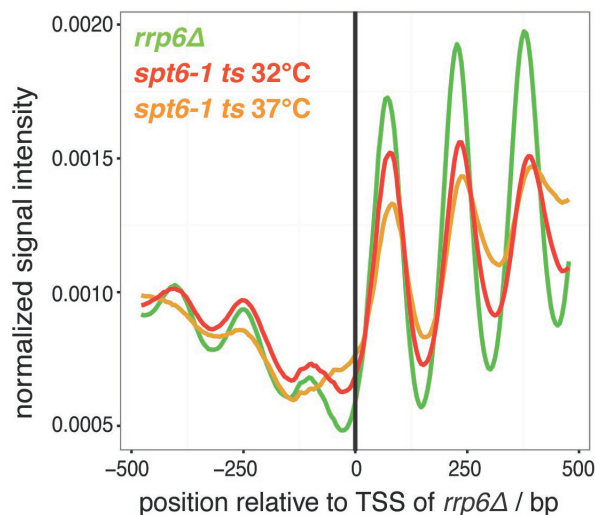
We performed the combination of CAGE-seq and MNase-seq of matching yeast cultures also for additional conditions: wild type grown in minimal medium EMM, and three mutants, *rrp6Δ*, *spt6-1 ts* and *hrp1Δ hrp3Δ* (Table 2.1). In previous publications of the field, MNase-seq data for mutant strains are always aligned at TSSs annotated for the wild type strain, simply because the TSS annotation for the mutant strains are not available. For the first time, we obtained the annotation of the TSSs for all mutants which enabled to align the nucleosome data at the true corresponding TSSs. We aligned the nucleosome data for

all conditions and mutants to their corresponding TSSs or to the TSSs of the *rrp6Δ* mutant, which we defined above as our reference. In the case of wild type cells grown in YES or EMM medium, the nucleosome patterns looked quite similar with regard to the amplitude if aligned to the corresponding versus the *rrp6Δ* TSSs (Figure 2.6 A versus C). However, a clear difference between both alignment versions was observed for the *spt6-1 ts* and the *hrp1Δ hrp3Δ* mutants (Figure 2.6 B versus D). The disturbed nucleosome organization downstream of the +1 nucleosome (= lower amplitude), which is consistent with published data sets (Pointner *et al.*, 2012; DeGennaro *et al.*, 2013), was observable for both chromatin factor mutants only if the *rrp6Δ* TSSs were used for alignment (Figure 2.6 D), while the chromatin pattern for the *spt6-1 ts* mutant looked almost like the reference *rrp6Δ* pattern – besides slightly wider spacing – if the corresponding TSSs were used. The pattern of the *hrp1Δ hrp3Δ* mutant looked disturbed in any case including a slightly tighter spacing (Figure 2.6 B and D). This argues that previously published effects of mutations on nucleosome patterns may have been misjudged due to the use of inappropriate TSS alignment points.



**Figure 2.6 Alignment of the same MNase-seq data at TSSs annotated for the *rrp6Δ* mutant (our reference) or for the corresponding mutant affects the nucleosome patterns. A-D Composite plots of MNase-seq data for indicated strains and conditions aligned to corresponding (A and B), or to *rrp6Δ* TSS annotation (B and C).**



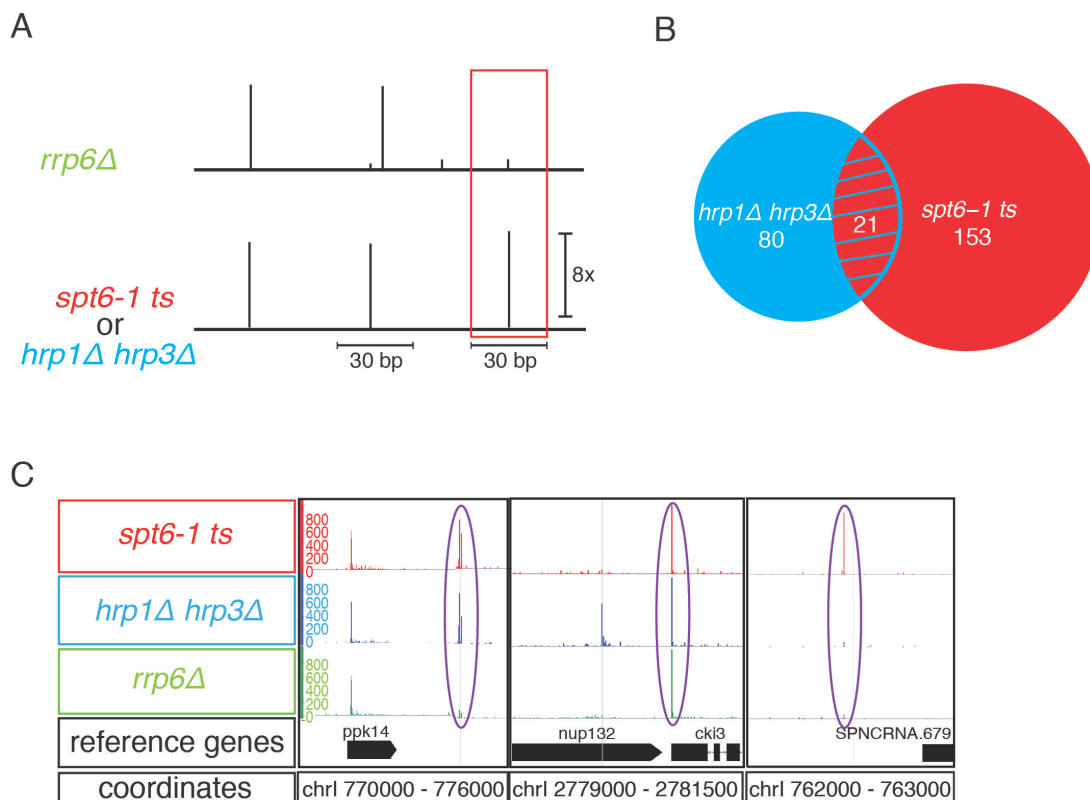


**Figure 2.7 Nucleosome pattern was less disturbed for *spt6-1 ts* grown at 32°C compared to 37°C.** Composite plot of MNase-seq data for indicated strains and conditions aligned to *rrp6Δ* TSS annotation.

Worth mentioning, for our CAGE-seq analysis we used less restrictive growth conditions for the *spt6-1 ts* mutant (32°C) to call the most prominent CSCT-TSSs. Previous work by DeGennaro *et al.*, 2013 used 37°C to show the disturbed genic arrays in this mutant (DeGennaro *et al.*, 2013). Indeed, our comparison of nucleosome data of *spt6-1 ts* grown at 32°C vs. 37°C revealed a less disturbed nucleosome pattern for *spt6-1 ts* grown at 32°C (Figure 2.7; as we did not have CAGE-seq data for this strain grown at 37°C we could only use the TSS annotation of *rrp6Δ* as common reference). We conclude that the CSCT-TSSs detected by CAGE-seq in the *spt6-1 ts* mutant at 32°C (see below chapter 2.1.3) appeared already even though an impairment of the nucleosome pattern was only slightly detectable by MNase-seq under these conditions. This argues that we chose conditions where only the most prominent CSCT-TSSs came up in this mutant.




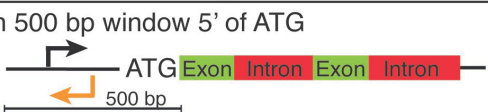

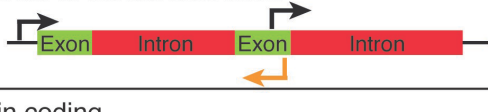
### 2.1.3 Definition and annotation of newly characterized CSCTs in chromatin factor mutants and additional transcripts in wild type cells grown in minimal medium (EMM)

To characterize features of a promoter region, we focused on a specific subset of TSSs and we defined them as follows. The exosome mutant *rrp6Δ* was used as our reference, because we were able to capture not only the canonical transcripts but also those, which are degraded in wild type cells by the fast exosome degradation system, but are probably nonetheless true wild type transcripts. We defined those transcripts that came up only in the chromatin factor mutants, *spt6-1 ts* or *hrp1Δ hrp3Δ*, but not in *rrp6Δ* as CSCTs. We decided to use the chromatin factor mutants, because it was described that their disrupted nucleosome organization led to increased cryptic transcription (Pointner *et al.*, 2012; DeGennaro *et al.*, 2013). The threshold for calling a CSCT-TSS was set very stringently. A CSCT-TSS peak had to be at least 8-fold higher compared to any TSS peak within a 30 bp window (= 15 bp up- and downstream) in the *rrp6Δ* mutant (Figure 2.8 A and C). By the analogous criteria, we annotated another subset of transcripts that came up in minimal EMM versus full YES media for wild type *S. pombe* cells.



**Figure 2.8** Annotation of CSCTs showed only a small overlap of CSCTs between the chromatin factor mutants *hrp1Δ hrp3Δ* and *spt6-1 ts*. **A** Schematic representation of the criteria for calling a CSCT. **B** Venn diagram of CSCTs in the *hrp1Δ hrp3Δ* and *spt6-1 ts* mutants. **C** Genome browser shot showing examples for localization of transcripts that are either present in all three mutants, *rrp6Δ*, *hrp1Δ hrp3Δ* and *spt6-1 ts* (middle), or only in *hrp1Δ hrp3Δ* and *spt6-1 ts* (left) or only in *spt6-1 ts* (right).

We identified 101 CSCTs in the *hrp1Δ hrp3Δ* mutant, 174 CSCTs in the *spt6-1 ts* mutant (Figure 2.8 B) and 62 EMM-specific transcripts (Figure 2.9). Interestingly, there was only a small overlap of 21 between the CSCTs in both chromatin factor mutants. The larger fraction of not shared CSCTs may indicate two classes of CSCTs, for example, due to different ways how chromatin is disturbed or how transcription is initiated in each mutant. We examined the localization of the CSCTs in both chromatin factor mutants and in the EMM-specific TSSs in wild type cells grown in EMM. The most CSCT-TSSs and EMM-specific TSSs were located in exons of protein coding genes, especially in antisense orientation (Figure 2.9). Given the *S. pombe* genome size of 12,841,905 bp and counting each strand separately as a potential TSS, there are 25,683,810 potential TSSs. Out of these, 12,587,270 (= 49%) are within exons and 447,360 (= 1.7%) are within introns. The actual numbers of CSCT-TSSs in exons and introns, respectively, corresponds to 63%/1.9% for *hrp1Δ hrp3Δ*, 60%/2.2% for *spt6-1 ts*, and 79%/4.8% for the EMM conditions. So CSCTs came up in exons and introns with higher probability than expected by random distribution ( $p$ -value < 0.0001, chi-square analysis with expected and observed values and two degrees of freedom). Interestingly, this was not mainly due to higher transcription in the immediate neighborhood as about half (*hrp1Δ hrp3Δ*) or even more than half (*spt6-1 ts*) of the exon-based CSCTs were antisense to not much expressed exons.

Localization of CSCT-TSSs and EMM-specific TSSs	<i>hrp1Δ hrp3Δ</i>	<i>spt6-1 ts</i>	wild type in EMM
Total Number	101	174	62
Exon 	64	105	49
Intron 	2	4	3
Antisense to exon 	60	82	25
Within 500 bp window 5' of ATG 	13	38	25
Antisense to non-transcribed exon 	31	51	5
Antisense to transcribed exon 	29	31	20
Protein coding	50	90	45
ncRNA	14	15	4

**Figure 2.9** The majority of the transcripts are located in the antisense exon region. Genomic localization of CSCTs in chromatin factor mutants *hrp1Δ hrp3Δ* and *spt6-1 ts* and additional transcripts in wild type cells grown in EMM.

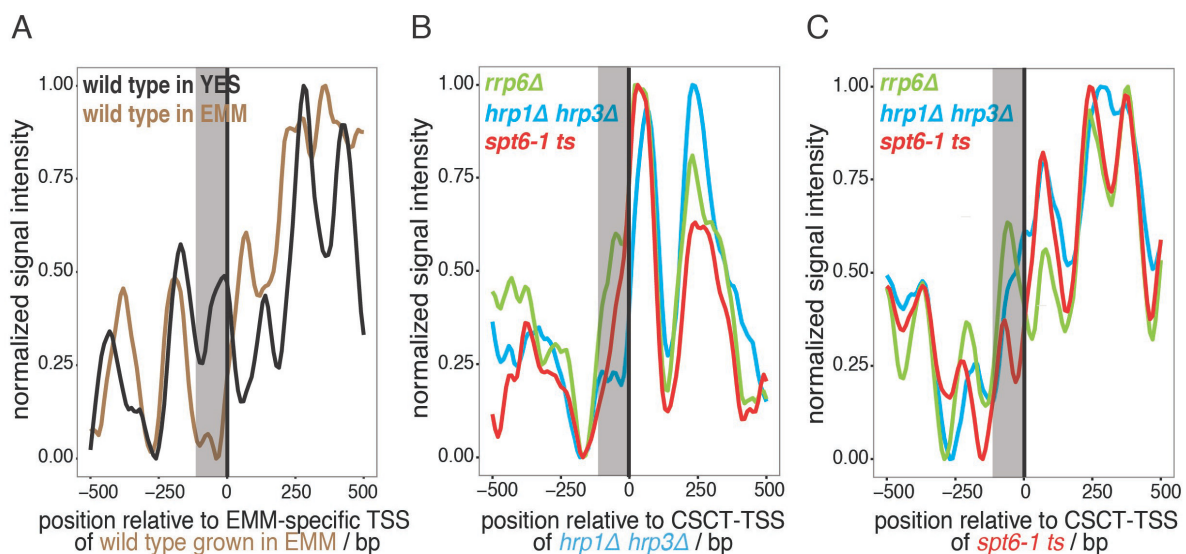
## 2.1.4 Features of CSCTs in the chromatin factor mutants

### 2.1.4.1 CSCT-TSSs localize to the very 5' flank of a corresponding +1 nucleosome

We asked how the nucleosome organization looked like at the CSCT-TSSs and the EMM-specific TSSs, specifically, if the appearance of these novel transcripts correlated with the appearance of new NDRs. We aligned the MNase-seq nucleosome data of wild type cells, grown in YES medium or EMM, always to the EMM-specific TSSs. Only the data derived from growth in EMM showed an NDR upstream of the TSS (grey area in Figure 2.10 A) and a corresponding +1 nucleosome at the canonical position relative to the TSS, i.e., the TSS was at the very 5' flank of the +1 nucleosome (compare with Figure 2.6). In contrast, the grey area was occupied by a peak in wild type cells grown in YES medium.

For the CSCT-TSSs in the *hrp1Δ hrp3Δ* and *spt6-1 ts* mutants we made a similar observation. A +1 nucleosome at the canonical position flanked the CSCT-TSSs only in the corresponding mutants (Figure 2.10 B and C). An NDR was not always very pronounced, but the occupancy levels upstream of the CSCT-TSSs were always lowest in the strain that actually expressed the respective CSCTs.

So it became clear that the nucleosome organization changed if the condition- or mutant-specific TSSs came up. It seemed that the canonical position of a corresponding +1 nucleosome was the more important chromatin feature than a pronounced NDR. Strictly speaking, we cannot distinguish if these chromatin features are cause or consequence of the usage of these novel TSSs. But as the experimental perturbation was the deletion/ablation of a chromatin factor leading to chromatin changes, we assume that the use of the novel TSSs was the consequence rather than the cause for these observed chromatin changes.

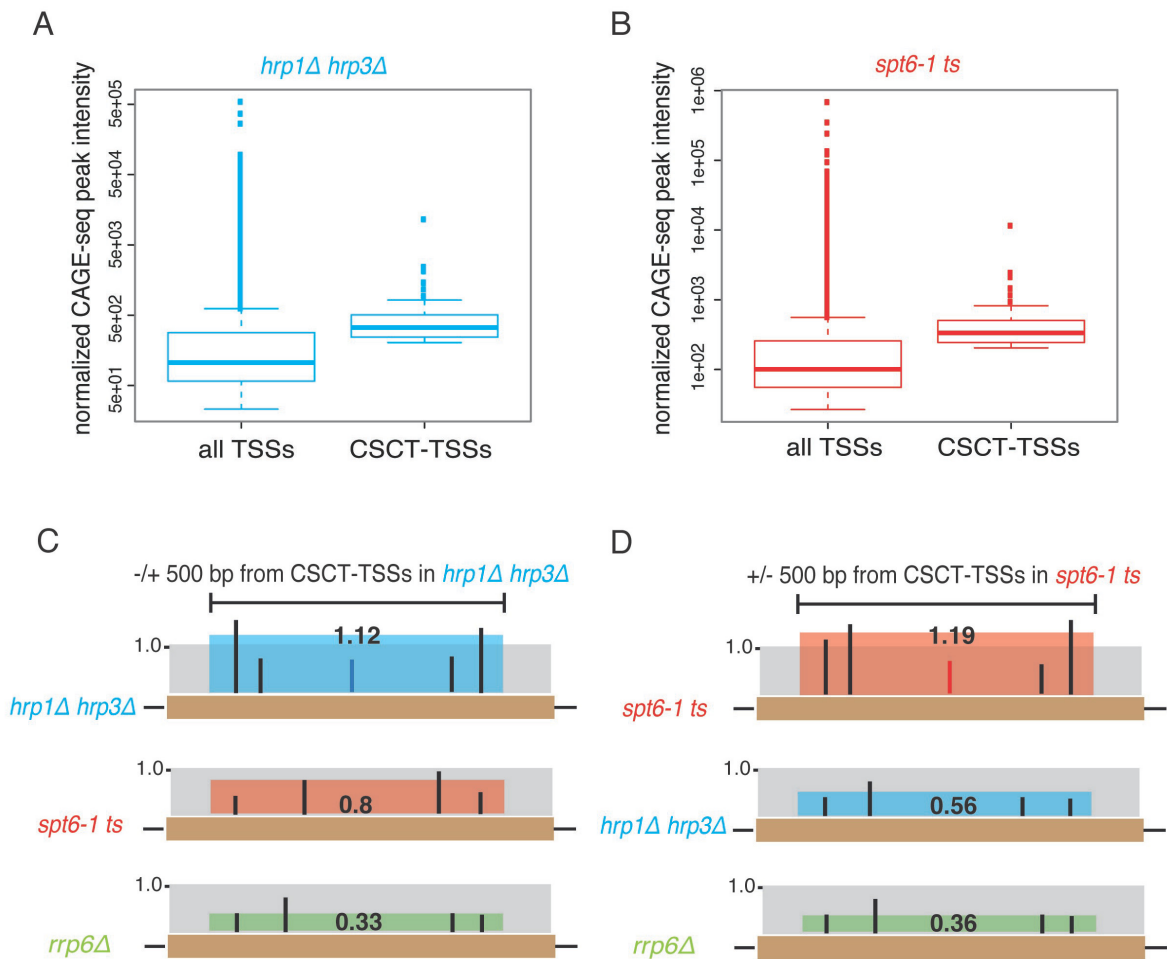


**Figure 2.10 Nucleosome organization at EMM-specific TSSs and CSCT-TSSs revealed that these TSSs are at the 5' flank of a corresponding +1 nucleosome. A** Composite plots of MNase-seq data of wild type cells grown in YES medium or EMM aligned to EMM-specific TSSs. **B-C** Composite plots of MNase-seq data of *rrp6Δ*, *hrp1Δ hrp3Δ* and *spt6-1 ts* strains aligned to CSCT-TSSs from *hrp1Δ hrp3Δ* (**B**) or *spt6-1 ts* (**C**).

#### 2.1.4.2 CSCT-TSSs are located in regions with more than average expression levels

To further characterize the CSCT-TSSs, we first determined their expression levels in comparison to all TSSs. CAGE signal intensity is a very good measure for expression level (Kawaji *et al.*, 2014). The CSCTs' expression levels were on average higher than the genomic average (Figure 2.11 A and B). This was somewhat expected because the CSCTs were defined by an 8-fold increased expression level relative to surrounding transcripts in the *rrp6Δ* reference strain. Nonetheless, it was not a priori clear if this criterion would also lead to higher expression levels relative to the whole-genome average. So this analysis confirms that the selected CSCTs corresponded to strongly expressed and not just spurious transcripts.

Second, we asked if only the CSCTs were highly expressed or also their genomic neighborhood in the same strain. We analyzed if the average transcription levels in the regions 500 bp up- and downstream of the CSCTs were changed compared to the genome-wide average in the mutants where the CSCTs came up. The CSCTs were excluded from the calculation, i.e., did not contribute with their relatively high expression level to the calculated average expression of their neighborhood. Nonetheless, this neighboring region was always more transcribed than the genome-wide average in the respective chromatin factor mutant where the CSCT was detected, but not for the same regions in the other strains where no CSCTs were expressed (Figure 2.11 C and D). There, the expression levels of the corresponding regions were even lower than average, always lowest in the *rrp6Δ* reference strain. So it appeared that CSCTs came up in regions where the average expression level was higher than the genome-wide average, but that it was lower in the same regions in both strains where these CSCTs did not come up.

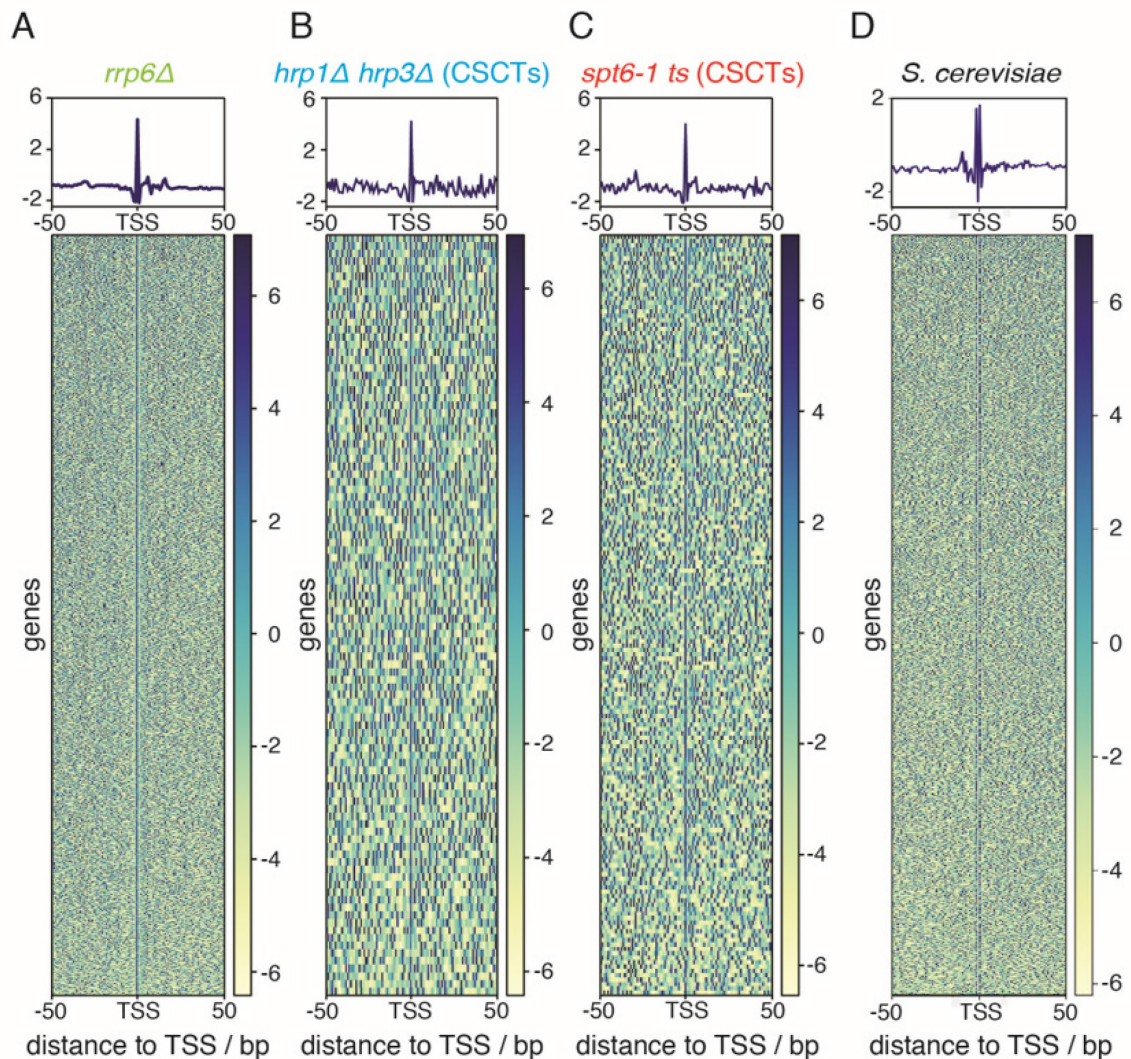


**Figure 2.11 CSCTs are highly expressed and located in relatively upregulated regions.** **A-B** Box plots of expression level distributions for all transcripts (TSSs) and the CSCTs in the *hrp1Δ hrp3Δ* (**A**) or the *spt6-1 ts* (**B**) mutant. **C-D** Schematic representation of CSCT neighborhood regions and upregulation of non-CSCT-transcripts in these regions for *hrp1Δ hrp3Δ* (**C**) or *spt6-1 ts* (**D**). Numbers in the center of the neighborhood region as well as height of colored boxes relative to the grey box representing the genome average give the ratio of the average expression level in this region relative to the whole-genome average expression level in the same strain. Whole-genome average expression level was set to 1.

### 2.1.4.3 CSCT-TSSs share distinctive DNA shape features with canonical TSSs

DNA shape is a further feature that we were interested in. DNA shape describes the orientation of the DNA bases in both strands relative to each other and probably reflects mainly electrostatic features in the minor groove of the DNA. Six different base pair orientations were described such as shift, slide, rise, tilt, roll and twist (Fujii *et al.*, 2007; Zhou *et al.*, 2013). DNA shape features may be calculated for free DNA by an algorithm developed in the Rohs group (Zhou *et al.*, 2013). We applied this algorithm to a 100 bp window centered on the TSSs. Indeed, we identified a peak for the DNA roll shape feature at the *rrp6Δ* TSSs as well as at the CSCT-TSSs in the *hrp1Δ hrp3Δ* and *spt6-1 ts* mutants (Figure 2.12 A, B and C). We asked if this striking feature was conserved in TSSs from other species, too. We repeated the same analysis for TSSs determined by TIF-seq in *S. cerevisiae* (Pelechano *et al.*, 2013). The DNA roll shape feature peak was visible at the

TSSs from *S. cerevisiae*, too, but less pronounced (note the different y-axis scales) than at TSSs in *S. pombe* (Figure 2.12 D).



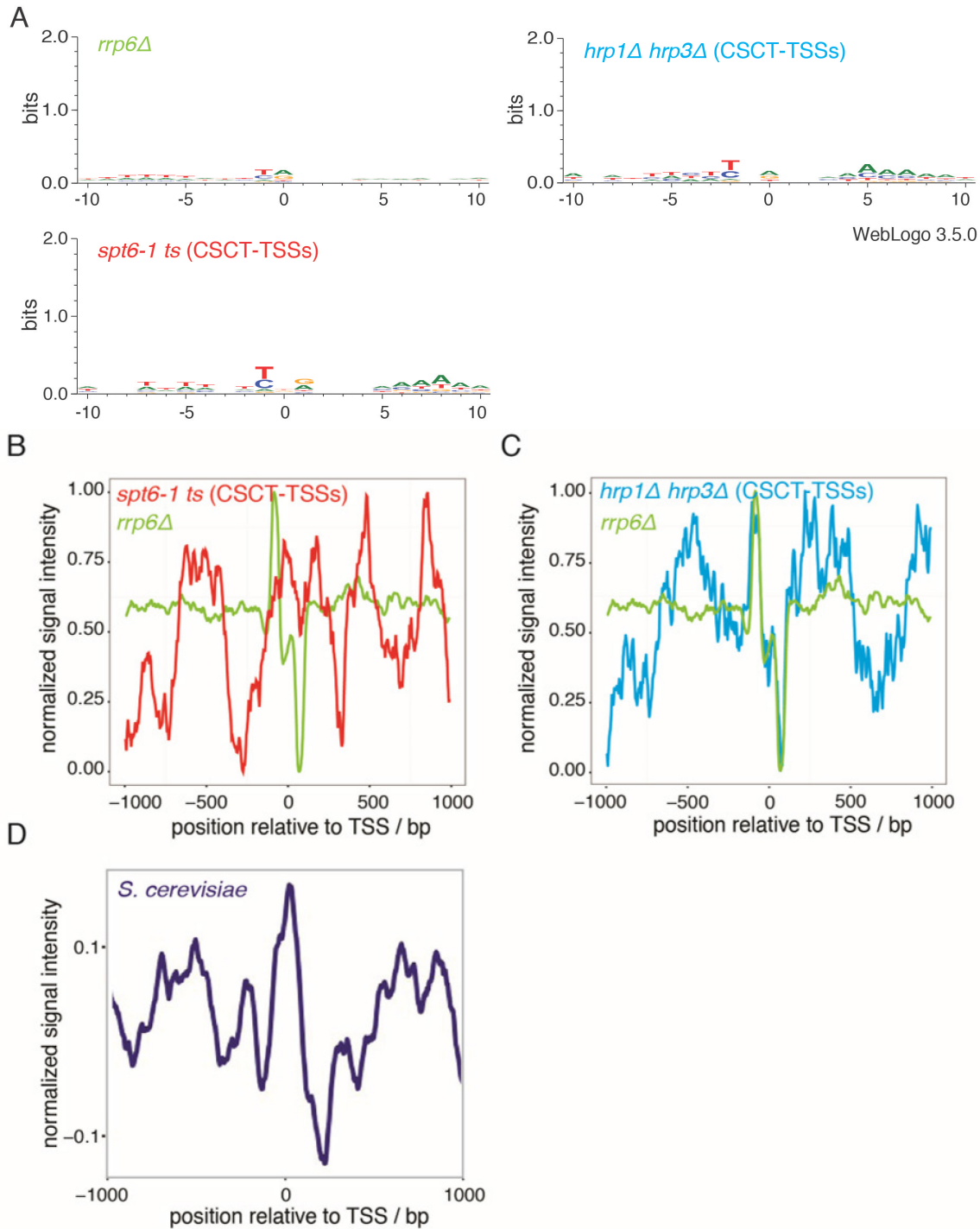
**Figure 2.12 DNA roll shape feature is enriched for *rrp6Δ* TSSs and CSCT-TSSs in the *hrp1Δ hrp3Δ* and *spt6-1 ts* strains. A-D** Composite plots and heat maps of calculated DNA roll shape feature for the *rrp6Δ* TSSs (A) and CSCT-TSSs in the *hrp1Δ hrp3Δ* (B) and *spt6-1 ts* mutants (C) and for wild type TSSs in *S. cerevisiae* (D) (analyzed data from (Pelechano *et al.*, 2013)).

#### 2.1.4.4 Some CSCT-TSSs are enriched for a GC skew signal

Li *et al.* described that promoter regions of wild type TSSs are enriched for the Initiator element (Li *et al.*, 2015). We confirmed this finding but note that this element is not present at the majority of TSSs, i.e., not strictly required for promoters (Figure 2.13 A). To characterize also the here newly annotated CSCTs in terms of sequence features, we analyzed the sequence around their TSSs with regard to base pair composition, motifs by position weight matrix as well as GC skew distributions. GC skew is defined as a strand-specific G over C enrichment.

We did not identify any enrichment of base pair composition or sequence motifs at or around the TSSs in the *rrp6Δ* strain or the TSSs of CSCTs (Figure 2.13 A). In contrast, we

saw a pronounced GC skew signal at the *rrp6Δ* TSSs and CSCT-TSSs in the *hrp1Δ hrp3Δ* mutant (Figure 2.13 C). Surprisingly, we did not detect GC skew enrichment at the CSCT-TSSs in the *spt6-1 ts* mutant (Figure 2.13 B). This observation coincides with the little overlap of CSCTs of both mutants (Figure 2.8). This might suggest that different sequence requirements are needed for the CSCT initiation of both mutants. A GC skew signal was less pronounced for wild type TSSs in *S. cerevisiae* (Figure 2.13 D) (Pelechano *et al.*, 2013).



**Figure 2.13 DNA sequence motifs and GC skew signals for *rrp6Δ* TSSs and *hrp1Δ hrp3Δ* CSCT-TSSs. A** Sequence motif analysis by position weight matrix at *rrp6Δ* TSS (left top panel), CSCT-TSSs for *hrp1Δ hrp3Δ* (right top panel), and *spt6-1 ts* (left bottom panel). **B-C** GC skew analysis for *rrp6Δ* TSSs and *spt6-1 ts* CSCT-TSSs (**B**) or *hrp1Δ hrp3Δ* CSCT-TSSs (**C**). **D** GC skew analysis for wild type TSSs in *S. cerevisiae* (analyzed data from (Pelechano *et al.*, 2013)).

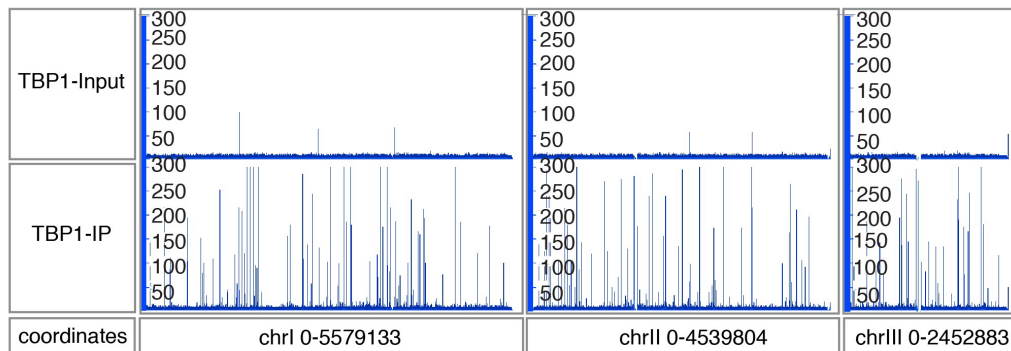


### 2.1.5 Annotation and characterization of Tbp1 binding by CHIP-seq

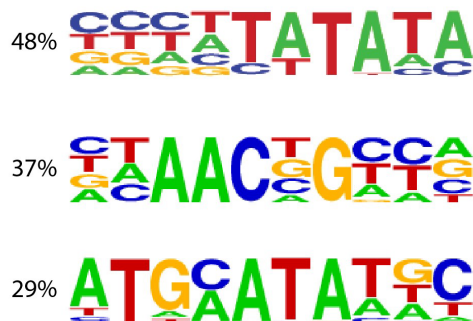
One classical element in promoter regions is the TATA box sequence motif, which is specifically bound by the Tbp1 protein in *S. pombe*. We annotated the Tbp1 binding sites in *S. pombe* wild type cells by CHIP-seq for the first time. We identified around 200 peaks of bound Tbp1 protein, i.e., detectable Tbp1 cross-linking at less than 5% of the genes (Figure 2.14 A). The genes bound by Tbp1 were mostly tRNA genes. We used these Tbp1 binding sites to annotate the underlying consensus sequences. We identified three major consensus sequences with a frequency of 48%, 37% and 29% (Figure 2.14 B). The most abundant sequence motif harbored the canonical TATA box (Smale and Kadonaga 2003). We asked how many *rrp6Δ* promoters harbored this TATA box. 11% of the *rrp6Δ* promoters showed this most prominent consensus sequence motif. Interestingly, the distribution of the distances between this sequence motif and the TSSs showed a prominent peak at 35 bp (Figure 2.14 C). Additionally, we found a substantial fraction (18%) of the CSCT promoters of the *spt6-1 ts* mutant to be enriched for this TATA box with a similar average distance of 35 bp (Figure 2.14 C). The average distance could not be reasonably determined for the CSCT promoters in the *hrp1Δ hrp3Δ* mutant as the number of CSCTs with TATA box was too low.

We divided the TSSs from wild type cells grown in YES medium into two classes, with or without TATA box motif. We asked if there were any differences with respect to DNA shape features or nucleosome organization. There were no major differences. The peak of the DNA roll shape feature was visible for both TSSs classes. As expected, we observed a peak for the DNA roll shape feature at the TATA box position due to the TATA box sequence there (Figure 2.14 D). The nucleosome organization aligned to the wild type TSSs of promoter regions with or without TATA box motif revealed no major difference (Figure 2.14 E).

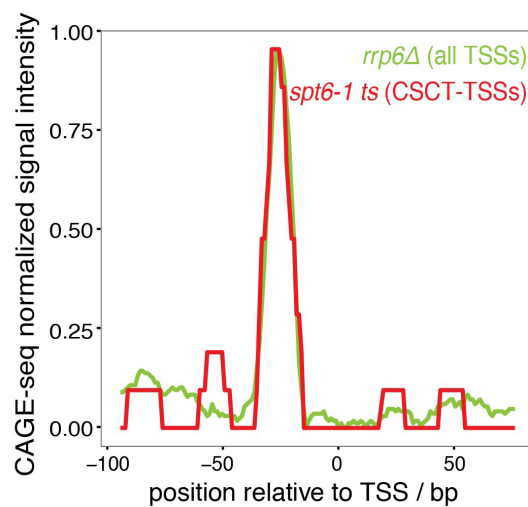
A



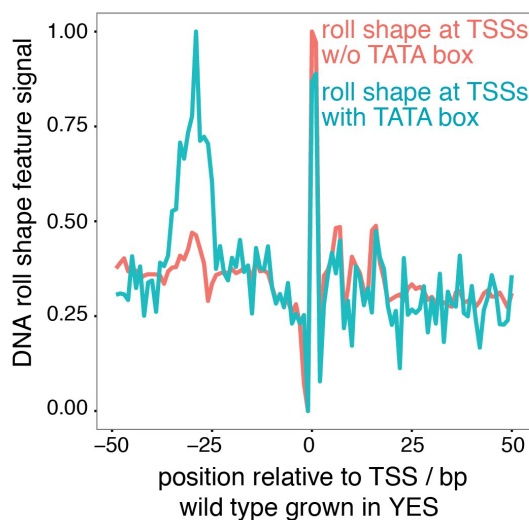
B



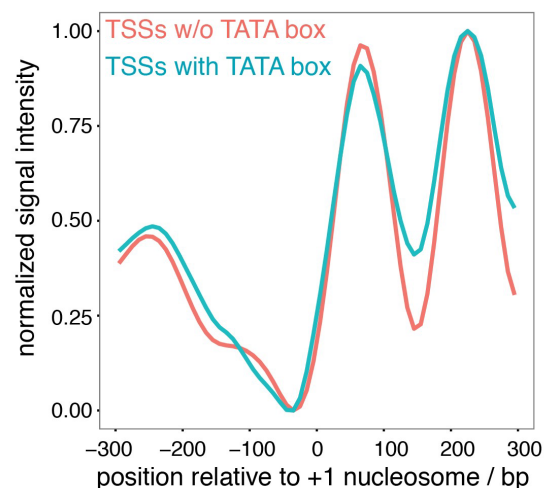
C



D



F



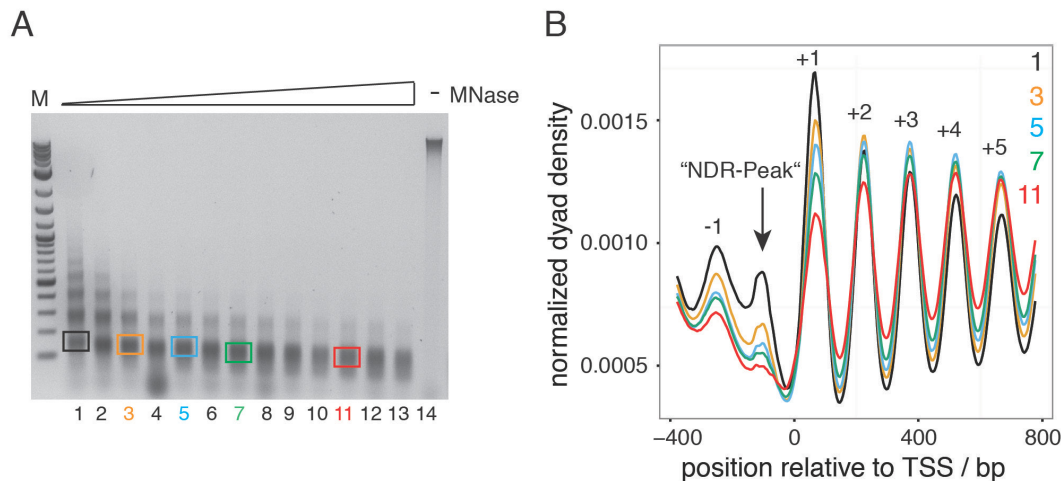
**Figure 2.14 Localization and characteristics of Tbp1 binding sites and TATA box motif.** **A** Genome browser shot of all Tbp1 binding sites for all three chromosomes in *S. pombe* as determined by CHIP-seq, one replicate shown ( $n = 2$ ). **B** Position weight matrix of the underlying binding sequences of Tbp1. **C** Composite plot of TATA box motif distribution for *rrp6Δ* TSSs and CSCT-TSSs of *spt6-1 ts*. **D** Composite plot of DNA shape for TSSs from wild type grown in YES medium, with or without TATA box motif. **F** Composite plot of MNase-seq data derived from wild type cells grown in YES medium aligned to wild type TSSs, with or without TATA box motif.

## 2.2 CHD1-dependent NDR-array pattern in *S. pombe*

One of the strongest effects on nucleosome positions and NDR-array patterns are observed in *S. pombe* and *S. cerevisiae* if a specific subset of genes encoding chromatin remodelers is deleted. In *S. pombe*, the double deletion mutant *hrp1Δ hrp3Δ* leads to an impairment of TSS-aligned regular nucleosome arrays over gene coding regions (Hennig *et al.*, 2012; Pointner *et al.*, 2012; Shim *et al.*, 2012). A comparable phenotype is seen in *S. cerevisiae* for the triple deletion mutant *chd1Δ isw1Δ isw2Δ* (Gkikopoulos *et al.*, 2011; Ocampo *et al.*, 2016). Notably, the MNase ladders are still observable in these mutant strains (Pointner *et al.*, 2012). This means that regularly spaced nucleosomes are present but not aligned to the TSSs in these mutant strains. This observation hints towards spacing and nucleosome array alignment being two separated processes. Additionally, the Chd1 chromatin remodeler in *S. cerevisiae* and the Hrp3 chromatin remodeler in *S. pombe* make the strongest contribution to this effect on nucleosome array alignment (Gkikopoulos *et al.*, 2011; Hennig *et al.*, 2012; Pointner *et al.*, 2012). Therefore, the CHD1 chromatin remodeler class seemed to be especially important for the alignment of nucleosome arrays to the TSSs. We examined the contribution of Chd1/Hrp3 and their domains to the generation of the aligned NDR-array pattern and the functional conservation of these domains between *S. cerevisiae* and *S. pombe*.

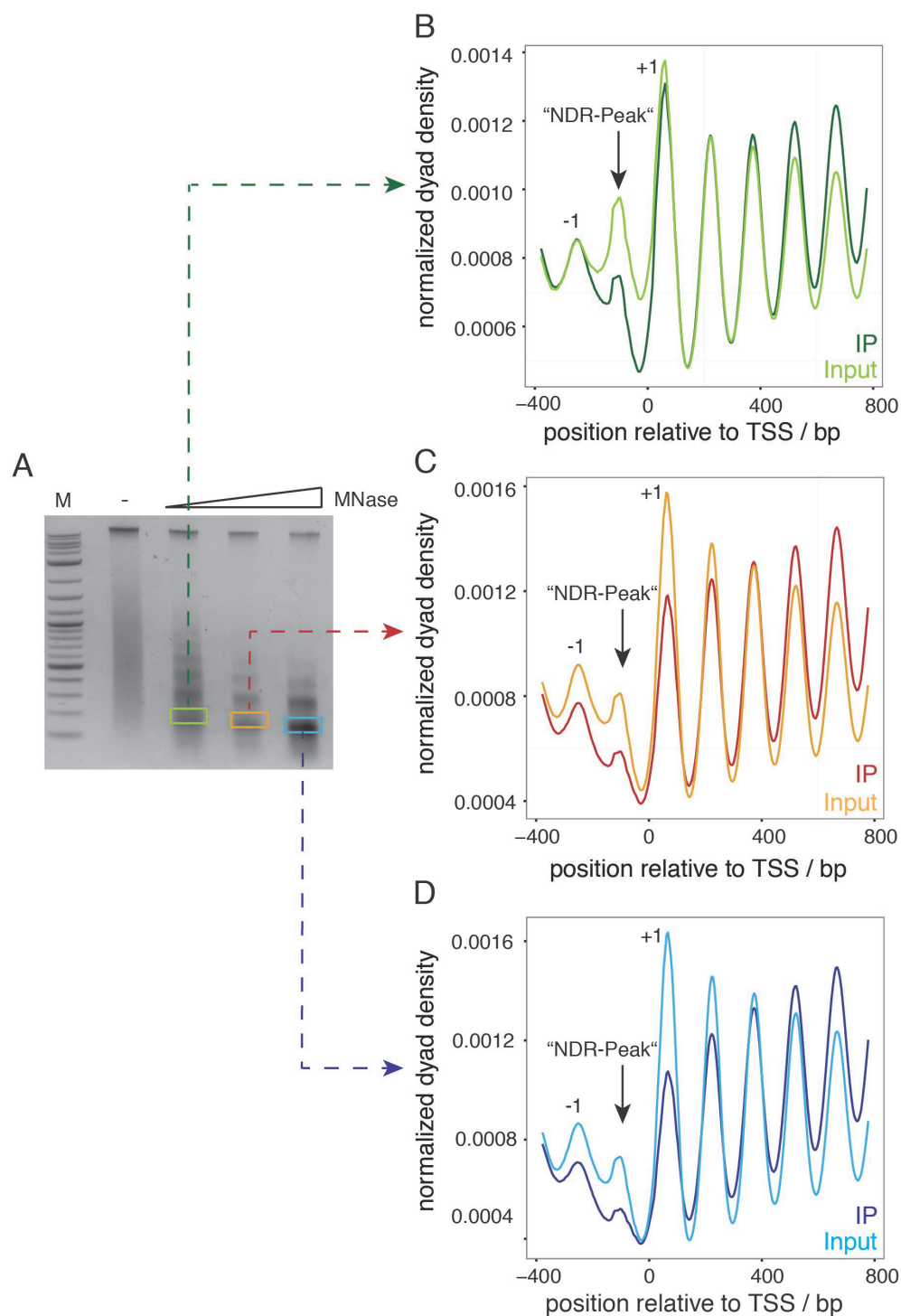
### 2.2.1 Effect of MNase digestion degree on the NDR-array pattern

As mentioned, one common way to display nucleosome positions and thereby show the NDR-array pattern is to align the dyad densities of the nucleosomes to a reference point in a composite plot. Here, we used the *rrp6Δ* TSSs as alignment point (chapter 2.1) and the nucleosome positions were determined by MNase-seq. In a composite plot, the peak position and height represent the nucleosome position and occupancy, respectively. MNase-seq is debated with regard to the peak heights as they are highly dependent on the MNase digestion degree (Weiner *et al.*, 2010; DeGennaro *et al.*, 2013). Therefore, the nucleosome occupancy results of MNase-seq experiments might be misleading as the MNase digestion degree is difficult to control or normalize for, especially if comparing different samples among each other. To demonstrate the effects of MNase digestion degree on NDR-array patterns, we used five different MNase concentrations on the same chromatin sample derived from *S. pombe* wild type cells. We could observe concentration dependent MNase laddering patterns (Figure 2.15 A). This MNase titration experiment showed that the +1 nucleosome peak height decreased with higher MNase concentration (Figure 2.15 B). Additionally, lower digestion degrees showed a peak in the region that is largely nucleosome depleted (= NDR) at usually used digestion degrees. Accordingly, the height of this “NDR-Peak” also decreased with increasing MNase concentration. Conversely, the array peaks downstream of the +1 nucleosome seemed to be more pronounced if a higher MNase concentration was applied to the chromatin sample.



**Figure 2.15 Apparent nucleosome occupancy is highly dependent on MNase digestion degree, especially in the NDR region.** **A** MNase ladders resulting from different MNase digestion degrees of the same chromatin preparation, separated by agarose gel electrophoresis, one replicate shown ( $n = 1$ ). M: 2-Log DNA marker (NEB). **B** Composite plots of MNase-seq data of the same MNase digestions as shown in panel **(A)** (indicated by corresponding colors and labeled according to the lanes where the respective samples were analyzed in panel **(A)**) aligned to *rrp6 $\Delta$*  TSSs.

As NDRs are occupied by many factors and complexes, e.g. the PIC, that may protect from MNase digestion, especially at low digestion degrees, we wished to see if the “NDR-Peak” indeed corresponded to nucleosomes. We performed MNase-seq coupled to anti-H3-ChIP. This allowed us to capture specifically those DNA fragments that are bound to histone H3. The MNase-anti-H3-ChIP approach was performed with three different MNase concentrations on the same chromatin sample (Figure 2.16). For direct comparison between general MNase protection and protection by particles containing histone H3, we also analyzed the corresponding input material, which corresponds to a usual MNase-seq analysis. The most pronounced differences in MNase protection patterns between samples without and with anti-H3-ChIP were that the height of the +1 nucleosome peak, the “NDR-Peak”, and also somewhat of the -1 nucleosome peak decreased in the latter. This difference increased with increasing digestion degree (Figure 2.16 B-D).



**Figure 2.16 The “NDR-Peak” originates, at least in part, from nucleosomes.** **A** MNase ladders resulting from different MNase digestion degrees of same *S. pombe* wild type chromatin preparation, separated by agarose gel electrophoresis (here shown for Input fraction), one replicate shown ( $n = 1$ ). M: 2-Log DNA marker (NEB). **B-D** Composite plots of MNase-seq (Input) or MNase-anti-H3-ChIP-seq (IP) data generated from the mononucleosomal DNA shown in panel **(A)** (corresponding color coding) aligned to *rrp6Δ* TSSs.

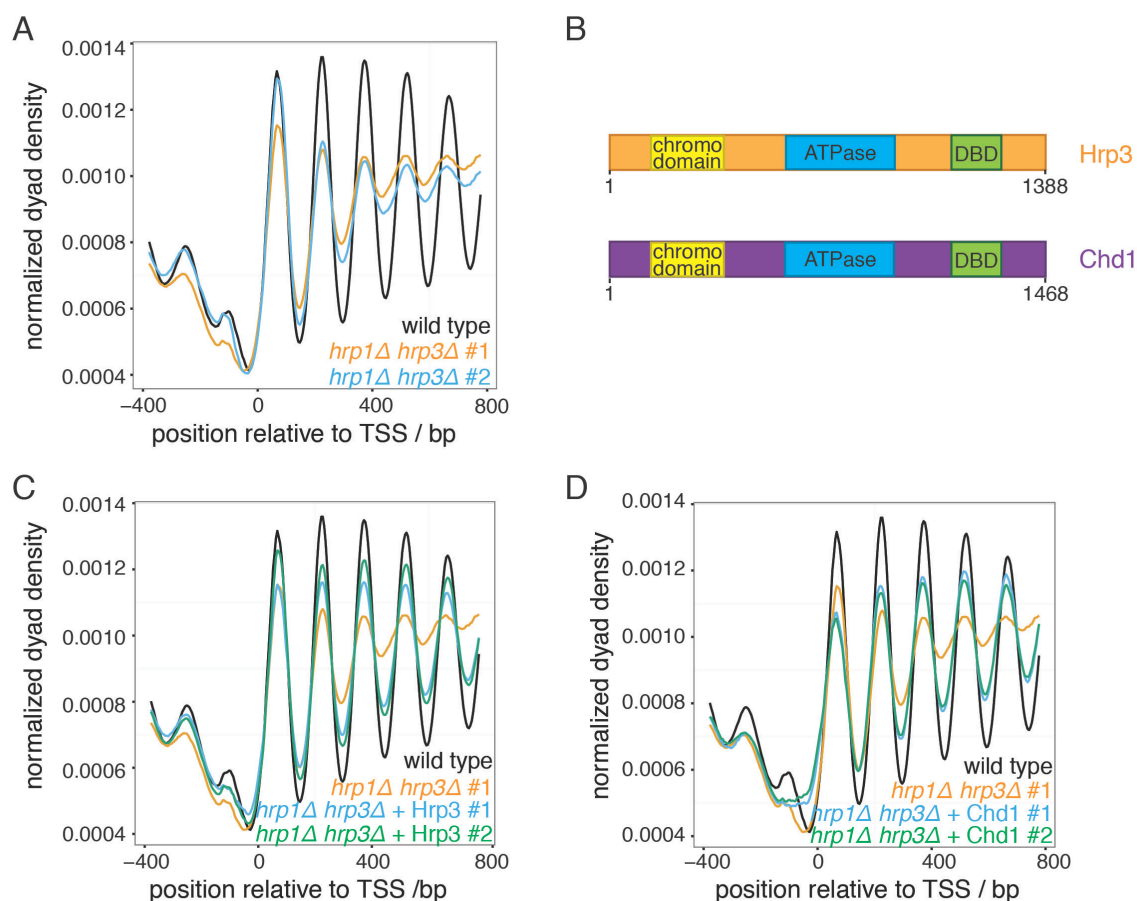
Taken together, we could confirm that nucleosome occupancy is highly dependent on MNase digestion degree whereas nucleosome positions were not affected. Thus, to judge if a factor has an effect on the nucleosomal NDR-array pattern, we mainly took changes in

peak positions rather than peak height as read-out. The “NDR-Peak” was observed in MNase-seq as well as in MNase-anti-H3-ChIP-seq, although much less pronounced in the latter. So it seemed, at least in part, to originate from nucleosomes. That the +1 (and -1) peak heights decreased with application of the anti-H3-immunoprecipitation step, while peaks of the genic arrays increased may argue for cross-linking and/or precipitation biases depending on the nucleosome position relative to the TSS. It may also originate from the molecular composition of the nucleosomes at the respective positions, i.e., depend on other factors bound to the nucleosomes.

### **2.2.2 Role of CHD1 chromatin remodelers in the generation of NDR-array patterns assessed by *in vivo* complementation assay in the *hrp1Δ hrp3Δ* mutant**

We were interested in both deletion mutants, *chd1Δ isw1Δ isw2Δ* in *S. cerevisiae* and *hrp1Δ hrp3Δ* in *S. pombe* (Gkikopoulos *et al.*, 2011; Hennig *et al.*, 2012; Pointner *et al.*, 2012). Both show a similar phenotype regarding impaired genic nucleosome arrays, but differ regarding the affected chromatin remodeler classes (CHD1 and ISWI versus CHD1 only in *S. cerevisiae* versus *S. pombe*, respectively). Additionally, both yeasts are far diverged, so that the evolutionary conservation of these chromatin remodelers and their function would be interesting.

We used an *in vivo* complementation assay where we reintroduced CHD1 chromatin remodelers into the *S. pombe* deletion strain *hrp1Δ hrp3Δ*. The resulting NDR-array patterns were analyzed by MNase-seq. We compared the NDR-array pattern of the complemented strain with that of the double deletion strain. We confirmed the disturbed nucleosome pattern of the *hrp1Δ hrp3Δ* deletion strain also by MNase-seq (Figure 2.17 A), since the previous work in our group applied MNase-chip (Pointner *et al.*, 2012). We wished to see if the Hrp3 chromatin remodeler was able to rescue this disturbed NDR-array pattern. Indeed, the disturbed NDR-array pattern was rescued as the peaks over the gene coding regions were more pronounced in the Hrp3 rescue strain compared to those in the double deletion mutant, especially at the +3, +4 and +5 nucleosome positions (Figure 2.17 C). We tested the Chd1 chromatin remodeler from *S. cerevisiae* in the *hrp1Δ hrp3Δ* deletion strain. Surprisingly, also this heterologous chromatin remodeler could rescue the phenotype (Figure 2.17 D). Both rescues, by Hrp3 or Chd1 in the *hrp1Δ hrp3Δ* mutant, worked similarly well with regard to the resulting NDR-array pattern. One slight difference was that Chd1 did not rescue the additional “NDR-Peak”, the peak was only observed in the rescue with Hrp3 in *S. pombe*. The analogous rescue experiment in *S. cerevisiae* did not lead to the same observation (data not shown, see PhD thesis by Dr. Corinna Lieleg). Here, the Hrp3 chromatin remodeler was not able to rescue the disturbed NDR-array pattern in the *chd1Δ isw1Δ isw2Δ* in *S. cerevisiae*.



**Figure 2.17** Both CHD1 chromatin remodelers, Hrp3 from *S. pombe* and Chd1 from *S. cerevisiae*, can rescue the NDR-array pattern for the *hrp1Δ hrp3Δ* mutant in *S. pombe*. **A** Composite plots of MNase-seq data for *S. pombe* wild type cells and two biological replicates of the *hrp1Δ hrp3Δ* mutant with empty plasmid pJR-A (orange #1 and blue #2, n = 2) aligned to *rrp6Δ* TSSs. **B** Domain organization (not to scale) of *S. pombe* Hrp3 and *S. cerevisiae* Chd1 chromatin remodelers. DBD: DNA binding domain. **C** Composite plots as in panel (A), but for two biological replicates of the *hrp1Δ hrp3Δ* mutant carrying plasmid pJR-A\_HRP3 expressing full length Hrp3 (blue #1 and green #2, n = 2). **D** As in panel (C) but with plasmid pJR-A\_CHD1 expressing full length *S. cerevisiae* Chd1.

### 2.2.3 Effectiveness of Chd1/Hrp3 hybrid constructs in the rescue of NDR-array pattern in the *hrp1Δ hrp3Δ* mutant

Another question was to pinpoint which domain of the chromatin remodeler Chd1 in *S. cerevisiae* and which domain of the chromatin remodeler Hrp3 in *S. pombe* might play an important role in the generation of the NDR-array pattern. We divided the Chd1 and Hrp3 chromatin remodelers into three main parts, i.e., the chromodomain, the ATPase and the DBD domain (Figure 2.17 B, Figure 2.18 A-F) and tested six correspondingly different Chd1/Hrp3 hybrid constructs (Table 2.3, Table 2.4 and Table 2.5) in the *chd1Δ isw1Δ isw2Δ* mutant in *S. cerevisiae* (see PhD thesis by Dr. Corinna Lieleg) and in the *hrp1Δ hrp3Δ* mutant in *S. pombe* to see if the domains are exchangeable and take over similar functions with regard to generating the NDR-array pattern. Interestingly, all but one of these hybrid constructs could rescue the NDR-array pattern in the *chd1Δ isw1Δ isw2Δ* mutant in *S. cerevisiae* but showed tighter spacing (Table 2.3).

**Table 2.3 Chd1/Hrp3 hybrid constructs tested in complementation assay in the *chd1Δ isw1Δ isw2Δ* mutant in *S. cerevisiae*.** Results taken from PhD thesis by Dr. Corinna Lieleg.

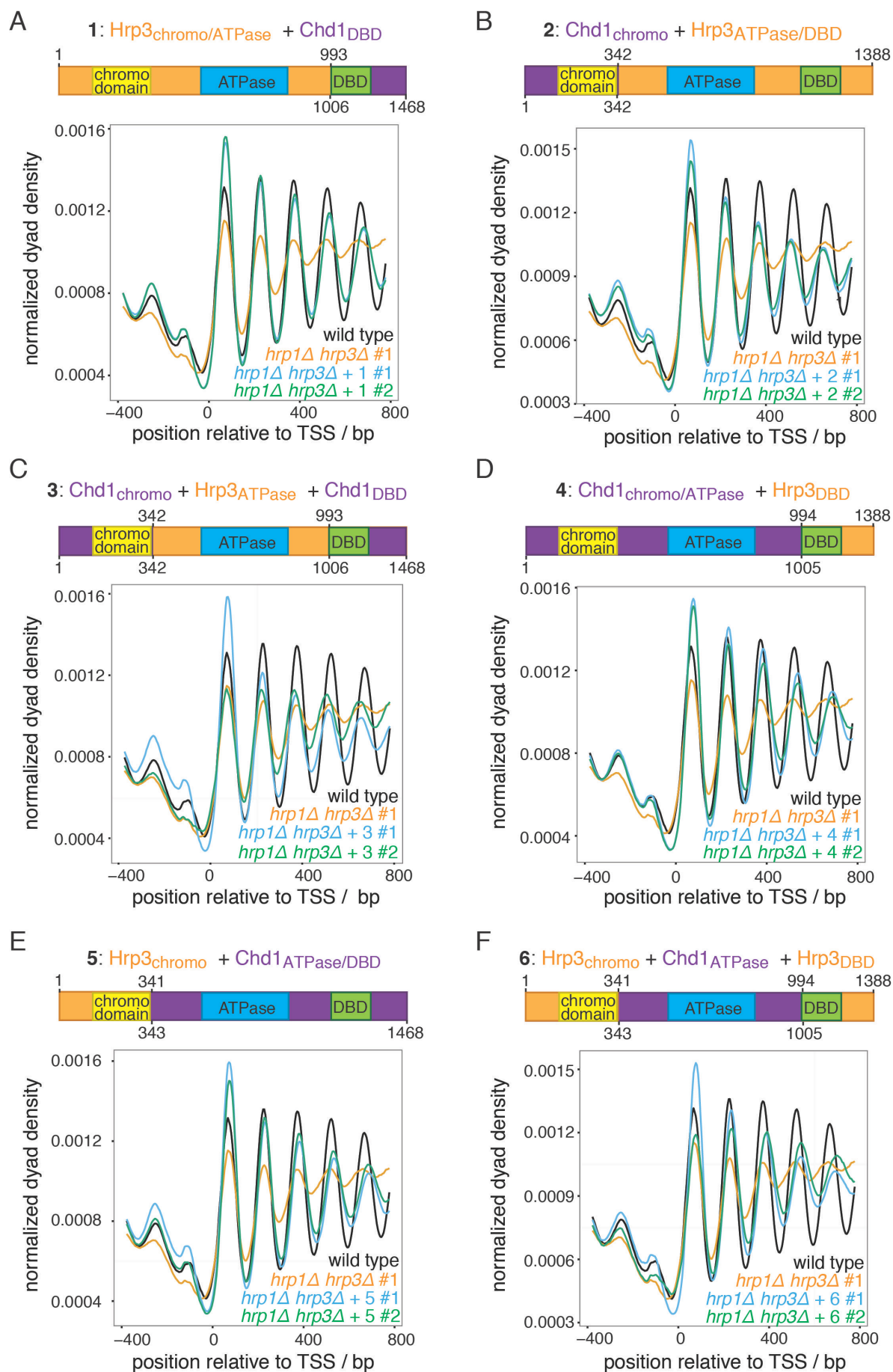
Constructs				NDR-array pattern rescue	Spacing (compared to wild type)
Chd1				YES	tighter
Hrp3				NO	-
No.	Chromodomain	ATPase	DBD		
I	Hrp3	Hrp3	Chd1	YES	tighter
II	Chd1	Hrp3	Hrp3	NO	-
III	Chd1	Hrp3	Chd1	YES	tighter
IV	Chd1	Chd1	Hrp3	YES	tighter
V	Hrp3	Chd1	Chd1	YES	tighter
VI	Hrp3	Chd1	Hrp3	YES	tighter

The analogous complementation approach, done in this thesis project here for *S. pombe* with the same constructs No. 1 to 6 as in the PhD project by Dr. Corinna Lieleg, but expressed from a different *S. pombe* plasmid, showed that all six hybrid constructs could rescue NDR-array patterns in the *hrp1Δ hrp3Δ* mutant (Figure 2.18). This was somewhat to be expected as already full length Chd1 could rescue the NDR-array pattern in *S. pombe* (Figure 2.17 D). However, the resulting NDR-array patterns for the hybrid constructs were more different from the wild type pattern. The hybrid constructs, 1, 4, 5 and 6, resulted in a downstream shift of the +1 nucleosome peak as well as in wider spacing compared to wild type (Figure 2.18 A, D, E, F). Conversely, the constructs 2 and 3 showed a tighter spacing (Figure 2.18 B and C). It is quite surprising that the combination of Chd1 chromodomain and Hrp3 ATPase domain in constructs 2 and 3 led to an even tighter spacing as the *S. pombe* wild type spacing is already the tightest known (Lantermann *et al.*, 2010; Lieleg *et al.*, 2015). The short spacing (given in bp, Table 2.4) for all constructs which may seem too short given the canonical length for mononucleosomal DNA of 147 bp (Luger *et al.*, 1997) may result due the MNase trimming activity, since MNase digestion degrees may vary from experiment to experiment.

**Table 2.4 Chd1/Hrp3 hybrid constructs tested in complementation assay in the *hrp1Δ hrp3Δ* mutant in *S. pombe*.** Spacing was calculated by dividing the distance between the +1 and +5 nucleosome peaks by four.

Constructs				NDR-array pattern rescue	Spacing (compared to wild type)
Hrp3				YES	145 bp
Chd1				YES	145 bp
No.	Chromodomain	ATPase	DBD		
1	Hrp3	Hrp3	Chd1	YES	150 bp (+3.5%)
2	Chd1	Hrp3	Hrp3	YES	140 bp (-3.5%)
3	Chd1	Hrp3	Chd1	YES	140 bp (-3.5%)
4	Chd1	Chd1	Hrp3	YES	150 bp (+3.5%)
5	Hrp3	Chd1	Chd1	YES	150 bp (+3.5%)
6	Hrp3	Chd1	Hrp3	YES	155 bp (+6.7%)





**Figure 2.18** For Figure legend, see next page.

**Figure 2.18 All Chd1/Hrp3 hybrid constructs are able to rescue the NDR-array pattern in the *hrp1Δ hrp3Δ* mutant in *S. pombe*.** A-F Composite plots of MNase-seq data of the *hrp1Δ hrp3Δ* mutant in *S. pombe* with plasmids pJR-A\_1 (A), pJR-A\_2 (B), pJR-A\_3 (C), pJR-A\_4 (D), pJR-A\_5 (E) and pJR-A\_6 (F) aligned to *rrp6Δ* TSSs (Table 2.5). Two biological replicates are shown (blue #1 and green #2, n = 2). Plasmids encoding the Chd1/Hrp3 hybrid constructs indicated by the schematic representation (not to scale) with start- and endposition of amino acids of corresponding domain given in numbers.

Taken together, all Hrp3/Chd1 hybrid constructs rescued NDR-array patterns in the *hrp1Δ hrp3Δ* mutant in *S. pombe*, i.e. both chromatin remodelers are somewhat exchangeable in this yeast, in contrast to *S. cerevisiae*. Therefore, the function of both chromatin remodelers in generating NDR-array patterns seems evolutionary well-conserved. Nonetheless, the domain-wise complementation showed some differences in detail.

## 2.2.4 Supplementary materials

Wild type strain was (h- 972) and the double deletion mutant strain *hrp1Δ hrp3Δ* (Table 2.1). The pJR-A plasmid (high copy number plasmid with regulatable expression system (thiamine-repressible nmt1 promoter), adenine marker) was used to express the constructs in the *hrp1Δ hrp3Δ* strain (Moreno *et al.*, 2000). The Gibson cloning strategy was used to clone the constructs (Table 2.5) (Gibson *et al.*, 2009). The pJR-A plasmid was cut using the restriction enzymes XhoI and SmaI (NEB).

**Table 2.5 Cloning strategies to obtain plasmid constructs for *in vivo* complementation approach for *S. pombe***

Name	Domain structure	Primers (Table 2.7)	Template for PCR (Table 2.6)	Final plasmid constructs
1	Hrp3 $\Delta$ DBDChd1 $\Delta$ DBD	151, 156	pEG202_1	pJR-A_1
2	Chd1 $\Delta$ chromoHrp3 $\Delta$ chromo	153, 154	pEG202_2	pJR-A_2
3	Chd1 $\Delta$ chromoHrp3 $\Delta$ chromo $\Delta$ DBDChd1 $\Delta$ DBD	153 + 156	pEG202_3	pJR-A_3
4	Chd1 $\Delta$ DBDHrp3 $\Delta$ DBD	153 + 154	pEG202_4	pJR-A_4
5	Hrp3 $\Delta$ chromo Chd1 $\Delta$ chromo	151 + 156	pEG202_5	pJR-A_5
6	Hrp3 $\Delta$ chromoChd1 $\Delta$ chromo $\Delta$ DBDHrp3 $\Delta$ DBD	151 + 154	pEG202_6	pJR-A_6
<b>Hrp3</b>	full length Hrp3	151 + 154	pEG202-HRP3	pJR-A_HRP3
<b>Chd1</b>	full length Chd1	153 + 156	pEG202-CHD1	pJR-A_CHD1

**Table 2.6 Cloning strategies to obtain plasmid constructs for *in vivo* complementation approach for *S. cerevisiae* (see PhD thesis by Dr. Corinna Lieleg)**

Name	Domain structure	Primer (Table 2.7)	Template for PCR	Final plasmid constructs
1	Hrp3 $\Delta$ DBDChd1 $\Delta$ DBD	23+24 25+26	genomic <i>S. pombe</i> DNA genomic <i>S. cerevisiae</i> DNA	pEG202_1
2	Chd1 $\Delta$ chromoHrp3 $\Delta$ chromo	27+28 29+30	genomic <i>S. cerevisiae</i> DNA genomic <i>S. pombe</i> DNA	pEG202_2
3	Chd1 $\Delta$ chromoHrp3 $\Delta$ chromo $\Delta$ DBDChd1 $\Delta$ DBD	27+28 25+26 24+29	genomic <i>S. cerevisiae</i> DNA genomic <i>S. pombe</i> DNA genomic <i>S. cerevisiae</i> DNA	pEG202_3
4	Chd1 $\Delta$ DBDHrp3 $\Delta$ DBD	27+31 32+33	genomic <i>S. cerevisiae</i> DNA genomic <i>S. pombe</i> DNA	pEG202_4
5	Hrp3 $\Delta$ chromoChd1 $\Delta$ chromo	34+35 26+36	genomic <i>S. pombe</i> DNA genomic <i>S. cerevisiae</i> DNA	pEG202_5
6	Hrp3 $\Delta$ chromoChd1 $\Delta$ chromo $\Delta$ DBDHrp3 $\Delta$ DBD	37+38 34+35 32+33	genomic <i>S. pombe</i> DNA genomic <i>S. cerevisiae</i> DNA genomic <i>S. pombe</i> DNA	pEG202_6
<b>Hrp3</b>	full length Hrp3	5+6	genomic <i>S. pombe</i> DNA	pEG202-HRP3
<b>Chd1</b>	full length Chd1	3+4	genomic <i>S. cerevisiae</i> DNA	pEG202-CHD1

**Table 2.7 Primer sequences used for cloning strategies (Table 2.5 and Table 2.6)**

No.	Sequence
151	CTTTGTTAAATGGCCTCGAGATGAGTACAAGTGCTATAG
153	GTAAATGGCCTCGAGATGGCAGCCAAGGATATTTCTACTG
154	CATGTATGAAAAGATGAAGTAGCCCGGGTAAAGGAATG
156	GATAACAGAGTCTCAAAGAAGTGACCCGGTAAAGGAATG
3	GAGAGAGGATCCATGGCAGCCAAGGATATTTT
4	GGAGCGCCCATGGTCACTTCTTTTGAGACTCTG
5	GAGAGA GGATCCATGAGTACAAGTGCTATAG
6	GGAGCGCCTCGAGCTACTTCATCTTTTCATAC
23	AATCCCAGGGGATCCATGAGTACAAGTGCTATAGCACTTGC
24	AATAGAGTCCATGTCCTCATCTTTAAGCATTGCTTTTGC
25	ATGCTTAAAGATGAGGACATGGACTCTATTGGTGAATCGG
26	GGTCGACTCGAGTTACTTCTTTTGAGACTCTGTTATCTTG
27	AATCCCAGGGGATCCATGGCAGCCAAGGATATTTT
28	TGACTCACTTTCTTCTCTGTTTTGAAAATGTTTCACTTG
29	TTTTCAAACAGAGAAGAAAGTGAGTCAGATGATAGTTC
31	CCTTTTCCAGTAAAACATTAGCTCTTGCTCTTCTTCTAG
32	GAAGAGCAAGAGCTAATGTTTTACTGGAAAAGGAAATTCG
33	CAGGTCGACTCGAGCTACTTCATCTTTTCATACATGCTG
34	GAATCCCAGGGGATCCATGAGTACAAGTGCTATAGCACTTG
35	GTGGGAGGATCTTAGAGTTTTCTTTCTTTGAAATGCCTG
36	GCATTTCAAGAAAGAGAAAACCTAAGATCCTCCACAATATTC
37	CAGGCATTTCAAGAAAGAGAAAACCTAAGATCCTCCAC
38	CTTTCCAGTAAAACATTAGCTCTTGCTCTTCTTCTAGAAG

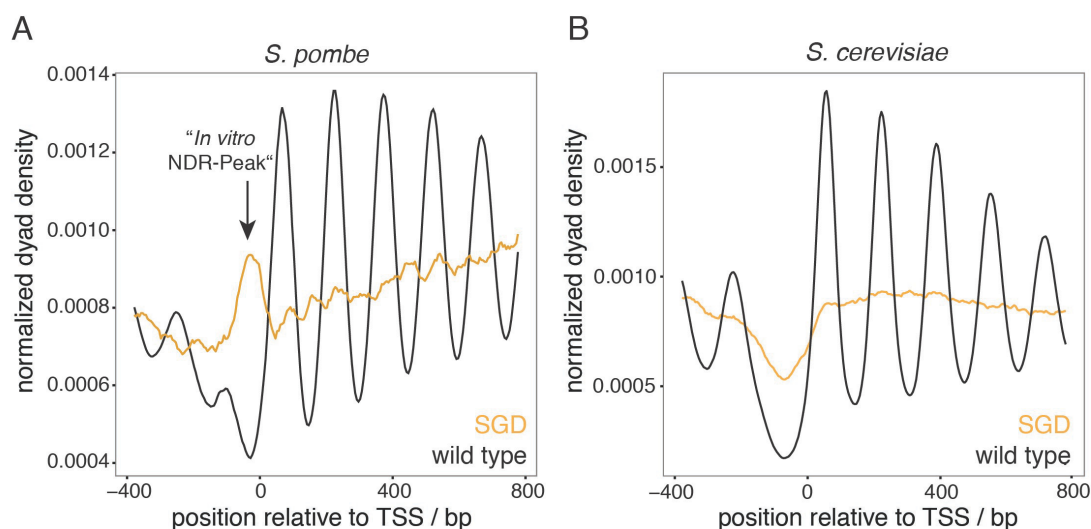
## 2.3 *In vitro* reconstitution systems for genome-wide *in vivo*-like nucleosome positioning

Several *in vivo* mutant and *in vitro* reconstitution studies for *S. cerevisiae* showed that chromatin remodelers and GRFs play an important role in nucleosome positioning mechanisms (Badis *et al.*, 2008; Parnell *et al.*, 2008; Hartley and Madhani 2009; Gkikopoulos *et al.*, 2011; Tsankov *et al.*, 2011; Zhang *et al.*, 2011; Hennig *et al.*, 2012; Pointner *et al.*, 2012; van Bakel *et al.*, 2013; Krietenstein *et al.*, 2016; Ocampo *et al.*, 2016). *In vivo*, a combination of deletions is necessary to see major genome-wide effects on the nucleosome patterns, e.g., the *chd1Δ isw1Δ isw2Δ* mutant in *S. cerevisiae* or the *hrp1Δ hrp3Δ* mutant in *S. pombe* (chapter 2.2) (Gkikopoulos *et al.*, 2011; Hennig *et al.*, 2012; Pointner *et al.*, 2012). Such redundant contribution of multiple factors hampers the determination of the contribution of one particular factor *in vivo*. Therefore, an *in vitro* approach, based on salt gradient dialysis (SGD) chromatin reconstitution and addition of extracts or purified factors, was used to determine which factors are necessary or sufficient and have a direct role in nucleosome positioning for *S. cerevisiae* (Wippo *et al.*, 2011; Zhang *et al.*, 2011; Krietenstein *et al.*, 2012; Krietenstein *et al.*, 2016). We wished to establish an analogous *in vitro* reconstitution system for the reconstitution of genome-wide *in vivo*-like nucleosome patterns also for *S. pombe*. With this we should be able to compare conserved or diverged nucleosome positioning mechanisms between both yeasts, which may be especially interesting as both yeasts differ in their use of chromatin remodeler classes (Pointner *et al.*, 2012).

### 2.3.1 *In vitro* reconstitution using whole cell extract from *S. pombe*

Our *in vitro* reconstitution system is a two-step approach. First, chromatin is assembled by SGD using purified histone octamers and a genomic plasmid library. Second, the SGD chromatin is incubated with factors to be tested for their nucleosome positioning activity. The outcome is assessed by MNase-seq. We compared the nucleosome pattern of reconstitution experiments to the *in vivo* nucleosome pattern (the same wild type *S. pombe* MNase-seq data was used for the following figures).

The nucleosome pattern of SGD chromatin using an *S. pombe* plasmid library, which contained DNA inserts covering the whole genome, did not show any *in vivo*-like nucleosome pattern (Figure 2.19 A). This was somewhat expected as this pure SGD approach also did not yield the *in vivo* pattern for *S. cerevisiae* (Figure 2.19 B) (Kaplan *et al.*, 2009; Zhang *et al.*, 2009; Zhang *et al.*, 2011). Comparing the *S. pombe* and *S. cerevisiae* SGD chromatin, the nucleosome pattern upstream of the TSS attracted most attention. In *S. cerevisiae*, the NDR seen there *in vivo* seemed to be rather pronounced already *in vitro*, whereas in *S. pombe* even a peak was located upstream of the TSS where *in vivo* the NDR resides (Figure 2.19). The other features of the nucleosome pattern, such as the +1 nucleosome or the nucleosome array, were not reconstituted in either yeast by just using histone octamers and DNA during SGD.



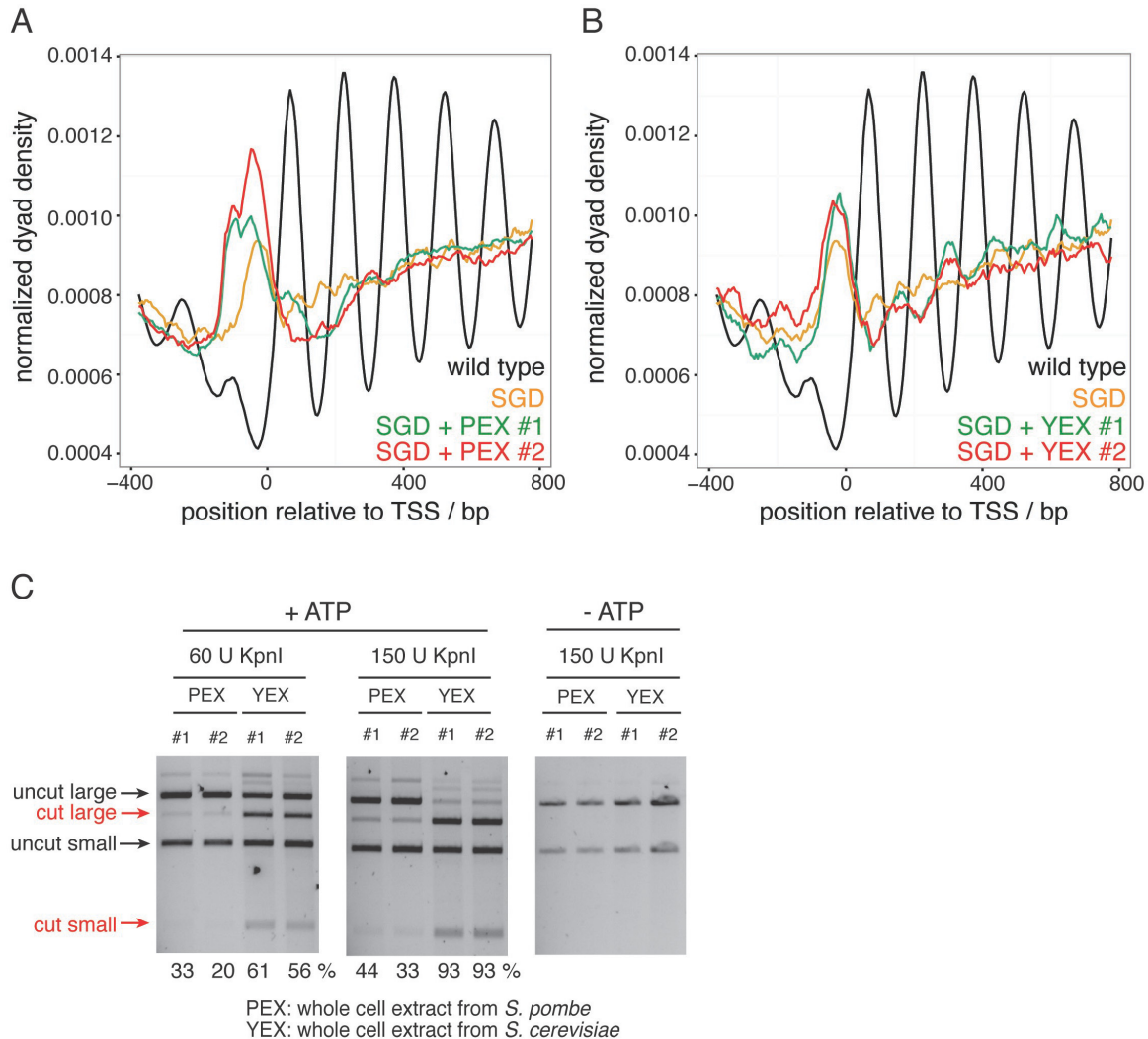
**Figure 2.19 Genome-wide nucleosome pattern of SGD chromatin for *S. pombe* revealed a peak in the *in vivo* NDR in contrast to the SGD chromatin for *S. cerevisiae*.** **A** Composite plots of MNase-seq data of SGD chromatin for *S. pombe* (orange) and of chromatin in wild type cells (black) aligned to *rrp6Δ* TSSs, one replicate shown ( $n = 2$ ). **B** As panel **(A)** but for *S. cerevisiae* (*S. cerevisiae* MNase-ChIP-seq data set from (Krietenstein *et al.*, 2016)).

Next, we asked which factors may change the nucleosome pattern of this SGD chromatin starting material towards a more *in vivo*-like nucleosome pattern. As a first step, we tested a whole cell extract from *S. pombe* (PEX). PEX should include all factors that may be important to generate an *in vivo*-like nucleosome pattern. For *S. cerevisiae*, the same approach could already show that the *S. cerevisiae* whole cell extract (YEX) was able to reconstitute an *in vivo*-like nucleosome pattern *in vitro* (Zhang *et al.*, 2011). Additionally, it was shown that the mechanism is ATP-dependent. Therefore, we wished to test the PEX extract in the *in vitro* reconstitution system for *S. pombe*. In the presence of PEX and ATP in the *in vitro* reconstitution system, the peak upstream of the TSS, where the *in vivo* nucleosome pattern shows an NDR, became higher, broader and shifted a bit upstream compared to the SGD chromatin pattern (Figure 2.20 A). Overall, the *in vivo*-like nucleosome pattern was not reconstituted in contrast to the same approach for *S. cerevisiae*. Additionally, we were interested if the YEX had any effect on the *S. pombe* SGD chromatin. YEX did change the SGD pattern, but we observed no clear difference between the effect of YEX versus PEX on SGD chromatin (Figure 2.20 A and B).

As we knew already from the work with YEX and purified chromatin remodeling enzymes applied to *S. cerevisiae* SGD chromatin that chromatin remodelers are key to nucleosome positioning (Krietenstein *et al.*, 2016), we wondered if the PEX had not enough remodeling activity and if this may be the reason why PEX did not generate a more *in vivo*-like nucleosome positioning pattern. We tested the ATP-dependent remodeling activity of the PEX and compared it to that of the YEX.

For this, we used the KpnI restriction enzyme accessibility assay (Lieleg *et al.*, 2015; Krietenstein *et al.*, 2016). The principle of this assay is that a plasmid is assembled with histone octamers by SGD. The plasmid harbors an array of 25 strong 601 nucleosome positioning sequences. After SGD, the 601 sequences should be occupied with histone

octamers. One of the 601 sequences harbors a unique KpnI restriction enzyme site. The KpnI enzyme is able to cut the plasmid only if the histone octamers are remodeled such that this particular 601 sequence is accessible. The remodeling activity was estimated by the ratio of the sum of cut small and large versus the sum of cut small, cut large and uncut large fragments as quantified after ethidium bromide staining. Two different KpnI concentrations were used to check saturation of the assay (Figure 2.20 C).



**Figure 2.20** *S. pombe in vivo*-like nucleosome pattern could not be reconstituted by incubation of SGD chromatin with whole cell extract from *S. pombe* (PEX). **A** Composite plots of MNase-seq data of SGD chromatin for *S. pombe* alone (orange) or incubated with PEX (two biological replicates: red #1 and green #2), and of wild type cells (black) ( $n = 3$ ) aligned to *rrp6Δ* TSSs. **B** Same as in panel (A) but for incubation with *S. cerevisiae* whole cell extract YEX ( $n = 3$ ). **C** KpnI restriction enzyme accessibility assay with KpnI activities and ATP as indicated for *S. pombe* SGD chromatin incubated with PEX or YEX as in panels (A and B) ( $n = 2$ ). Remodeling activity by this assay was estimated as the ratio of the sum of cut small and large versus the sum of cut small, cut large and uncut large bands according to band intensities after agarose gel electrophoresis and ethidium bromide staining (percentages below lanes) using AIDA software v.4.27 (Raytest).

---

Using the KpnI restriction enzyme accessibility assay revealed that both PEX and YEX were able to remodel nucleosomes and that the remodeling activity was ATP-dependent (Figure 2.20 C). Even though saturation was not reached and both technical replicates for PEX differed substantially, it was nonetheless clear that PEX had less specific remodeling activity than YEX as it always generated much lower KpnI accessibility per time and amount of extract protein. This lower remodeling activity might explain why we did not observe a genome-wide *in vivo*-like nucleosome pattern in the *in vitro* reconstitution system for *S. pombe* as shown for *S. cerevisiae* with the similar *in vitro* approach (Zhang *et al.*, 2011).

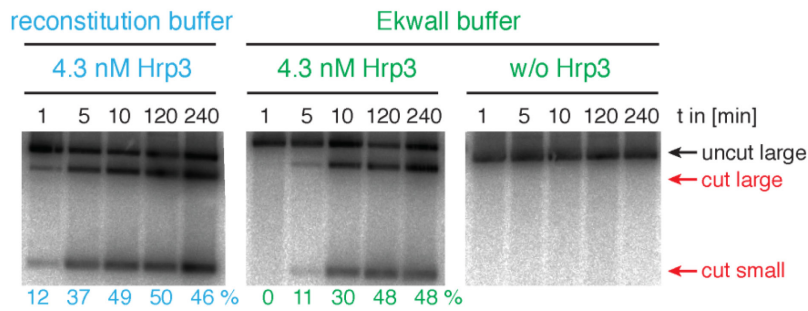
### 2.3.2 *In vitro* reconstitution using purified chromatin remodelers Hrp1 and Hrp3

Since the PEX did not reconstitute the *in vivo*-like nucleosome pattern, we applied a candidate approach to test individual *S. pombe* factors. Krietenstein *et al.* showed nicely that incubation of SGD chromatin with purified factors from *S. cerevisiae* was able to reconstitute *in vivo*-like nucleosome patterns in the presence of ATP (Krietenstein *et al.*, 2016). This *in vitro* reconstitution system using purified factors allowed the dissection of the individual contributions of the purified factors to the nucleosome pattern. Suitable candidates for *S. pombe* were homologous chromatin remodelers, such as Hrp1 and Hrp3, as both are crucial for maintaining nucleosome arrays over gene coding regions *in vivo* (Hennig *et al.*, 2012; Pointner *et al.*, 2012). In collaboration with Punit Prasad (Ekwall group), we purified both remodelers as tagged proteins from *S. pombe*, and used them in the *in vitro* reconstitution system.

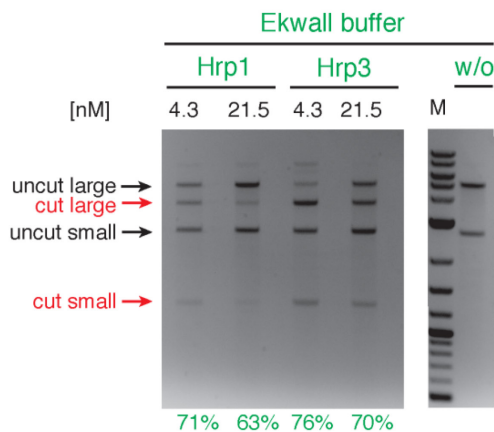
First, the remodeling activity of both chromatin remodelers was tested in the KpnI restriction enzyme accessibility assay. We tested these chromatin remodelers in two different buffer systems, one from our group (reconstitution buffer) and one from the Ekwall group (Ekwall buffer). In the latter, the purification protocols for these remodelers were established (Pointner *et al.*, 2012). Both chromatin remodelers were able to remodel nucleosomes in both buffers (here shown for Hrp3, Figure 2.21 A). Hrp3 showed somewhat faster remodeling kinetics at early time points in the reconstitution buffer (Figure 2.21 A) (Pointner *et al.*, 2012; Krietenstein *et al.*, 2016). Testing two different remodeler concentrations in the Ekwall buffer showed that both remodelers were more active at the lower concentration (Figure 2.21 B), and maybe the specific remodeling activity of Hrp3 was slightly higher than that of Hrp1.

After confirming that purified Hrp1 and Hrp3 were active, we examined if they, alone or in combination and either in reconstitution or in Ekwall buffer, were able to reconstitute genome-wide *in vivo*-like nucleosome patterns, fully or partially, on SGD chromatin for *S. pombe*. However, the *in vivo*-like nucleosome pattern was not reconstituted under any of these conditions (Figure 2.21 C-E). Instead, the peak in the *in vivo* NDR that was already generated by SGD became even more pronounced. This was reminiscent of the effect of PEX and YEX on the SGD pattern (Figure 2.20 A and B).

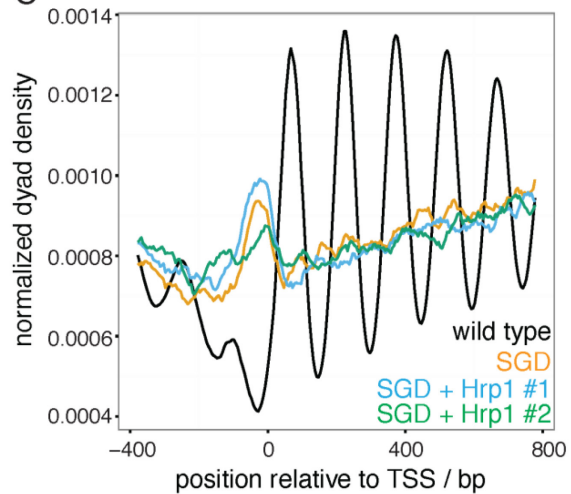
A



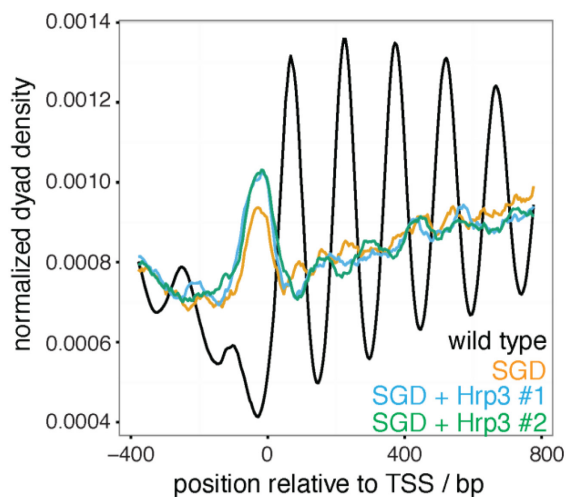
B



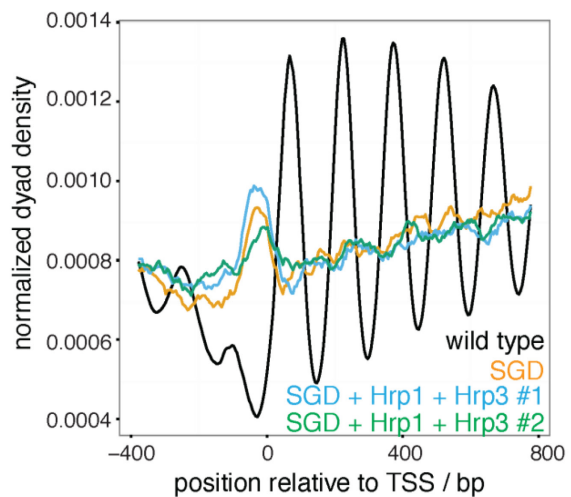
C



D



E

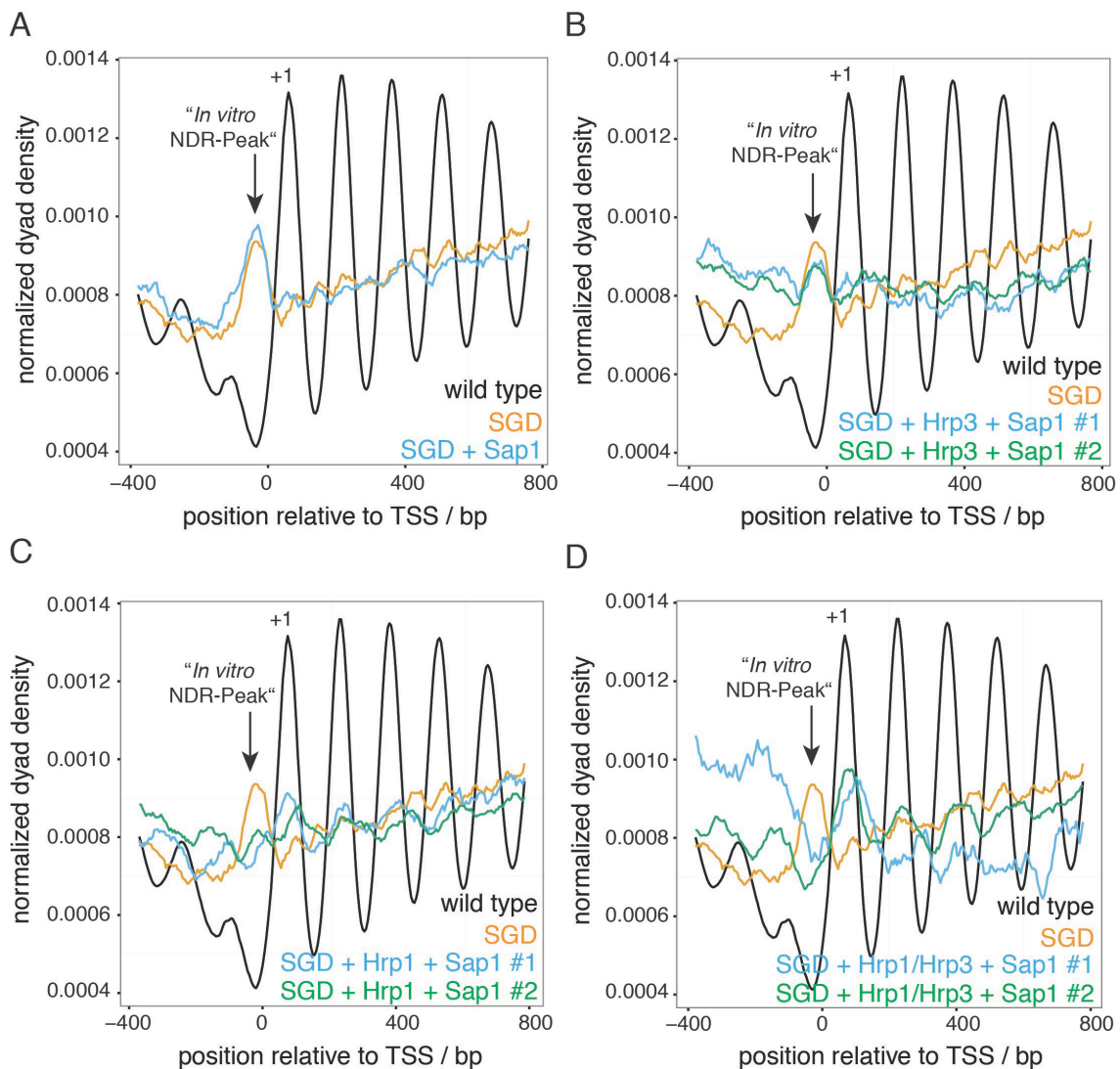


**Figure 2.21** *In vivo*-like nucleosome patterns could not be reconstituted by incubation of SGD chromatin with purified Hrp1 and Hrp3 chromatin remodelers from *S. pombe*. **A** KpnI restriction enzyme accessibility assay as in Figure 2.20 C but with Hrp3 at the indicated concentrations, time points and buffer conditions, and using Southern blotting for detection (therefore the uncut small fragment is not visible). **B** As panel (A) but for the indicated remodeler concentrations and buffer conditions and for 240 min incubation using ethidium bromide for detection. M: 2-Log DNA marker (NEB). **C-E** Composite plots of MNase-seq data as in Figure 2.20 A and B, but for *S. pombe* SGD chromatin (orange) incubated with the indicated remodelers, each at 4.3 nM and in reconstitution buffer (blue #1, n = 2) or Ekwall buffer (green #2, n = 1) aligned to *rrp6Δ* TSSs.



### 2.3.3 *In vitro* reconstitution using purified chromatin remodelers Hrp1 and Hrp3 and the GRF Sap1 as barrier

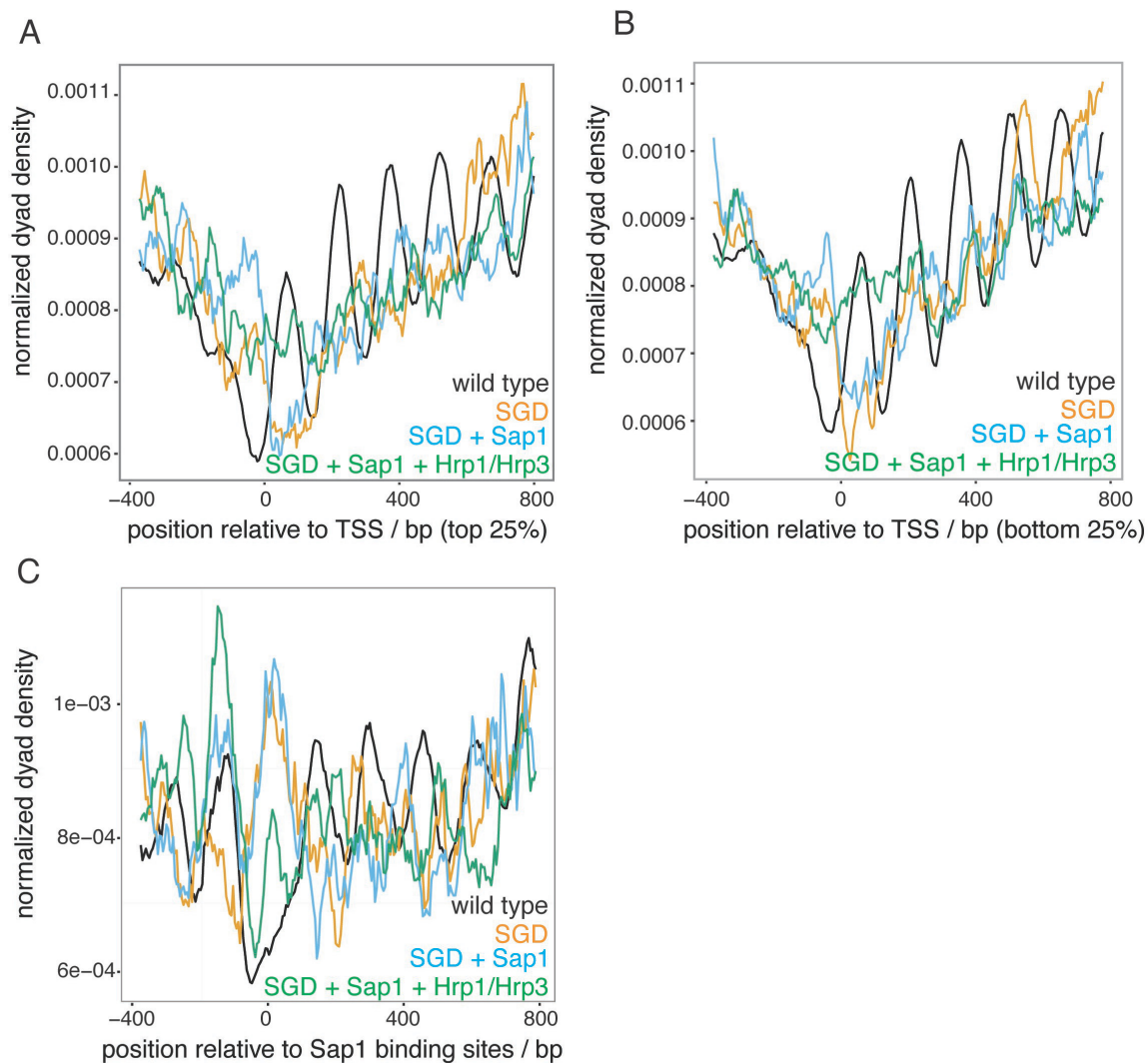
Since the chromatin remodelers failed to reconstitute *in vivo*-like nucleosome patterns on their own, we wondered if other factors could assist the chromatin remodelers. *In vivo*, GRFs were shown to be involved in nucleosome organization. The inactivation of GRFs leads to the gain of nucleosome occupancy at the binding sites of the GRFs (Badis *et al.*, 2008; Hartley and Madhani 2009). In *S. pombe*, Sap1 was discussed to be a potential GRF (Tsankov *et al.*, 2011). The inactivation of Sap1 leads to higher nucleosome occupancy at the Sap1 binding sites, which are otherwise in NDRs. In addition, the chromatin remodeler ISW2 combined with the GRFs Abf1 or Reb1 from *S. cerevisiae* could generate a nucleosome pattern that was dependent on the GRFs and their binding sites (Krietenstein *et al.*, 2016). Therefore, the GRFs acted as a barrier from where or against which the chromatin remodeler ISW2 could set the nucleosomes into arrays. Accordingly, we checked whether Sap1 is a barrier factor in the *S. pombe* reconstitution system. Sap1 was tested with and without the chromatin remodelers Hrp1 and/or Hrp3 with either the reconstitution buffer or the Ekwall buffer (Figure 2.22). Sap1 alone was not able to change the nucleosome organization (Figure 2.22 A). This was expected as no remodeling activity is described for Sap1 and nucleosomes do not move much *in vitro* under our reconstitution conditions without an ATP-dependent remodeler (Zhang *et al.*, 2011; Krietenstein *et al.*, 2016). Also with Sap1 and Hrp3 there was not much change (Figure 2.22 B). In contrast, Sap1 together with Hrp1 led to a slight but noteworthy change, especially in the *in vivo* NDR (Figure 2.22 C). The prominent “*In vitro* NDR-Peak” of the SGD chromatin was moved towards the position where the +1 nucleosome was observed *in vivo*. This effect became even stronger if the SGD chromatin was incubated together with Sap1, Hrp1 and Hrp3 (Figure 2.22 D). This argued for some barrier-dependent nucleosome positioning by the remodelers, at least by Hrp1. Nonetheless, there was no further *in vivo*-like nucleosome organization visible such as nucleosome arrays over the gene coding regions.



**Figure 2.22** The *in vivo*-like nucleosome pattern could not be reconstituted by incubation of SGD chromatin with the chromatin remodelers Hrp1 and Hrp3 and the GRF Sap1 from *S. pombe*. A-D Composite plots of MNase-seq data of wild type cells (black) or SGD chromatin for *S. pombe* (orange) incubated with Sap1 (A) Sap1 and Hrp3 (B), Sap1 and Hrp1 and (C) Sap1 and Hrp1/Hrp3 (D) in reconstitution buffer (blue #1,  $n = 1$ ) or Ekwall buffer (green #2,  $n = 1$ ) aligned to *rrp6Δ* TSSs.

As the composite plots so far included all genes, we wondered if the barrier effect may be more pronounced for genes with Sap1 binding sites in their promoter NDRs. First, we used the Sap1 binding site annotation from Tsankov *et al.* 2011 and ranked the genes with Sap1 binding sites according to the degree of nucleosome occupancy change at the Sap1 binding sites upon ablation of Sap1 (Tsankov *et al.*, 2011). The nucleosome occupancy change was defined as difference of nucleosome occupancy between the wild type and *sap1 ts* strain grown at restrictive conditions. The top 25% genes showed a high nucleosome occupancy change and a Sap1 binding site motif. The bottom 25% genes showed lower or no nucleosome occupancy change and almost no Sap1 binding sites (Tsankov *et al.*, 2011). Unfortunately, there was no clear nucleosome pattern observable, neither for the top 25% nor for the bottom 25% genes (Figure 2.23 A and B).

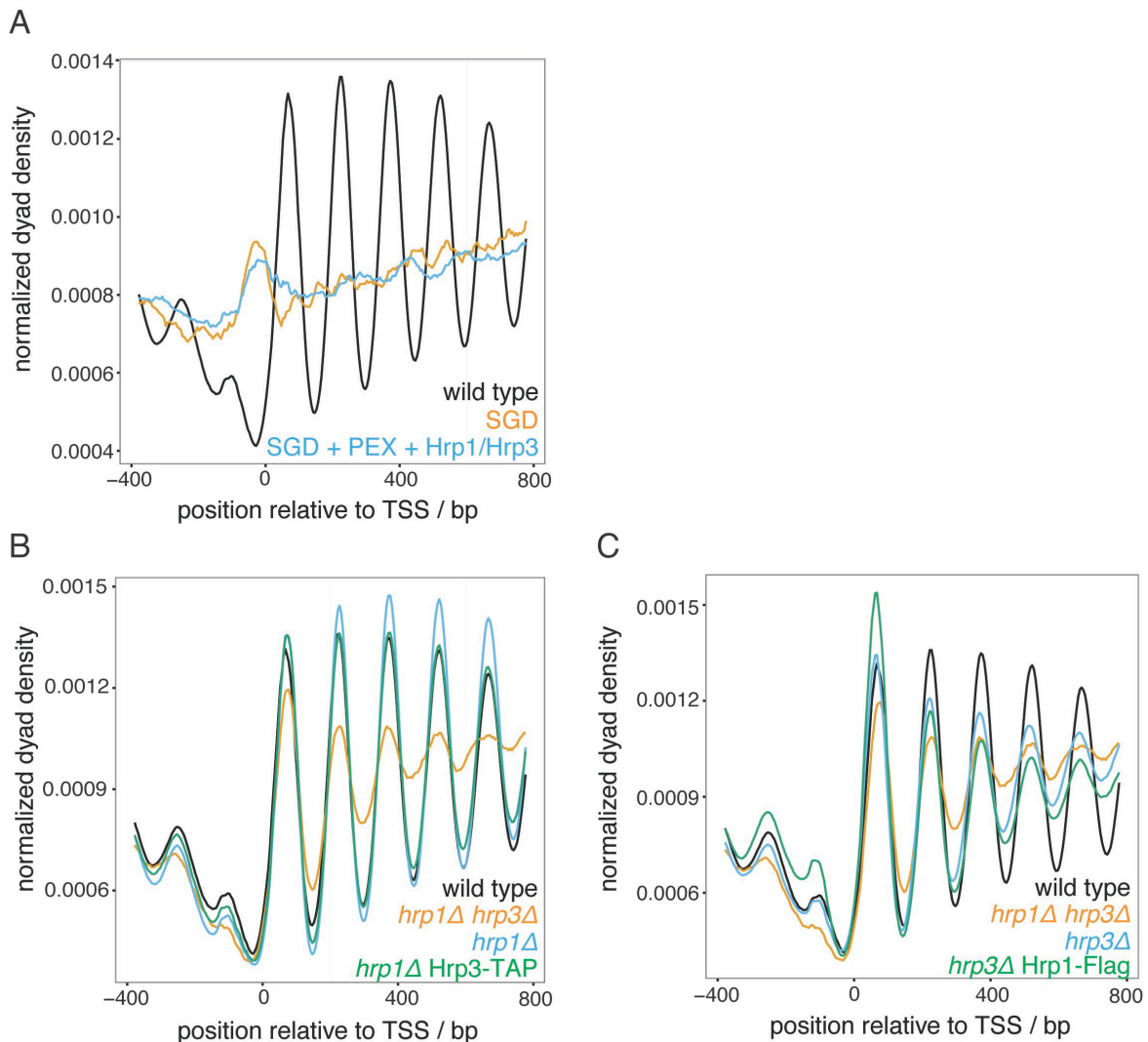
Second, we annotated Sap1 binding sites using the published binding motif for a position weight matrix analysis and aligned the MNase-seq data to these Sap1 binding sites (Figure 2.23 C). There was a slight difference between the patterns of SGD, SGD with Sap1 and SGD with Sap1 and Hrp1/Hrp3, but, unfortunately, there was no nucleosome pattern at Sap1 binding sites, here shown for Sap1 and Hrp1/Hrp3.



**Figure 2.23 Nucleosome pattern at the Sap1 binding sites and at genes with or without Sap1 binding sites.** **A-B** MNase-seq data of wild type cells (black) and of *S. pombe* SGD chromatin (orange) incubated with Sap1 (blue) and Hrp1, Hrp3 remodelers (green). Data were aligned to aligned to *rrp6Δ* TSSs with only the top **(A)** or bottom **(B)** 25% of genes (1106 and 1105 genes, respectively) with regard to nucleosome pattern changes upon ablation of Sap1 *in vivo* (Tsankov *et al.*, 2011). **C** MNase-seq data of wild type cells (black) and of *S. pombe* SGD chromatin (orange) incubated with Sap1 (blue) or Sap1/Hrp1/Hrp3 (green). Data were aligned at Sap1 binding sites (504 Sap1 binding sites), which were determined by Sap1's PWM (Badis *et al.*, 2008).

As neither the PEX alone nor purified candidate remodelers, with or without GRF, were able to transform the SGD chromatin pattern into something much more *in vivo*-like, we tried to boost the PEX, which was otherwise a bit poor regarding remodeling activity, by adding the purified remodelers. The idea behind this was that the PEX probably contained a variety of GRFs, which could help to guide the Hrp1/Hrp3 chromatin remodelers to

position nucleosomes into the right nucleosome organization. Unfortunately, the PEX supplemented with the Hrp1 and Hrp3 chromatin remodelers was still not able to reconstitute the *in vivo*-like nucleosome pattern (Figure 2.24 A).



**Figure 2.24** The *in vivo*-like nucleosome pattern could not be reconstituted by incubation of SGD chromatin with the chromatin remodelers Hrp1 and Hrp3 and PEX from *S. pombe*. The tag of Hrp1 and Hrp3 did not compromise their function *in vivo*. **A** Composite plots of MNase-seq data of wild type (black) and SGD chromatin for *S. pombe* (orange) incubated with PEX and Hrp1/Hrp3 (blue,  $n = 1$ ) aligned to *rrp6Δ* TSSs. **B-C** Composite plots of *in vivo* MNase-seq data of wild type (black,  $n = 2$ ) and *hrp1Δ hrp3Δ* (orange,  $n = 2$ ), *hrp1Δ* (blue,  $n = 2$ ) and *hrp1Δ Hrp3-TAP* (green,  $n = 2$ ) (**B**) or *hrp3Δ* (blue,  $n = 2$ ) and *hrp3Δ Hrp1-Flag* (green,  $n = 2$ ) (**C**) *S. pombe* strains aligned to *rrp6Δ* TSSs.

We wondered if addition of the tag to the chromatin remodelers for protein purification could be problematic for their remodeling activity and could cause a functional problem (prompted by personal communication by Tamas Fisher). Therefore, we checked by MNase-seq the *in vivo* nucleosome patterns of the strains used for remodeler purification. In these strains, the tagged chromatin remodeler was the only copy of this remodeler type and the other remodeler type was absent by deletion of the corresponding gene. The respective nucleosome pattern was compared to the pattern of the corresponding strain with the untagged remodeler version. In addition, the *hrp1Δ hrp3Δ* double mutant was

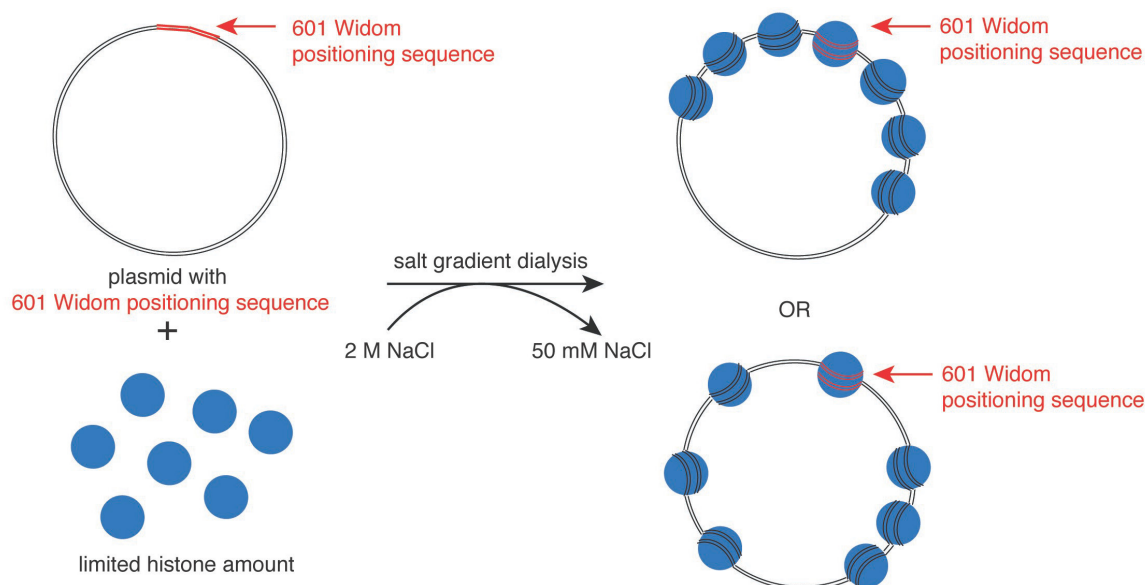
also assessed as a positive control for the major effect on nucleosome organization in the absence of both functional chromatin remodelers, Hrp1 and Hrp3. With this type of assay, we did not see a relevant difference between tagged or untagged versions of Hrp1 or Hrp3 (Figure 2.24 B and C). Therefore, the tags did not seem to influence the remodeling activity and function of these chromatin remodelers.

Taken together, neither the PEX whole cell extract nor three purified candidate factors from *S. pombe* were able to reconstitute the genome-wide *in vivo*-like nucleosome pattern. Nonetheless, there are more potential candidates that need to be tested in the *in vitro* reconstitution system, such as other chromatin remodeler classes, like INO80 or SWI/SNF.

### 2.3.4 Cooperativity between nucleosomes during SGD chromatin assembly

One striking observation in the context of reduced nucleosome density *in vivo* and *in vitro* was that closely spaced MNase ladders were still visible arguing for close packing of nucleosomes (= nucleosome clusters). For example, *S. cerevisiae* cells lacking the Nhp6a and Nhp6b proteins contain less nucleosomes than wild type cells, but the digest of the chromatin with MNase led to MNase ladders with wild type spacing (Celona *et al.*, 2011). A similar observation was made *in vitro* if SGD chromatin with low nucleosome density was digested with MNase, the same spacing was obtained compared to high nucleosome density (Lieleg *et al.*, 2015). *In vivo*, one explanation might be that other factors keep the nucleosome together. *In vitro*, exclusively DNA and histones are present during salt gradient dialysis. Hence, further factors are excluded to keep the nucleosome together. Cooperativity during nucleosome assembly may explain why nucleosomes stay together at low nucleosome density also in the absence of other factors. We wished to deal with the question if the nucleosomes assemble in a cooperative manner during salt gradient dialysis, or if they assemble randomly.

To distinguish between these alternatives we designed different plasmids each containing just one 601 Widom positioning sequence. The 601 Widom positioning sequence should function as a high affinity site for the histones during SGD assembly, i.e., become preferentially assembled into a nucleosome even at low nucleosome density. If nucleosome assembly were cooperative, the nucleosome at the 601 sequence could serve as a seed and lead to preferential assembly of flanking nucleosomes relative to assembly on other parts of the plasmid. Conversely, if assembly were at random, the neighborhood of the 601 sequence should show similarly abundant closely packed arrays as any other region of the plasmid (Figure 2.25). The plasmids were assembled with a range of histone concentrations and digested at different MNase concentrations. The resulting DNA fragments were detected by Southern blot analysis using DNA probes recognizing the 601 Widom positioning sequence or a DNA sequence distant to the 601 Widom positioning sequence, called backbone probe.

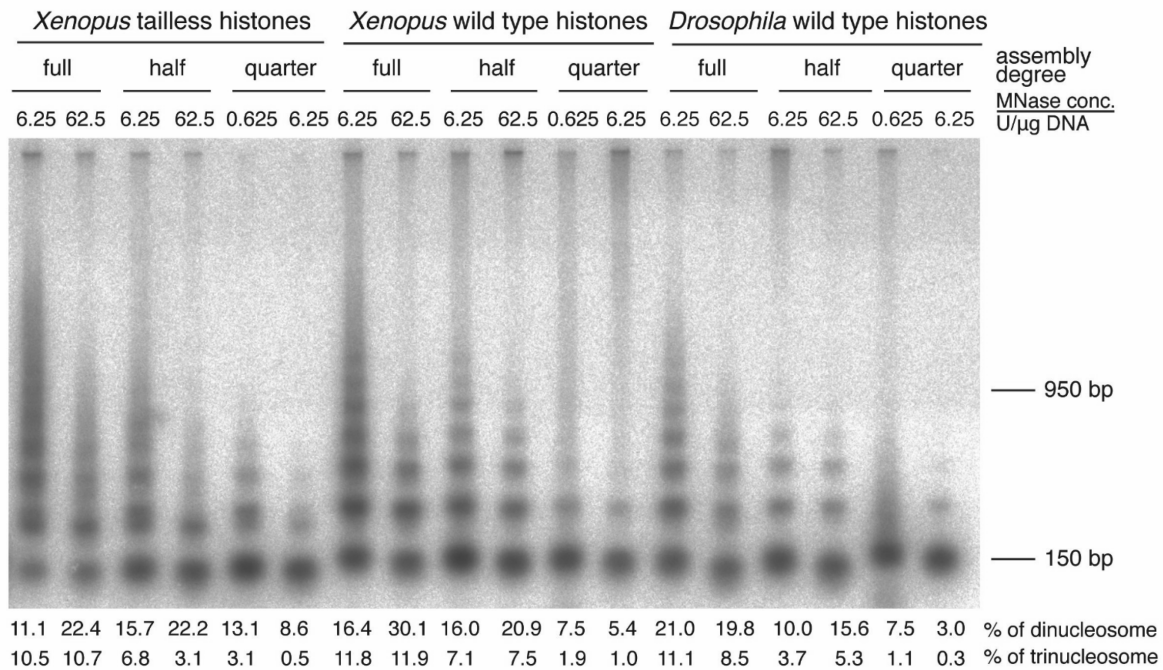


**Figure 2.25 Experimental concept to test cooperativity during salt gradient dialysis nucleosome assembly.** Plasmids were assembled into chromatin with limited amounts of histone octamers. Plasmids harbored a 601 Widom positioning sequence (highlighted in red). The idea would be that 601 Widom positioning sequence functions as a seed; if chromatin assembly by salt gradient dialysis was cooperative the histone octamers should preferentially assemble around the 601 Widom sequence and we would see nucleosome clusters preferentially around the 601 Widom positioning sequence. If histone octamers were randomly distributed over the plasmid, we would not see an enrichment of nucleosome clusters around the 601 Widom positioning sequence.

#### 2.3.4.1 Nucleosome cluster formation is independent of assembly degree and histone-tails during SGD chromatin assembly

We tested different SGD assembly degrees (full, half and quarter according to a lab-internal standard) by varying the histone amount relative to a fixed DNA concentration of the same plasmid. We also used histones derived from different species. We observed MNase ladders indicative of nucleosome clusters for all three assembly degrees with the extent of the MNase ladders depending on both the MNase concentration and the assembly degree (Figure 2.26).

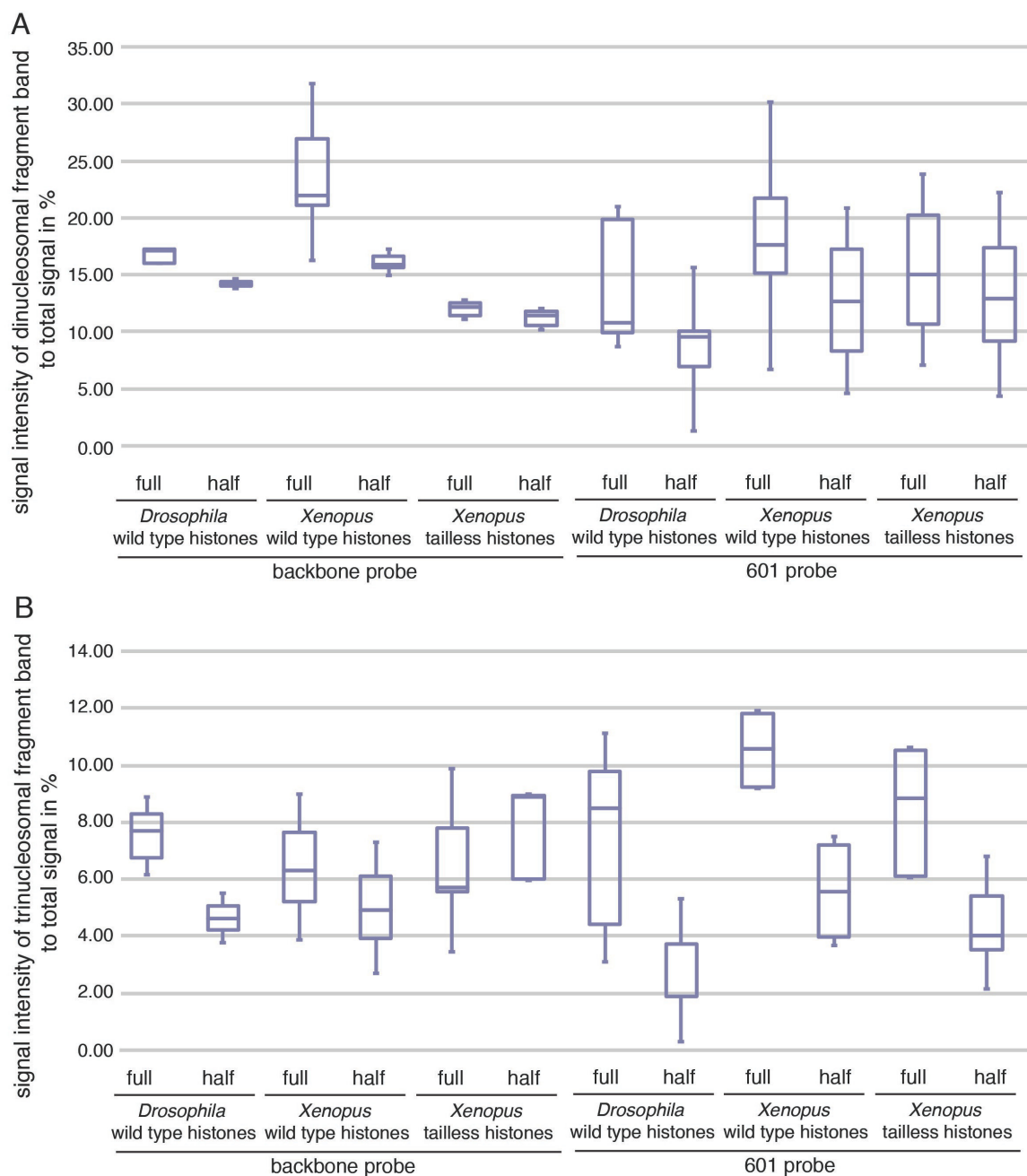
We asked if the observed nucleosome cluster formation might depend on the histone-tails due to their interactions with DNA and/or neighboring nucleosomes. So we repeated similar experiments with all tailless histone octamers. We still observed nucleosome clusters (Figure 2.26).



**Figure 2.26 Nucleosome clusters were visible for all tested conditions.** SGD chromatin was assembled with the indicated assembly degrees and histones and digested by the indicated MNase concentrations. MNase digestion fragments were visualized by Southern blot probing against the 601 positioning sequence. Calculation of signal intensities of di-/trinucleosomal fragments compared to total signal intensities of corresponding lane was done as described in chapter 4.2.12.

The occurrence of di- and especially trinucleosomal fragments was taken as indicator of clusters with tightly spaced nucleosomes. Exact quantification of these fragments from such MNase digests is not possible as the digestion is always a limit digest and does not reach a plateau as it would eventually digest even the nucleosomes. Therefore, each digestion degree corresponds to an arbitrary intermediate state and the intensity of each band depends on this digestion degree. Nonetheless, the maximum intensity of a band at any of the tested digestion degrees provides an estimate of the minimal abundance of the corresponding, for example, di- or trinucleosomal state. The cluster abundance may be even higher at a different, but not tested digestion degree. Calculating the signal intensity of the tri- and also the dinucleosomal band relative to total signal intensity of the corresponding lane revealed that such conservative estimation still corresponded to an appreciable fraction derived from dinucleosomal or trinucleosomal fragments (Figure 2.27). This was not only true for fully assembled chromatin, but, more importantly, also for half-assembled chromatin, and also for histones derived from different species. There was no clear difference between the region around the 601 Widom positioning sequence or the backbone region. The calculation for tailless histones resulted in similar nucleosome cluster frequency as for histones with tails. This observation seemed to hint towards a cooperativity during SGD chromatin assembly, although no “seed-effect” for the 601 sequence was apparent. However, it was not a priori clear if the observed cluster frequency may still be compatible with a random, non-cooperative assembly.



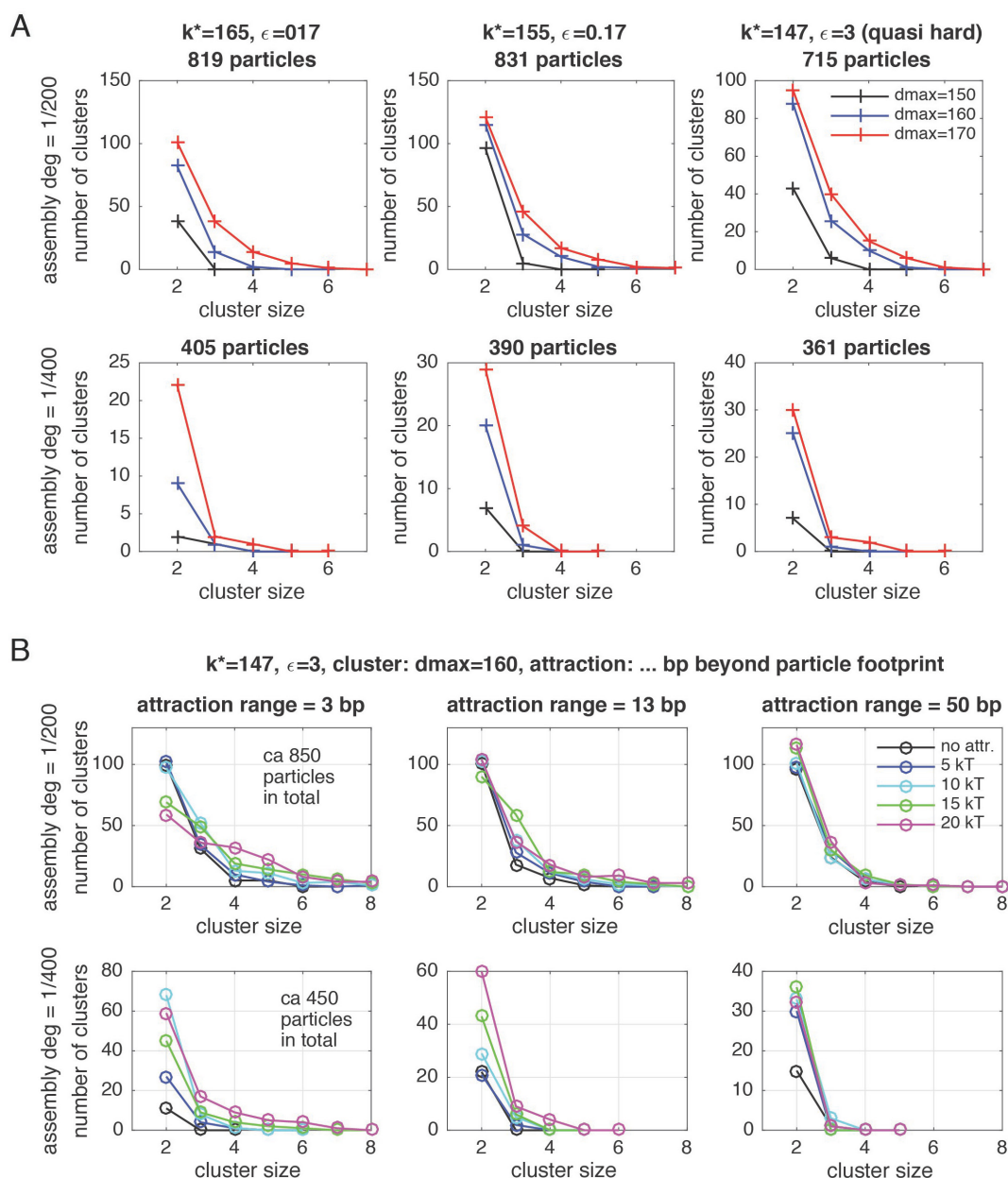


**Figure 2.27 Substantial fraction of digested SGD chromatin derived from di/trinucleosomal fragment.**  
**A** Box plot of signal intensity quantification of the dinucleosomal fragment bands derived from different Southern blot analyses ( $n = 3$ ). Calculation of signal intensities of dinucleosomal fragment compared to total signal intensity of corresponding lane was done as described in chapter 4.2.12. Quarter assembly degrees were not considered due to high variations in the MNase digestion degree.  
**B** As described in panel **(A)** but for the trinucleosomal fragment bands.

#### **2.3.4.2 Simulation of nucleosome assembly revealed that the observed cluster frequency can hardly be explained without cooperativity**

In order to estimate which frequency of nucleosome clusters could be expected by random assembly and how cooperativity alters this frequency we turned to simulations. For simulation without cooperativity we varied parameters such as nucleosome-nucleosome interaction, assembly degree and center-to-center distance of nucleosomes in a cluster (= how close together nucleosomes have to be to constitute a “cluster”) (Figure 2.28 A) (Osberg *et al.*, 2014; Osberg *et al.*, 2015). We found that for the center-to-center distance  $d_{max} = 160$  bp, which corresponds to a 14 bp linker and about to the spacing observed by MNase ladders, clusters with more than two nucleosomes were exceedingly rare, less than 3% at the half assembly degree (Figure 2.28 A). However, our experiments yielded percentages of trinucleosome clusters that were clearly higher than 3%, even up to 10% (Figure 2.27 B).

We then investigated how cooperativity increased the cluster frequency (Figure 2.28 B). As expected, increasing cooperativity significantly increased cluster frequencies. The strongest effects were observed for short range attractions (3 bp), where clusters of three to six nucleosomes are boosted from almost non-existence (Figure 2.28 A) to an appreciable fraction of the total number of nucleosomes (Figure 2.28 B). This calculation supports the notion that the cluster fractions observed in the experiments argue for a certain degree of cooperativity (interaction energy of at least 10 kT) during SGD chromatin assembly and can hardly be explained by a random distribution of nucleosomes.



**Figure 2.28 Cooperativity significantly increases nucleosome cluster frequency.** **A** Histograms of the number of nucleosomes clusters of various sizes (where the size is the number of nucleosomes in a cluster). We produced ensembles of nucleosomes positioned on DNA respecting steric hindrance but without cooperativity, namely for soft-core repulsion with a nucleosome footprint range of  $k^* = 165$  bp (left column) and  $k^* = 155$  bp (middle column) both with stiffness of  $\epsilon = 0.17$ , and, for comparison, for quasi-hard-core nucleosomes footprint  $k^*=147$  and stiffness  $\epsilon= 3$  (right column), each for full (top row) and half (bottom row) assembly degree. Assembly degree = 1/200 correspond to full assembly degree and assembly degree = 1/400 corresponds to half assembly degree. We then defined a maximum center-to-center distance (dmax) for when nucleosomes are counted as belonging to a cluster (dmax = 150, 160 and 170 bp, shown black, blue, red). Number of particles used for simulation were indicated in the corresponding graph. **B** Histograms of cluster frequencies, using dmax = 160 bp (compare to blue lines in graphs without cooperativity, panel **A**). We again produced ensembles of nucleosomes on DNA, this time with nucleosome-nucleosome attraction to model cooperative assembly. We chose three exemplary attraction ranges, quasi-contact interaction (3 bp, left column), attraction range equals linker length (middle column) and a longer range attraction of 50 bp (right column). For each, we produced nucleosome ensembles for varying attraction strength (shown in different colors). Assembly degree = 1/200 correspond to full assembly degree and assembly degree = 1/400 corresponds to half assembly degree.

### 2.3.4.3 Supplementary materials

The plasmid containing one 601 Widom sequence (V1\_601) was constructed using the plasmid pFBDM\_ACF1\_DominoB\_Flag\_N (V1) (kind gift of Dr. Kenneth Börner) and the 601 Widom sequence derived from the 601-25mer designer array (Lieleg *et al.*, 2015). The plasmid pFBDM\_ACF1\_DominoB\_Flag\_N was digested with PmeI according to standard protocols as described on [www.neb.de](http://www.neb.de). The 601 Widom sequence was amplified according to standard protocols as described on [www.neb.com](http://www.neb.com) using primers (601\_F/R) and the plasmid 601-25mer designer array. Digested plasmid pFBDM\_ACF1\_DominoB\_Flag\_N and amplified 601 Widom sequence were ligated according to standard protocols as described on [www.neb.com](http://www.neb.com) and transformed into *E. coli* (chapter 4.1.2). The probes for Southern blot analysis were amplified according to standard protocols as described on [www.neb.de](http://www.neb.de) using primers (601\_F/R) for 601 Widom sequence probe or primers hyb\_outside601\_R/F and plasmid V1\_601 (Table 2.8).

**Table 2.8 Primer sequences used for cloning of V1\_601 plasmid and for probe amplification**

Name	Sequence
601_F	CAGGATGTATATATCTGACAC
601_R	CGGCACCGGGATTCTCCAGG
hyb_outside601_R	GCTGGCCTTTTGCTCACATG
hyb_outside601_F	GTATCTTATAGTCCTGTC

---

## **3 Discussion**

### 3.1 Promoter organization in *S. pombe*

In this thesis, we used CAGE-seq to perform genome-wide TSS annotation and detailed analysis of the promoter structure in *S. pombe*, not only for the wild type strain, but also for an exosome mutant and two chromatin factor mutants. Here, the main focus was the identification of minimal criteria for promoter structure by looking at a specific subset of TSSs, the CSCT-TSSs arising in the chromatin factor mutants, *spt6-1 ts* and *hrp1Δ hrp3Δ*.

#### 3.1.1 TSS annotation by CAGE-seq revealed a close overlap with other high-resolution TSS annotations

The wild type TSS annotation in *S. pombe* was recently investigated by different groups, since high-resolution TSS annotation in *S. pombe* was not available, so far (Li *et al.*, 2015; Booth *et al.*, 2016; Eser *et al.*, 2016). The TSS annotation was improved by RNA-seq with improved annotation algorithm (Eser *et al.*, 2016), or CAGE-seq (Li *et al.*, 2015) and Pro-cap-seq (Booth *et al.*, 2016), with the latter two techniques specifically mapping the 5' cap of the transcript, which is the exact start position of the transcript. Booth *et al.* compared their TSS annotation derived from Pro-cap-seq with the recently published TSS annotation derived from RNA-seq by Eser *et al.*, 2016 and ascertained a close overlap between both TSS annotations. We also wished to compare our CAGE-seq data sets with already published CAGE-seq data sets (Li *et al.*, 2015). However, this turned out to be difficult. The correlation of both raw data was low. In this context, we faced the problem that there is no standardized method for the comparison or correlation of this kind of transcriptome data (personal communication by Vicente Pelechano) and that the usual correlations are mainly influenced by the noise rather than by the actual TSS peaks. On the other hand, the quality and quantity of TSS annotation does not only depend on the methods used to define the TSSs (RNA-seq vs. CAGE-seq), but also on the bioinformatical strategy. We reanalyzed the published Li *et al.*, 2015 data set with our own bioinformatical pipeline to overcome the problem of different settings and criteria. In total we identified less TSSs compared to their pipeline (4347 vs. 7859), which underlines how critical and different the results of annotation methods could be. Nevertheless, we decided to use relative distance analysis (Favorov *et al.*, 2012) for comparison between data sets, and nucleosome data for validation of accuracy (Figure 2.2 and Figure 2.4). By both criteria, both data sets agree very well. The nucleosome structure was more pronounced if nucleosome data are aligned to our TSSs. The alignments of nucleosome data to the TSSs from Booth *et al.*, 2016, Eser *et al.*, 2016 and Li *et al.*, 2015 overlapped well with the alignment of same nucleosome data to our TSS annotation (Figure 2.4 C-E) (Li *et al.*, 2015; Booth *et al.*, 2016; Eser *et al.*, 2016).

Interestingly, using our TSS annotation for the alignment of nucleosome data revealed that the +1 nucleosome is more downstream as compared to the previous TSS annotations from Lantermann *et al.*, 2010 and Rhind *et al.*, 2011 (Figure 2.4 A and B) (Dutrow *et al.*, 2008; Lantermann *et al.*, 2010; Rhind *et al.*, 2011). This is interesting

because it shows how critical it is to use an adequate method for TSS annotation, in this case a method which is specific to map the start site of transcripts. Otherwise it might change the interpretation of results.

Furthermore, we annotated not only the TSSs from wild type strain, but also from different mutant strains using CAGE-seq. The TSS annotation of different strains allowed us to align the nucleosome data to their corresponding TSSs for the first time (Figure 2.6). In the *spt6-1 ts* mutant the nucleosome pattern seemed to be less compromised when aligned to the corresponding TSSs compared to *rrp6Δ* TSSs (Figure 2.6 B and D). There was a slight difference in case of the alignment of the *hrp1Δ hrp3Δ* nucleosome data to their corresponding TSSs vs. *rrp6Δ* TSSs. These differences indicate that it is crucial to use the proper TSS annotation to avoid misinterpretation of effects.

Taken together, the comparison of our TSS annotation to the published TSS annotations, using relative distance analysis and chromatin structure as quality criteria, indicates that our TSS annotation by CAGE-seq is reliable.

### **3.1.2 Promoters with sharp or broader TSS peak distribution harbored both similar chromatin structure in *S. pombe***

Our TSS annotations of wild type and *rrp6Δ* mutant cells revealed that the promoters in *S. pombe* can be divided into at least two different classes depending on sharp or broader TSS peak distribution (Figure 2.3 and Table 2.2). This is consistent with the findings of Li *et al.*, 2015. They defined four different promoter classes due to the TSS peak distribution (single dominant peak, broad with a single dominant peak, broad with bi- or multi- peaks, and generally broad distribution). Our and their analyses confirmed that the majority of promoters harbors a sharp TSS distribution. The appearance of promoters with diverse TSS peak distributions in *S. pombe* shows the diversity and complexity of transcription regulation in a unicellular organism. Two promoter classes, sharp vs. broad, are found in higher eukaryotes, whereby the TSS peak distribution shows a clear bimodal characteristic. The sharp promoters are less prominent in higher eukaryotes (Carninci *et al.*, 2006; Suzuki *et al.*, 2009; Ni *et al.*, 2010). There, sharp promoters harbor core promoter elements such as TATA box motif, Inr or BRE (Juven-Gershon *et al.*, 2008). In mammals, the CpG islands, which are not present in *S. pombe*, are associated with broad promoter structure (Lenhard *et al.*, 2012). The different regulation mechanisms of different promoter classes and their characteristics, such as DNA sequence motifs, transcription factor binding sites or presence of histone variants/modifications, still need further investigations in *S. pombe*.

Two promoter-associated nucleosome organizations are discussed in *S. cerevisiae* (Tirosh and Barkai 2008). One promoter class is described to harbor a stereotypical NDR-array pattern with an NDR closely upstream of the TSS and well-positioned +1/-1 nucleosomes up- and downstream of the NDR. The other promoter class harbors a more dynamic nucleosome organization with non-stereotypical but promoter-specific nucleosome

organizations in the promoter region. Consistent with the findings in *S. cerevisiae* promoter regions, different promoter classes in higher eukaryotes also have diverse nucleosome organizations. Broad promoters harbor a defined and stereotypical nucleosome organization, whereas sharp promoters seem to have more individual or less organized nucleosome pattern (Rach *et al.*, 2011). However, while the two types of promoter nucleosome organizations in mammals correlates with the occurrence of single vs. multiple TSSs, we did not find differences in the nucleosome pattern between the promoters with sharp vs. broader TSS peak distribution in *S. pombe* (Figure 2.5). Both promoter classes showed the same stereotypical nucleosome pattern such as the NDR, +1 nucleosome and nucleosome arrays over the gene coding region. They harbored similar NDR lengths and +1 nucleosome fuzziness, which might indicate that TSS positions and +1 nucleosome positions do not in general have a direct causal relationship. Another interesting aspect would be to look at chromatin-associated features such as histone variants or histone modifications, and if there is any distinction between the promoter classes. For example the histone variant H2A.Z is found at the +1 nucleosome position in promoter regions (Guillemette *et al.*, 2005; Raisner *et al.*, 2005; Albert *et al.*, 2007; Buchanan *et al.*, 2009).

### **3.1.3 Minimal criteria to define a promoter region in *S. pombe***

We looked at the TSSs, which are exclusively present in the chromatin factor mutants, *spt6-1 ts* and *hrp1Δ hrp3Δ*, and seemed to be blocked by the chromatin structure in our reference conditions, the exosome mutant *rrp6Δ*. We defined the *rrp6Δ* mutant as our reference to exclude all transcripts that occur in wild type strains, no matter if usually detected or “cryptic” due to fast RNA degradation by the exosome degradation system. The novel occurrence of CSCTs in the absence of chromatin factors was already reported in literature, but their TSSs and other features and characteristics of the CSCTs were not investigated in *S. pombe*, or any other species, so far (Cheung *et al.*, 2008; Pointner *et al.*, 2012; Shim *et al.*, 2012; DeGennaro *et al.*, 2013; Uwimana *et al.*, 2017). The CSCTs are mostly found at exons in antisense direction (Figure 2.14). This is consistent with previous findings that *spt6-1 ts* and *hrp1Δ hrp3Δ* are required for repression of antisense transcripts in *S. pombe* (Pointner *et al.*, 2012; Shim *et al.*, 2012; DeGennaro *et al.*, 2013). This seems to be conserved among *S. pombe* and *S. cerevisiae*. Increased antisense transcription also arises in the *spt6-1004* mutant in *S. cerevisiae*, which is equivalent to the *spt6-1 ts* mutant in *S. pombe* (Cheung *et al.*, 2008; Uwimana *et al.*, 2017). The number of our identified CSCTs seems to be quite low (Figure 2.8 B), especially if compared to the number of identified cryptic transcripts in the *S. cerevisiae spt6-1004* mutant (Uwimana *et al.*, 2017). There might be several reasons for the different numbers such as the methods used to annotate the cryptic transcripts (RNA-seq vs. CAGE-seq, as well as different bioinformatics, e.g., different thresholds), the used reference strains (wild type vs. *rrp6Δ* mutant) and growth conditions (*spt6-1004* mutant grown at fully restrictive conditions of 37°C and *spt6-1 ts* mutant grown at less restrictive conditions of 32°C). Using CAGE-seq enabled the



---

detection of transcripts with 5'-cap structure, which is specific for start sites of transcripts, and truncated transcripts are neglected. The advantage of using the *rrp6Δ* mutant as reference was that it enabled the annotation of transcripts in the chromatin factor mutants, which are specific for these mutants. Using less restrictive growth conditions enabled the detection of the strongest transcripts, since they already arose under less restrictive conditions.

We assume that such CSCT-TSSs represent fortuitous promoters that did not evolve as bona fide functional promoters, i.e., are hardly ever used in wild type cells. Nonetheless, these CSCT-TSSs may come up also in wild type cells under special circumstances, e.g., starvation or meiosis, or may correspond to transcripts that are rapidly degraded by pathways not affected in the *rrp6Δ* mutant, e.g., the cytosolic exosome or the RNAi pathway. Fortunately, the Bähler group made available to us so far unpublished RNA-seq data for all of these conditions or respective mutant strains. We annotated the TSSs of these RNAs and compared them to our CSCT-TSSs. We saw only a small overlap (for *spt6-1 ts* mutant 49 out of 173 CSCT-TSSs and 25 for *hrp1Δ hrp3Δ* out of 100 CSCT-TSSs). This confirms the assumption of fortuitous promoters as the CSCTs seem to be specific for disrupted chromatin structure conditions and do not correspond to TSSs that are used in wild type cells or under any other conditions or rapidly degraded by any of the known RNA degradation pathways. Therefore, these CSCT-TSSs should allow characterizing the minimal features sufficient for transcription initiation as such without convolution by additional features, like regulation, that probably evolved for promoters that are actually functional in wild type cells.

What are the minimal promoter features according to the analysis of the fortuitous CSCT-TSSs? We looked at chromatin organization around the CSCT-TSSs, average expression levels around the CSCT-TSSs, DNA features such as DNA shape and DNA motifs. We showed a relationship to the +1 nucleosome position, a location for CSCT-TSSs in generally upregulated regions, an enrichment of the DNA roll shape for all TSSs and a GC skew for some TSSs.

The identified CSCT-TSSs in the chromatin factor mutants *spt6-1 ts* and *hrp1Δ hrp3Δ* barely overlap indicating two classes (Figure 2.8 B). This observation might have several implications. First, the chromatin disruption is different in both mutants. Second, the initiation of these transcripts might be regulated through different mechanism.

Speaking for a similar mechanism of transcription initiation, the following features were shared features of the CSCT-TSSs in both chromatin factor mutants. The first feature is the chromatin structure around the CSCT-TSSs. We observed a defined position of the CSCT-TSS relative to the +1 nucleosome (Figure 2.10). The CSCT-TSSs are localized to the very 5'-flank of the corresponding +1 nucleosome. This feature is shared with the canonical TSSs and therefore seems to be an important relationship between any TSS and +1 nucleosomes in *S. pombe*. Strictly speaking, we cannot conclude if this +1 nucleosome position is causally responsible for the appearance of CSCT-TSSs. But our finding that multiple TSSs in a promoter do not lead to more fuzzy +1 nucleosomes argues that +1 nucleosomes are prior to TSSs and not the other way around. Regarding the classical

hypothesis that the appearance of new NDRs in chromatin mutants provides “windows of opportunity” for CSCTs (Kaplan *et al.*, 2003), we did see an NDR upstream to the CSCT-TSSs, but it was less pronounced than for the canonical TSSs. So it seems that the NDR formation is not a major requirement for transcription initiation, but rather the +1 nucleosome position. The localization of TSSs at the +1 nucleosome 5'-flank was described for canonical TSSs in *S. cerevisiae* and *S. pombe*, whereas in higher eukaryotes such as *Drosophila*, the TSS is positioned upstream to the +1 nucleosome in the NDR (Mavrigh *et al.*, 2008; Jiang and Pugh 2009; Lantermann *et al.*, 2010; Brogaard *et al.*, 2012). The +1 nucleosome presents an obstacle to RNA PolII passage, which may explain the observed +1 nucleosome/TSS relation for yeasts where selection of transcription start site may be regulated by +1 nucleosome positioning. In contrast, RNA PolII running into the +1 nucleosome may impact transcription pausing rather than initiation in higher eukaryotes (Mavrigh *et al.*, 2008; Gilchrist *et al.*, 2010). Of note, while the chromatin organization at the CSCT-TSSs seemed shared, it was observed at different genomic locations arguing for the above possibility of differentially disturbed chromatin structures in both mutants.

Other chromatin features such as histone modification and histone variants might be further determinants and would expand the requirements for CSCT-TSSs. In *S. pombe*, the histone variant H2A.Z as well as histone modification H3K4me3 were enriched at the +1 nucleosome position and downstream to canonical TSSs (Buchanan *et al.*, 2009; Pointner *et al.*, 2012; Li *et al.*, 2015). Both histone marks could be potential hallmarks for CSCT-TSS regions, but are unlikely to be causal.

Together with the common chromatin structure, the CSCTs share one other feature; they arise in regions where transcription is upregulated relative to the genome average (Figure 2.11 C and D). The location of the upregulated regions differed in both chromatin factor mutants. So the upregulation might be a consequence of disrupted chromatin structure that is permissive for transcription initiation. This supports again the conclusion that chromatin structure is disturbed in different ways in both mutants.

One further feature, which is shared among the CSCT-TSSs and the *rrp6Δ* TSSs, is the DNA roll shape, which was never studied before at TSSs (Figure 2.12 A-C). For comparison and better understanding if this is a special feature for TSS selection in *S. pombe*, we also analyzed the DNA shape at TSSs in *S. cerevisiae* (Figure 2.12 D). The DNA roll shape was less pronounced at TSSs in *S. cerevisiae* compared to TSSs in *S. pombe*. This might indicate that DNA roll shape is a major requirement for TSS selection in *S. pombe*, but not in *S. cerevisiae*. Structural analysis of budding yeast RNA PolII transcription initiation complex revealed that DNA recognition by RNA PolII is based on bendability of DNA in the promoter regions (Engel *et al.*, 2017). Both findings might indicate that DNA structure properties, such as DNA shape or DNA bendability, might drive TSS selection.

Regarding the possibility of different transcription initiation mechanisms leading to the small overlap of CSCT-TSSs in both chromatin factor mutants, we found one DNA sequence feature, GC skew, that differed between both. GC skew analysis showed a clear signal at the CSCT-TSSs of *hrp1Δ hrp3Δ* similar to that at the canonical *rrp6Δ* TSSs, but not

at the CSCT-TSSs of *spt6-1 ts* (Figure 2.13 B and C). This may indicate that the canonical *rrp6Δ* TSSs and the CSCT-TSSs of *hrp1Δ hrp3Δ* follow similar transcription initiation requirements and mechanism but not the *spt6-1 ts* CSCT-TSSs. Also, the GC skew signal seems not to be conserved among *S. pombe* and *S. cerevisiae*, since the GC skew signal was less pronounced in *S. cerevisiae* compared to *S. pombe* (Figure 2.13 D). If this GC skew signal is indeed indicative of a distinct initiation mechanism cannot be decided at present.

In summary, different criteria are important for the selection of CSCT-TSSs. We identified a +1 nucleosome/TSS relationship, a location of CSCT-TSSs in an upregulated region, DNA roll shape for all and an enrichment of GC skew for some TSSs. Some questions still remain, e.g., whether all criteria are needed simultaneously for the selection of CSCT-TSSs, or if the CSCTs have any biological function such as transcription regulation or if they encode proteins. Transcription regulation through ncRNA is already described and would be interesting to investigate for the newly identified CSCTs (Mellor *et al.*, 2016; Quinn and Chang 2016). In *S. pombe*, one example for a regulative ncRNA is the promoter transcript of the *fbp1* gene which contributes to the regulation of promoter chromatin opening (Hirota *et al.*, 2008). In higher eukaryotes, cryptic transcripts arise if DNA methyltransferase and histone deacetylase are downregulated, and these cryptic transcripts are translated into products with potentially abnormal functions and may contribute to carcinogenesis (Brocks *et al.*, 2017).

### 3.1.4 Characterization of TATA box motif containing promoters in *S. pombe*

For the first time, the Tbp1 binding sites were identified by ChIP-seq in *S. pombe* and the enriched, underlying TATA box motif was annotated based on such binding data and not just via a presumed sequence motif (Li *et al.*, 2015). Tbp1 protein binds preferentially tRNA genes and is enriched in 5% of *S. pombe* genes (Figure 2.14). The TATA box motif is enriched at 11% and 18% of the *rrp6Δ* TSSs and CSCTs in *spt6-1 ts*, respectively. The number of TATA box motifs enriched at canonical promoters varies from 10-20% in *S. cerevisiae* (Rhee and Pugh 2012) and up to ca. 40% in *Drosophila* (Kutach and Kadonaga 2000; Smale and Kadonaga 2003). The TATA box motif is found in the cryptic promoters in *spt6-1004* mutant in *S. cerevisiae* (Uwimana *et al.*, 2017). Nevertheless, the TATA box motif does not seem to be one of the main determinants of cryptic promoters in *S. cerevisiae* and *S. pombe*.

One common feature of *S. pombe* shared with higher eukaryotes is that the TATA box motif has a canonical distance to the TSSs of around 35 bp (Figure 2.14 C) (Struhl 1989; Li *et al.*, 2015). In *S. cerevisiae*, the TSS-TATA box motif distance has a broader distribution between 40 bp and 120 bp (Smale and Kadonaga 2003). The identified canonical distance between TATA box motif and TSSs of around 35 bp in *S. pombe* is consistent with previous studies, which used consensus sequence analysis to identify the TATA box motif (Li *et al.*, 2015). This common feature might indicate that the Tbp1-mediated transcription initiation follows similar mechanism in *S. pombe* and higher eukaryotes.

Previous studies in *S. cerevisiae* suggested that promoters with TATA box motif have a different nucleosome organization than promoter without TATA box motif (Ioshikhes *et al.*, 2006; Albert *et al.*, 2007; Tirosh *et al.*, 2007). We could not confirm this observation for *S. pombe* (Figure 2.14 E). Here, the nucleosome pattern at promoters with and without TATA box motif was quite similar.

### 3.2 Nucleosome pattern at promoter regions in *S. pombe*

In the context of nucleosome patterns at promoter regions, “fragile” nucleosomes are highly discussed, especially for *S. cerevisiae* promoter regions (Weiner *et al.*, 2010; Xi *et al.*, 2011; Kubik *et al.*, 2015; Chereji *et al.*, 2017; Kubik *et al.*, 2017; Chereji *et al.*, 2018). These “fragile” nucleosomes are more sensitive to MNase than other nucleosomes. MNase-dependent techniques are often used to map nucleosome positions. Several problems of MNase-dependent techniques are discussed: MNase sequence bias might lead to enrichment of distinct fragments, and additionally, it is hard to distinguish between DNA derived from nucleosome vs. DNA protected by other factors, both might cause nucleosome occupancy changes and misinterpretation of the results (Horz and Altenburger 1981; Weiner *et al.*, 2010; Xi *et al.*, 2011). Using ChIP-based methods should, at least in part, overcome the problem since histone proteins are selected by the ChIP step. Still, controversial observations were made for “fragile” nucleosomes using ChIP-based methods (Kubik *et al.*, 2015; Chereji *et al.*, 2017; Kubik *et al.*, 2017).

On the one hand, Chereji *et al.* could not detect “fragile” nucleosomes at promoter regions by ChIP-based method. Their suggestion was that the promoter regions are occupied by factors, such as transcription factor, chromatin remodelers etc., rather than “fragile” nucleosome and therefore this occupied promoter region by these factors is erroneously assigned to nucleosomes (Chereji *et al.*, 2017). Their observation is in agreement with the finding that the hydroxyl-radical approach failed to detect “fragile” nucleosome in *S. cerevisiae* promoter regions (Brogaard *et al.*, 2012). “Fragile” nucleosomes in *S. cerevisiae* promoter region were not discussed using a further developed hydroxyl-radical approach (Chereji *et al.*, 2018).

On the other hand, Kubik *et al.* and others claim to detect “fragile” nucleosome in *S. cerevisiae* promoter regions (Weiner *et al.*, 2010; Xi *et al.*, 2011; Kubik *et al.*, 2015; Kubik *et al.*, 2017). Kubik *et al.* used also ChIP-seq and they argued that difference between their study and study by Chereji *et al.*, 2017 may be due to the fact that they used different ChIP conditions (Kubik *et al.*, 2015; Kubik *et al.*, 2017). Chereji *et al.* used a different epitope tag approach to detect histones and this might cause that they missed to detect “fragile” nucleosomes in *S. cerevisiae* promoter region (Chereji *et al.*, 2017). Therefore, the existence of “fragile” nucleosomes in *S. cerevisiae* promoter regions seems not to be completely clarified.

The “fragile” nucleosomes in promoter regions are not only discussed for *S. cerevisiae*, but also for *Drosophila* (Chereji *et al.*, 2016). Notably, Chereji *et al.* observed that the DNA fragment length pulled down by ChIP is shorter than canonical nucleosomal DNA fragment length, arguing for partially unwrapped nucleosomes rather than “fragile” nucleosomes of canonical structure.

Collectively, both for *S. cerevisiae* and for *Drosophila*, the evidence for “fragile” nucleosomes is highly controversial and probably not sufficient.

We analyzed the nucleosome structure at the promoter region in *S. pombe* by MNase-seq using various MNase concentrations to digest the same chromatin and we saw a peak in

the promoter regions, the “NDR-Peak” (Figure 2.15). The occupancy of this “NDR-peak” was highly dependent on the MNase digestion degree. This observation would agree with the observation made in *S. cerevisiae* as well as in *S. pombe* that nucleosome occupancy is highly dependent on MNase digestion degree (Weiner *et al.*, 2010; DeGennaro *et al.*, 2013; Kubik *et al.*, 2015; Kubik *et al.*, 2017). Using MNase-anti-H3-ChIP-seq suggested that the “NDR-peak” originated from nucleosomes, at least in part (Figure 2.16). This would argue for the existence of “fragile” nucleosomes in the *S. pombe* promoter regions. In contrast to *S. cerevisiae*, in *S. pombe* “fragile” nucleosomes in promoter regions were also detected by the hydroxyl-radical approach and this would agree with our findings by MNase-anti-H3-ChIP-seq (Moyle-Heyrman *et al.*, 2013) and might suggest the existence of “fragile” nucleosomes in *S. pombe* promoter regions as a species specific feature. Nevertheless, we might look at partially unwrapped nucleosomes rather than “fragile” nucleosomes as discussed by Chereji *et al.*, 2016 for *Drosophila* and this would need further investigations.

### 3.3 NDR-array pattern formation in *S. pombe*

We investigated the role of CHD1 chromatin remodelers in NDR-array pattern formation at promoters in *S. pombe*. We used two strategies; first, an *in vivo* complementation approach and second, an *in vitro* reconstitution approach, both involving MNase-seq to trace the formation of NDR-array patterns.

#### 3.3.1 NDR-array pattern formation by CHD1 chromatin remodelers *in vivo*

We could show that Chd1 from *S. cerevisiae* could rescue the NDR-array pattern in the *hrp1Δ hrp3Δ* mutant in *S. pombe* (Figure 2.17). Swapping experiments of CHD1 genes between *S. cerevisiae* and *K. lactis* by others underline our findings that the Chd1 chromatin remodelers from different yeasts may be exchangeable and the mechanism of generating NDR-array patterns through Chd1 is evolutionary conserved (Hughes and Rando 2015). Nonetheless, an analogous experiment, expressing Hrp3 in the *chd1Δ isw1Δ isw2Δ* mutant in *S. cerevisiae*, could not rescue the NDR-array pattern (PhD thesis by Dr. Corinna Lieleg). The swapping experiments between the far-diverged yeasts, *S. cerevisiae* and *S. pombe* (lineage split ca. 350 million years ago (Hoffman *et al.*, 2015)), only worked for *S. pombe*. In contrast, the swapping experiments between the less-diverged yeasts, *S. cerevisiae* and *K. lactis* (lineage split ca. 100 million years ago (Rozpedowska *et al.*, 2011)), worked for both yeasts (Hughes and Rando 2015). One explanation for this difference in exchangeability of the CHD1-type remodelers might be due to the dissimilar evolution between *S. pombe* and *S. cerevisiae* for example of their recruitment mechanism of CHD1 chromatin remodelers. Additionally, in the context of NDR-array pattern formation, the *S. cerevisiae* Chd1 chromatin remodeler has to deal/compete with additional factors, for example with the ISWI chromatin remodeler class, which is not found in *S. pombe*. On this ground *S. cerevisiae* Chd1 might have evolved a property to deal with the ISWI chromatin remodelers that is not present in Hrp3, but may be required in *S. cerevisiae*, even in the absence of ISWI remodelers, as in the *chd1Δ isw1Δ isw2Δ* mutant.

The *in vivo* complementation approach in *S. cerevisiae* showed that the C-terminal part of Chd1 plays a crucial role in NDR-array pattern formation and might be involved in the recruiting mechanism (PhD thesis by Dr. Corinna Lieleg). This finding is supported by the result that the Chd1/Hrp3 hybrid construct, where the ATPase domain and DBD domain originate from Hrp3, is not able to restore the NDR-array pattern in the *chd1Δ isw1Δ isw2Δ* mutant in *S. cerevisiae* (PhD thesis by Dr. Corinna Lieleg). In contrast all Chd1/Hrp3 hybrid constructs are able to restore the NDR-array pattern in the *hrp1Δ hrp3Δ* mutant in *S. pombe* (Figure 2.18). We assume that during evolution a different recruitment mechanism or different requirements are adapted in *S. cerevisiae*, in which the ATPase/DBD domains play a crucial role. The exact region or mechanism for Chd1/Hrp3 for recruitment is unknown. Further investigation of recruitment mechanism in *S. pombe* is an additional interesting point.

The spacing activity of Chd1 and Hrp3 was previously described in several *in vitro* (Stockdale *et al.*, 2006; Pointner *et al.*, 2012; Lieleg *et al.*, 2015), or *in vivo* (Ocampo *et al.*, 2016) studies, or investigated in swapping experiments of CHD1 chromatin remodelers between *S. cerevisiae* and *K. lactis* (Hughes and Rando 2015). These swapping experiments revealed that the N-terminal part of *K. lactis* Chd1 has a major contribution to the nucleosome spacing activity and might be involved in the recruiting mechanism of Chd1 (Hughes and Rando 2015). These results are in good agreement with our results. The *in vivo* complementation approach using different Chd1/Hrp3 hybrid constructs in *S. pombe* as well as in *S. cerevisiae* led to different nucleosome spacing/nucleosome repeat length (Table 2.3 and Table 2.4). The hybrid constructs with the N-terminal Chd1 chromodomain and Hrp3 ATPase domain showed tighter nucleosome spacing, whereas other Chd1/Hrp3 hybrid constructs revealed wider spacing in *S. pombe*. Nevertheless, the exact regions responsible for nucleosome spacing activity could not be assigned, despite the swapping experiments and the recently published structure of Chd1-nucleosome complex (Farnung *et al.*, 2017).

In context of the nucleosome spacing activity of the different Chd1/Hrp3 hybrid constructs, it is challenging to quantify the exact differences in the nucleosome distances just by investigating the TSS-aligned composite plot. Ocampo *et al.* developed an algorithm to determine nucleosome spacing using MNase-seq data (Ocampo *et al.*, 2016). We applied this algorithm to determine the different nucleosome spacing of Chd1/Hrp3 hybrid constructs. Unfortunately, using this algorithm we faced the problem that the MNase digestion degree contributes the most to the nucleosome spacing distribution (data not shown). Ocampo *et al.* used paired-end MNase-seq data for their algorithm to determine the nucleosome spacing. This improves the exact determination of nucleosome positions, since both ends of DNA fragments are sequenced. Accordingly, we also used paired-end MNase-seq data, but this did not solve the issue of MNase digestion degree influence on spacing quantification by the Ocampo *et al.* algorithm.

Taken together, the *in vivo* complementation approach revealed an interesting evolutionary difference between *S. cerevisiae* and *S. pombe*. Chd1 and Hrp3 contribute to the NDR-array pattern formation in *S. cerevisiae* and *S. pombe*, but the exact domain responsible for aligning arrays to the +1 nucleosomes or for spacing activity could not be assigned yet.



### 3.3.2 NDR-array pattern formation investigated by *in vitro* reconstitution approach

To dissect the direct, sufficient and necessary role of factors for the nucleosome positioning mechanism we tried to establish an *in vitro* reconstitution system for *S. pombe*. Such an *in vitro* reconstitution system was successfully used for *S. cerevisiae* (Zhang *et al.*, 2011; Krietenstein *et al.*, 2016). Unfortunately, the addition of whole cell extract from *S. pombe* (PEX), chromatin remodelers and GRF to the SGD chromatin of *S. pombe* did not result in a genome-wide *in vivo*-like nucleosome pattern by this *in vitro* reconstitution system (Figure 2.20 A and B, Figure 2.21 C-E). This is in contrast to the analogous experiments for *S. cerevisiae*, where both the addition of whole cell extract from *S. cerevisiae* (YEX) and/or of purified remodelers and GRFs to the *in vitro* reconstitution system leads to proper *in vivo*-like nucleosome pattern (Zhang *et al.*, 2011; Krietenstein *et al.*, 2016). There, the contribution of individual factors to this nucleosome pattern could be identified and a four-stage mechanism for generation of the nucleosome pattern was suggested including NDR formation, +1 nucleosome positioning, array formation and physiological spacing (Krietenstein *et al.*, 2016).

We speculate that the inability of PEX to reconstitute genome-wide *in vivo*-like nucleosome patterns might be due to the lower specific remodeling activity of PEX compared to YEX (Figure 2.20 C). There might be several reasons to explain the low remodeling activity. First, the extraction method, even though the exact same method works very well for *S. cerevisiae*, might not be suitable to extract all required factors from *S. pombe*. Second, the chromatin factors might lose their activity during preparation, for example, the proteins are not properly folded or the remodeling complexes are not properly assembled. Besides these technical problems, one other reason might be more biological, i.e., the processes required for proper nucleosome positioning along the *S. pombe* genome may require some sort of coordination that cannot be reconstituted in PEX. For example, ongoing transcription may be required or some sort of regulation through phosphorylation that is disturbed in PEX.

If too low specific remodeling activity of the PEX was limiting, we hoped to improve NDR-array pattern reconstitution by using purified candidate factors, especially the Hrp1 and Hrp3 remodelers that were already shown to play a major role in array alignment *in vivo* (Hennig *et al.*, 2012; Pointner *et al.*, 2012; Shim *et al.*, 2012). Nonetheless, also this did not help much so far. The Hrp1 and Hrp3 chromatin remodelers failed to reconstitute the genome-wide *in vivo*-like nucleosome pattern, alone or in combination with PEX or Sap1 (Figure 2.21 C-E, Figure 2.22 B-D, Figure 2.24 A). Notably, this result was not due to insufficient remodeling activity of our purified Hrp1 or Hrp3 chromatin remodelers since an ATP-dependent remodeling activity was demonstrated by KpnI restriction enzyme activity assay (Figure 2.21 A and B). For the combination of Hrp1/Sap1 with or without Hrp3, we saw a genome-wide change in nucleosome positioning (Figure 2.22 B-D). The prominent “*In vitro* NDR-Peak” of the SGD chromatin disappeared and a peak at the *in vivo* +1 nucleosome position arose. This result indicates that Hrp1 might be involved in a

barrier-dependent positioning mechanism. For *S. cerevisiae*, the chromatin remodelers ISW2, ISW1a and INO80, in combination with the GRFs Abf1 and Reb1 feature such a barrier-dependent nucleosome positioning mechanism and guide the +1 nucleosomes to their positions (Krietenstein *et al.*, 2016). Nevertheless, the results with purified Hrp1 and Hrp3 remain preliminary as the effect of Hrp1 was not as pronounced and clear as the analogous effects seen in the *S. cerevisiae* system. One explanation might be that Sap1 is not the proper recruitment/barrier factor for Hrp1. Surprisingly, Hrp3 had a negligible effect on SGD chromatin *in vitro* and this is in contrast to the *in vivo* observation. Here, the nucleosome pattern is most disturbed if the gene encoding for the Hrp3 chromatin remodeler is deleted (Hennig *et al.*, 2012; Pointner *et al.*, 2012; Shim *et al.*, 2012). This observation for *S. pombe* Hrp3 *in vitro* is in agreement with the observation for *S. cerevisiae* Chd1 *in vitro* (Krietenstein *et al.*, 2016). Also here, there was hardly any contribution to the genome-wide reconstitution of *in vivo*-like nucleosome patterns by Chd1 *in vitro*, although the *chd1Δ* deletion has a high impact on genome-wide nucleosome organization *in vivo* (Gkikopoulos *et al.*, 2011; Ocampo *et al.*, 2016). One explanation might be that CHD1 chromatin remodelers might act in a transcription-dependent manner, meaning they might be recruited by RNA PolII to gene bodies during transcription elongation, which is not reconstituted in the *in vitro* reconstitution system (Lee *et al.*, 2007; Smolle *et al.*, 2012; Krietenstein *et al.*, 2016).

We could not clearly show that Sap1 acts as a barrier and/or recruits the chromatin remodelers to the Sap1 binding sites/promoters enriched with Sap1 binding sites (Figure 2.23). This may be a technical problem or mean that Sap1 indeed has no barrier function such as Abf1, Reb1 etc. in *S. cerevisiae* (Krietenstein *et al.*, 2016). There might be several reasons why we did not observe a barrier function of Sap1. A proper annotation of Sap1 binding sites, which are truly used *in vivo* or *in vitro*, is missing, for example by ChIP-seq or even better by *in vitro* ChIP-seq, respectively. So our bioinformatical analysis may be misled by using not the proper annotation of Sap1 binding sites. Furthermore, only two chromatin remodelers were tested with Sap1. Sap1 might act/recruit other chromatin remodelers to the chromatin and serve as barrier with these remodelers to generate nucleosome arrays. Other GRFs such as Reb1, Rap1 and Abf1 in *S. cerevisiae* were described to participate in the NDR formation (Badis *et al.*, 2008; Parnell *et al.*, 2008; van Bakel *et al.*, 2013). However, their orthologs in *S. pombe* are either not present, as for Abf1, or may have a different function. As for *S. cerevisiae*, *S. pombe* Reb1 is a transcription termination factor, and *S. pombe* Rap1 is a telomere binding protein and involved in chromatin silencing at telomeres (Park *et al.*, 2002; Jaiswal *et al.*, 2015). The interesting question is if the barrier functions of Reb1 and Rap1 are also conserved in *S. pombe*. Testing these factors in the *in vitro* reconstitution system in *S. pombe* would reveal either evolutionarily conserved or diverged barrier functions of these factors.

In addition, there are other factors, especially chromatin remodelers, which could be good candidates to be tested for further improvement of the *in vitro* reconstitution system for *S. pombe*.

The RSC complex contributes to NDR formation in *S. cerevisiae*. This was shown *in vivo* as well as *in vitro* (Hartley and Madhani 2009; van Bakel *et al.*, 2013; Krietenstein *et al.*, 2016). The NDR formation by RSC is dependent on poly(dA:dT) sequences (Lorch *et al.*, 2014; Kubik *et al.*, 2015; Krietenstein *et al.*, 2016; Kubik *et al.*, 2017), which are enriched in NDRs in *S. cerevisiae* (Yuan *et al.*, 2005; Segal *et al.*, 2006; Kaplan *et al.*, 2009), but these poly(dA:dT) sequences are not enriched in *S. pombe* (Lantermann *et al.*, 2010; Moyle-Heyrman *et al.*, 2013). It is not clear if *S. pombe* RSC also preferentially recognizes poly(dA:dT) and if it has a role in promoter NDR formation. For *S. pombe*, the participation of RSC in generating nucleosome patterns could not be shown *in vivo* so far (Pointner *et al.*, 2012). In this context one open question remains if the used temperature-sensitive allele encoding the ATPase subunit of RSC might not show the complete phenotype and if the RSC complex is fully inactivated. This issue might be solved for example by using a degron inducible strain (Watson *et al.*, 2013). Some features are common between the RSC complexes of *S. cerevisiae* and *S. pombe*, for example the homologous and essential ATPase subunit as well as other orthologous subunits (Monahan *et al.*, 2008). One major difference is the missing Rsc3 subunit in *S. pombe*, which is suggested to be important for NDR formation in *S. cerevisiae* (Badis *et al.*, 2008). Taken together, maybe there are two different mechanisms for nucleosome positioning by RSC in both yeasts. This remains to be tested *in vivo* as well as *in vitro* for *S. pombe*.

Other candidates with missing proof for their contribution to nucleosome positioning for *S. pombe in vivo* as well as *in vitro* are the chromatin remodelers INO80 and SWI/SNF. These chromatin remodeler classes are present in both yeasts. INO80 positions the +1 nucleosome and generates aligned nucleosome arrays in *S. cerevisiae*. This activity is intrinsic to the INO80 complex (Krietenstein *et al.*, 2016). The SWI/SNF complex was purified from *S. pombe* and shows to facilitate *in vitro* transcription through nucleosome arrays (Bernal and Maldonado 2007; Monahan *et al.*, 2008): Testing these chromatin remodelers in the *in vitro* reconstitution system for *S. pombe* would enable the comparison of conserved or diverged nucleosome positioning mechanism for both yeasts. The ISWI chromatin remodeler class is missing in *S. pombe*, but *S. pombe* also has the chromatin remodeler Fun30. *S. pombe* Fun30 facilitates nucleosome disassembly during transcription elongation (Lee *et al.*, 2017) and may therefore also impact nucleosome array formation over gene bodies.

### 3.4 Cooperativity between nucleosomes during SGD chromatin assembly

Closely packed nucleosomes, nucleosome clusters, which are observed by regularly spaced MNase ladders occur also at reduced nucleosome density, observed *in vivo* as well as *in vitro* (Celona *et al.*, 2011; Lieleg *et al.*, 2015). We wondered why the nucleosomes stay together and asked if the nucleosome assembly is cooperative or random, in particular under the specific conditions of SGD chromatin assembly.

Already early studies of nucleosome assembly suggested cooperativity to be important for nucleosome formation (Forte *et al.*, 1989). Here, they measured the variation of nucleosome number on a given plasmid and assumed that this variation depends on nucleosome density and on the degree of cooperativity during assembly. In their model they did not take into account effects of neighboring nucleosomes, which should be considered since nucleosomes might assemble differently if neighboring nucleosomes are present. In contrast, we specifically defined cooperativity via the generation of tightly spaced nucleosome clusters.

Using Southern blot analysis of MNase-digested SGD chromatin we could show that a substantial fraction derived from nucleosome clusters (di- or trinucleosome fragments) even if the nucleosome density was reduced (Figure 2.26, Figure 2.27) indicating a cooperativity between nucleosomes. We observed nucleosome clusters for histones derived from different species and for tailless histones. Our simulation, where we assumed a certain attraction between nucleosomes during SGD assembly, revealed the expected increase in nucleosome cluster formation (Figure 2.28 B) and argued that the observed cluster frequency during SGD at low nucleosome density could hardly be explained without cooperativity.

The question arose what kind of molecular interactions is responsible for the cooperativity. One possible explanation, why nucleosomes favor cluster formation, might be that the nucleosomes are kept together by histone-tails interaction either with DNA or with neighboring nucleosomes. Studying nucleosome-nucleosome interactions by DNA origami force spectrometer revealed that nucleosome-nucleosome interaction is weak but indeed facilitated by histone tails (Funke *et al.*, 2016). Testing if histone tails were responsible for nucleosome cluster formation during SGD chromatin assembly we could not see a noticeable reduction of nucleosome cluster formation. This indicates that histone tails seem not to be involved in keeping nucleosomes together during SGD chromatin assembly, which is puzzling.

So, other aspects/molecular interactions seem to favor the nucleosome cluster formation, maybe, for example, the structure/bending of DNA during SGD assembly. Using supercoiled DNA compared to linearized DNA for SGD chromatin assembly favored nucleosome assembly and hints towards that conformation of DNA plays a role during SGD chromatin assembly (Patterton and von Holt 1993). The DNA bend around one histone octamer might be changed in a way that it might favor an assembly of a neighboring histone octamer. One other speculation might be, that the electrostatic

interactions between DNA and histone octamers might be changed during SGD chromatin assembly due to the high salt concentration used for SGD and this might favor a nucleosome cluster formation (Korolev *et al.*, 2007).



---

## 4 Materials and Methods

## 4.1 Molecular Biology

### 4.1.1 Generation of chemically competent *E. coli* cells

Over night (O/N) culture of *E. coli* (DH5 alpha) was inoculated in 100 ml LB medium and grown until  $OD_{600} = 1.0$  (PMQ II Spectrophotometer, Zeiss). After centrifugation (15 min, 4°C, 6000 g) cells were resuspended in 30 ml ice-cold TFBI buffer (30 mM KOAc, 100 mM KCl, 50 mM MnCl<sub>2</sub>, 15% (v/v) glycerol, pH 5.8) and incubated for 30 min on ice. Pelleted cells (5 min, 4°C, 1000 g) were resuspended in 4 ml ice-cold TFBII buffer (10 mM MOPS/NaOH, 75 mM CaCl<sub>2</sub>, 10 mM KCl, 15% (v/v) glycerol, pH 7.0) and incubated for 10 min on ice. 100 µl cell aliquots were flash frozen in liquid nitrogen and stored at -80°C.

### 4.1.2 Transformation of *E. coli*

Up to 1 µg of plasmid DNA was added to 50 µl chemically competent *E. coli* cells (DH5 alpha) and incubated for 30 min on ice. Heat shock was performed for 45 sec at 42°C. Subsequently, cells were cooled down for 2 min on ice, LB medium was added to the cells and cells were incubated for 1 h at 37°C. After centrifugation (2 min, RT, 900 g) cells were resuspended in 100 µl LB medium and plated onto LB-agar plates with corresponding antibiotics.

### 4.1.3 Plasmid isolation from *E. coli*

Plasmid DNA was isolated using NucleoSpin® Plasmid EasyPure, NucleoBond® Extra Midi from Macherey Nagel according to manufacturer's instructions.

### 4.1.4 Polymerase chain reaction (PCR), restriction enzyme digestion, DNA ligation and cloning

Routine PCRs were performed according to standard protocols as described on [www.neb.com](http://www.neb.com). Briefly, PCR was performed in a total volume of 50 µl PCR reaction mix (up to 200 µg DNA, 200 µM dNTP, 0.2 µM each forward/reverse primers and 1.25 U DNA Polymerase) (Taq DNA Polymerase or Phusion® High Fidelity DNA Polymerase, NEB) using following settings (1x 98°C for 30 s; 25-35x 98°C for 10 s, 50-72°C for 30 s and 72°C for 15-30 s/kb; 1x 72°C for 5 min, 4°C for ∞).

The restriction enzyme digestion and ligation of DNA were performed according to standard protocols as described on [www.neb.com](http://www.neb.com).

Standard cloning was performed as described in (Gibson *et al.*, 2009). Shortly, 15 µl Gibson cloning master mix (90 mM Tris/HCl pH 7.5, 5% PEG8000, 10 mM MgCl<sub>2</sub>, 0.25 mM dNTPs, 1 mM NAD<sup>+</sup>, 0.005 U T5 exonuclease, 0.033 U Phusion® High Fidelity DNA Polymerase, 5.33 U Taq Ligase (NEB)) was mixed with 5 µl plasmid/insert mix (ratio 1:2, at least 50 ng DNA). Reaction mix was incubated for 30 min at 50°C and half of the reaction volume was transformed into chemically competent *E. coli* cells.



#### 4.1.5 Cultivation of *S. pombe* cells

For CAGE-seq, MNase-seq, MNase-anti-H3-ChIP-seq and ChIP-seq *S. pombe* cells were grown either in sterile-filtered YES medium (5 g/l Yeast extract (Formedium), 30 g/l glucose, 250 mg/l each supplements (adenine, histidine, leucine, lysine, uracil) or EMM medium (12.3 g/l EMM w/o dextrose (Formedium), 20 g/l glucose, 1.35 g/l each supplements (adenine, histidine, leucine, lysine, uracil)).

For protein purification (Hrp1-FLAG and Hrp3-TAP), *S. pombe* cells were grown in YEA medium (5 g/l Yeast extract (Formedium), 20 g/l glucose, 2 g/l casoamino acids (Formedium), 100 mg/l each supplements (adenine, leucine, uracil)).

Pre-cultures of *S. pombe* cells were inoculated by adding 3-4 colonies to 10 ml medium and grown O/N at 30 or 32°C. O/N cell culture was diluted to  $2 \times 10^6$  cells/ml and grown for 8 h at 30 or 32°C. To induce the temperature shift for the strain *spt6-1 ts* (see chapter 2.1 and 2.1.2.2) *S. pombe* cells were grown to a density of  $5 \times 10^6$  cells/ml O/N at 30°C, transferred to pre-warmed incubator (37°C) and were grown for 2h at 37°C.

#### 4.1.6 Transformation of *S. pombe*

*S. pombe* cells were grown in YES medium to a density of  $5 \times 10^6$  cells/ml. 50 ml cells were centrifuged (5 min, RT, 800 g), washed once with 10 ml ddH<sub>2</sub>O and once with LiOAc/TE buffer (0.1 M LiOAc, 10 mM Tris/HCl, 1 mM EDTA, pH 8.0). Washed cells were resuspended in 1 ml LiOAc/TE buffer and aliquotized in 100 µl. Cells were mixed with 0.5 µg linearized DNA or 1 µg plasmid DNA and 10 µg carrier DNA (denatured Salmon sperm DNA) and incubated for 15 min at RT. After addition of 500 µl PEG/LiOAc buffer (40% (w/v) PEG8000, 0.1 M LiOAc, 10 mM Tris/HCl, 1 mM EDTA, pH 8.0), the cell mix was incubated for 50 min at 30°C. After addition of 50 µl DMSO the cell mix was incubated for 10 min at 42°C. The cells were washed once with ddH<sub>2</sub>O, plated onto corresponding selection agar plates and grown for at least 48 h at 30°C.

#### 4.1.7 Chromatin Immunoprecipitation (ChIP) of Flag-tagged Tbp1 and DNA preparation for ChIP-seq

To obtain the Flag-tagged Tbp1 strain, the construct was generated as follows: Standard PCR and Gibson cloning strategies were used to clone the plasmid pRS416\_TBP1\_2xFLAG\_KanMX6 (Table 4.1) (Gibson *et al.*, 2009). The plasmid pRS416 was cut using the restriction enzymes EcoRI and NotI (NEB). The plasmid construct pRS416\_TBP1\_2xFLAG\_KanMX6 was digested with PmeI (NEB) and the resulting TBP1\_FLAG\_KanMX6 DNA construct was transformed into *S. pombe* wild type strain (h- 972). The strain (*h- Tbp1-2xFLAG::KanMX6*) was used for ChIP.

**Table 4.1 Cloning strategy to obtain pRS416\_TBP1\_FLAG\_KanMX6 plasmid**

Primer	Sequence	Template for PCR
F1_tbp1_flag_F	GGTACCGGGCCCCCTCGAGGTCGACGGTATCGATAAGCTTG ATATCGGTTTAAACCGTTTTGCCGCTGTTATTATGCGTATCC	genomic <i>S. pombe</i> DNA
F1_tbp1_flag_R	CCAGTATTGTCTGAATTTGAAAACATCTCGAGACTATAAGGAT GACGATGACAAG	genomic <i>S. pombe</i> DNA
F2_tbp1_flag_F	CCAGTATTGTCTGAATTTGAAAACATCTCGAGACTATAAGGAT GACGATGACAAG	pFA6-FLAG-KanMX6
F2_tbp1_flag_R	CATTTGATGCTCGATGAGTTTTCTAAGGCATGTCAACAGTTAT CACACAGTTTTGTG	pFA6-FLAG-KanMX6
F3_tbp1_flag_F	CATTTGATGCTCGATGAGTTTTCTAAGGCATGTCAACAGTTAT CACACAGTTTTGTG	genomic <i>S. pombe</i> DNA
F3_tbp1_flag_R	CTTTGTATAATTCATTTTTTCATGATCGTGGTTTAAACGGCCGCC ACCGCGGTGGAGCTCCAGCTTTTGTCCCTTTAG	genomic <i>S. pombe</i> DNA

*S. pombe* cells (*h- Tbp1-2xFLAG::KanMX6*) were grown in 500 ml medium to a density of  $5 \times 10^6$  cells/ml and were cross-linked with 1% (v/v) methanol-free formaldehyde for 20 min at RT. Cross-linking was quenched by adding 125 mM glycine for 10 min at RT. After harvesting (5 min, 4°C, 800 g) cells were washed twice with ice-cold PEMS buffer (100 mM Pipes, 1.2 M sorbitol, 1 mM MgCl<sub>2</sub>, 1 mM EDTA, pH 7.5). Cells were resuspended in an equal volume of ice-cold IP buffer (50 mM Tris/HCl, 150 mM NaCl, 1 mM EDTA, 1% Triton X-100, 0.1% Igepal, pH 7.4), an equal volume of zirconium silicate beads (ZSB05, Biostep Süd GmbH) was added to the cells and cells were mechanically disrupted in the Precellys BeadBeater (settings: 3x30 sec at 6800 rpm with 5 min pause on ice, Peqlab). Disrupted cells were transferred into Covaris tubes (12x24 mm, Lot No. 001950, Covaris). Chromatin shearing was performed using Covaris machine S220 (Covaris) with following settings: 140 W, 200 cycles per burst, 20% duty factor for 25 min. The DNA length should be ca. 200 bp after shearing. After centrifugation (5 min, 4°C, 15000 g) the antibody was added to the supernatant in a new microcentrifuge tube and incubated O/N at 4°C. As antibody Anti-Flag® M2 magnetic beads (Sigma) were used according to manufacturer's instructions. Antibody beads were washed with 2x IP buffer, 2x CHIP Wash NaCl buffer I (10 mM Tris/HCl, 500 mM NaCl, 0.1% Igepal 630, 1 mM EDTA, pH 8.0), 2x CHIP Wash LiCl buffer II (10 mM Tris/HCl, 250 mM LiCl, 0.1% Igepal 630, 1 mM EDTA, pH 8.0) and once with TE buffer (50 mM Tris/HCl, 1 mM EDTA, pH 7.4). For reverse cross-linking, CHIP samples were incubated with TES buffer (50 mM Tris/HCl, 10 mM EDTA, 1% SDS, pH 7.4), treated with 1 mg/ml Proteinase K (Bioline) and incubated O/N at 65°C. DNA was prepared by phenol/chloroform extraction and isopropanol precipitation. DNA was dissolved in TE buffer (50 mM Tris/HCl, 1 mM EDTA, pH 8.0).

#### 4.1.8 Mononucleosomal DNA preparation for MNase-seq

Mononucleosomal DNA was prepared as described in (Lantermann *et al.*, 2009; Pointner *et al.*, 2012) with slight changes. *S. pombe* cells were grown in 500 ml medium to a density of  $5 \times 10^6$  cells/ml and were cross-linked with 0.5% (v/v) formaldehyde for 20 min at RT. Cross-linking was quenched by bringing to 125 mM glycine for 10 min at RT. Harvested

cells (5 min, 4°C, 800 g) were washed once with ice-cold ddH<sub>2</sub>O and incubated in 10 ml pre-incubation buffer (20 mM Na<sub>2</sub>HPO<sub>4</sub>, 20 mM citric acid, 40 mM EDTA, pH 8.0, 28.6 mM β-mercaptoethanol) for 10 min at 30°C. Cells were resuspended in 20 ml ice-cold Sorbitol/Tris buffer (1 M sorbitol, 50 mM Tris/HCl, pH 7.4, 10 mM β-mercaptoethanol) and lysed using Zymolyase T (10 mg for 5x10<sup>6</sup> cells/ml, MP Biomedicals) for 30 min at 30°C. Lysed cells were washed once in 40 ml Sorbitol/Tris buffer without β-mercaptoethanol and resuspended in ice-cold NP-buffer ((1 M sorbitol, 50 mM NaCl, 10 mM Tris/HCl, pH 7.4, 5 mM MgCl<sub>2</sub>, 1 mM CaCl<sub>2</sub>, 0.75% Igepal, 1 mM β-mercaptoethanol, 0.5 mM spermidine) 1x10<sup>6</sup> cells resuspended in 1 ml NP-buffer). Aliquots (1 ml lysed cells) were digested with serial dilutions of MNase (2-12 μl of 0.59 U/ml MNase (Sigma-Aldrich) in EX50 buffer (10 mM HEPES/NaOH pH 7.6, 50 mM NaCl, 1.5 mM MgCl<sub>2</sub>, 0.5 mM EGTA, pH 8.0, 10% (v/v) glycerol, 1 mM DTT, 0.2 mM PMSF)) for 20 min at 37°C. MNase digestion degree was chosen according to the ratio of mono- to dinucleosomal band (ca. 80% mononucleosomal band). MNase digestion was stopped by EDTA/SDS (final concentration 12.5 mM EDTA, 0.7% SDS). RNA was removed by 0.4 mg/ml RNase A (Roche) treatment for 45 min at 37°C. 1 mg/ml Proteinase K (Bioline) was added and reverse cross-linking during protease digest was performed at 65°C O/N. After precipitation (addition of 3 M KOAc pH 5.5 to final concentration of 0.7 M) and centrifugation (10 min, 4°C, 15000 g) DNA in supernatant was prepared by phenol/chloroform extraction and ethanol precipitation. The precipitation was performed in presence of 20 μg glycogen (Sigma-Aldrich) and at -20°C for 1 h. After centrifugation (25 min, 4°C, 15000 g) the pellet was washed once with 70% ethanol and resuspended in TE buffer (50 mM Tris/HCl, 1 mM EDTA, pH 8.0). Mononucleosomal DNA fragments were separated by 1.5% agarose gel electrophoresis in TAE buffer (40 mM Tris/HCl, 20 mM acetic acid, 1 mM EDTA, pH 7.6), cut out and purified by Freeze'N'Squeeze (Biorad) according to standard protocol.

#### 4.1.9 DNA preparation for MNase-anti-H3-ChIP-seq

MNase-digested samples were prepared as described in chapter 4.1.8. Briefly, *S. pombe* wild type cells (*h-* 972) were grown in 500 ml medium to a density of 5x10<sup>6</sup> cells/ml and cross-linked with 0.5% (v/v) formaldehyde for 20 min at RT. Cross-linking was quenched by bringing to 125 mM glycine for 10 min at RT. Harvest cells (5 min, 4°C, 800 g) were washed once with ice-cold ddH<sub>2</sub>O and incubated in pre-incubation buffer for 10 min at 30°C. Cells were resuspended in ice-cold Sorbitol/Tris buffer and lysed using Zymolyase T (10 mg for 5x10<sup>6</sup> cells/ml, MP Biomedicals) for 30 min at 30°C. Lysed cells were washed once in Sorbitol/Tris buffer without β-mercaptoethanol and resuspended in NP-buffer (1x10<sup>6</sup> cells resuspended in 1 ml NP-buffer). Aliquots (1 ml lysed cells) were digested with serial dilutions of MNase (2-12 μl, concentration 0.59 U/ml MNase (Sigma-Aldrich) in EX50 buffer) for 20 min at 37°C. After stopping the MNase digestion, a mix of anti-H3-antibody (Abcam, ab1791) and Magna ChIP™ Protein A Magnetic beads (Millipore, 16-661) was added to MNase treated cells (1 μg anti-H3-antibody/20 μl Magna ChIP™ Protein A Magnetic beads per 2 ml MNase-digested cells (1x10<sup>6</sup> cells in 1 ml NP-buffer)). The ChIP

sample was incubated overnight at 4°C on a rotating wheel and then washed with 2x IP buffer, 2x CHIP Wash NaCl buffer I, 2x CHIP Wash LiCl buffer II and once with TE buffer. For reverse cross-linking, the CHIP sample was incubated with TES buffer, treated with 1 mg/ml Proteinase K (Bioline) and incubated O/N at 65°C. DNA was prepared by phenol/chloroform extraction and ethanol precipitation. DNA was dissolved in TE buffer.

### 4.1.10 RNA extraction for CAGE-seq

RNA for CAGE-seq was prepared in the laboratory of Prof. Dr. Jürg Bähler (University College London) and Dr. Samuel Marguerat (Imperial College London) and sent for sequencing to DNAFORM (SourceBioScience).

## 4.2 Biochemistry

### 4.2.1 Preparation of embryonic *Drosophila* histone octamers

*Drosophila* histone purification was performed as described in (Faulhaber and Bernardi 1967; Simon and Felsenfeld 1979; Krietenstein *et al.*, 2012). 0-12 h *Drosophila* embryos were used for histone octamer purification. *Drosophila* embryos were washed through a sieve embryo collection apparatus, dechorionated in 3% sodium hypochlorite solution for 3 min at RT under stirring, washed first with 0.7% (w/v) NaCl, 0.04% (v/v) Triton X-100 and second with water for 5 min. The weight of the dechorionated embryos was determined and they were stored at -80°C. 50 g dechorionated embryos were resuspended in 50 ml lysis-2 buffer (15 mM HEPES/KOH, 10 mM KCl, 5 mM MgCl<sub>2</sub>, 0.1 mM EDTA, 0.5 mM EGTA, 17.5% (w/v) sucrose, 1 mM DTT, 0.2 mM PMSF, 1 mM sodium metabisulfite, pH 7.5) and homogenized using Yamato LSC LH-21 homogenizator (six-times, 1000 rpm). After filtration (Miracloth, Calbiochem Novabiochem Corporation) and centrifugation (15 min, 4°C, 6600 g) the soft nuclei pellet was resuspended in 50 ml suc-buffer (15 mM HEPES/KOH, 10 mM KCl, 5 mM MgCl<sub>2</sub>, 0.05 mM EDTA, 0.25 mM EGTA, 1.2% (w/v) sucrose, 1 mM DTT, 0.1 mM PMSF, 1x Complete™ EDTA-free protease inhibitor (Sigma-Aldrich), pH 7.5). The lipid layer above and hard bottom of the pellet should not be included. After centrifugation as above the nuclei pellet was resuspended in 30 ml suc-buffer and dounced 20 times with a glass dounce homogenizer with B pestle (Dounce Tissue Grinder, Wheaton/Fisher Scientific GmbH). The nuclei sample was warmed for 5 min to 26°C. 3 mM CaCl<sub>2</sub> was added and MNase digestion was started by adding 0.074 U MNase (0.59 U/ml MNase (Sigma-Aldrich) in EX50 buffer for 10 min at 26°C. Digestion was stopped by bringing to 10 mM EDTA. After centrifugation as above the pellet was resuspended in 6 ml TE-2 buffer (10 mM Tris/HCl, 1 mM EDTA, 1 mM DTT, 0.2 mM PMSF, pH 7.6) and incubated for 30-45 min at 4°C under constant rotating. After centrifugation (30 min, 4°C, 15322 g) the KCl concentration of the supernatant was adjusted to 0.63 M KCl with high salt buffer (2 M KCl, 0.1 M potassium phosphate, pH 7.2). The supernatant (15 min, 4°C,

15322 g) was filtered through 0.45  $\mu\text{m}$  and 0.22  $\mu\text{m}$  syringe filters and applied to a hydroxylapatite column (washed with low salt buffer (0.63 M KCl, 0.1 M potassium phosphate, 1 mM DTT, pH 7.2, Biorad)). Using an ÄKTA purifier system (GE) the hydroxylapatite column with bound histone octamers was washed with two column volumes of low salt buffer and histone octamers were eluted with high salt buffer. Elution fractions were checked by 4-20% gradient Coomassie SDS-PAGE (Biorad) and elution fractions containing histone octamers were pooled and concentrated using dialysis cup (10 kDa MWCO cut-off, Millipore). Histone octamers were stored at  $-20^{\circ}\text{C}$  in 2 M KCl, 0.1 M potassium phosphate, pH 7.2, 43% glycerol, 1x Complete™ EDTA-free protease inhibitor and 1 mM DTT. Protein concentration was determined by Nanodrop (Thermo Scientific) at 280 nm using  $\epsilon = 0.42 \text{ cm}^{-1} \text{ ml/mg}$ .

#### 4.2.2 Recombinant histone octamers

Recombinant *Xenopus laevis* histone octamers, wild type and all tailless, were obtained from the Protein Expression and Purification Facility (PEPF, Colorado State University). Histone octamer quality was determined as described in (Krietenstein *et al.*, 2012).

#### 4.2.3 Preparation of yeast whole cell extract

Yeast whole cell extract preparation was performed for *S. pombe* as described for *S. cerevisiae* (Wippo *et al.*, 2011; Zhang *et al.*, 2011; Krietenstein *et al.*, 2012). Briefly, *S. pombe* wild type cells (*h*- 972) were grown in 4x 500 ml medium to a density of  $5 \times 10^6$  cells/ml. After harvesting (15 min,  $4^{\circ}\text{C}$ , 6000 g) cells were washed with 200 ml ice-cold ddH<sub>2</sub>O and centrifuged again for 15 min at  $4^{\circ}\text{C}$  at 6000 g. Cells were washed once in 40 ml ice-cold extraction buffer (200 mM HEPES/KOH pH 7.5, 10 mM MgSO<sub>4</sub>, 20% (v/v) glycerol, 1 mM EDTA, 390 mM (NH<sub>4</sub>)<sub>2</sub>SO<sub>4</sub>, 1 mM DTT), and once in 40 ml ice-cold extraction buffer with 1x Complete™ EDTA-free protease inhibitor (Sigma-Aldrich). Between the washing steps, cells were harvested by centrifugation for 10 min at  $4^{\circ}\text{C}$  at 2047 g. Weight of pelleted cells was determined. Cells were transferred into a 10 ml syringe and pressed into liquid nitrogen to obtain “frozen spaghetti”. Frozen cells were stored at  $-80^{\circ}\text{C}$ . Electronic mortar (Retch RM100) was used for mild disruption of cells as following: electric mortar was cooled down with liquid nitrogen, setting 5.5 was used, 0.4 ml extraction buffer for one gram of cells were added while grinding and grinding was performed for ca. 30 min or until cells were fine powder. Disrupted cells were slowly thawed under stirring and ultracentrifugated for 2 h at  $4^{\circ}\text{C}$  at 82500 g. The clear phase between pellet and lipid layer, not including the fluffy layer above the pellet, was carefully transferred, and its volume determined. Ammonium sulfate was added stepwise (337 mg per ml cell lysate) while mixing and incubation for 30 min at  $4^{\circ}\text{C}$  to dissolve the powder. After a second incubation (30 min,  $4^{\circ}\text{C}$ , while rotating) the sample was centrifuged for 20 min at  $4^{\circ}\text{C}$  and 30300 g. The precipitate was resuspended in a small volume (500  $\mu\text{l}$ ) of dialysis buffer (20 mM HEPES/KOH, pH 7.5, 80 mM KCl, 10 or 20% (v/v) glycerol, 1 mM EGTA, 5 mM DTT, 0.1 mM PMSF, 1 mM sodium metabisulfite) and dialyzed twice against

500 ml dialysis buffer for 1.5 h at 4°C using a dialysis cup (MWCO 3.5 kDa cut-off, Millipore). Protein concentration was determined by Nanodrop (Thermo Scientific) at 280 nm. 50 µl aliquots of whole cell extract were flash frozen and stored at -80°C

### 4.2.4 TAP-tag purification of endogenous Hrp3

Hrp3-TAP purification was performed as described in (Pointner *et al.*, 2012). Briefly, *S. pombe* cells (*h- hrp1::ura4+ ade6-M210 leu1-32 ura4-D18 Hrp3-TAP::KanMX*) (Pointner *et al.*, 2012) were grown in 6x 2 l medium to a density of 25x10<sup>6</sup> cells/ml in YEA medium. Cells were harvested (6 min, 4°C, 3000 g), washed once with PBS buffer (144 mg/ml KH<sub>2</sub>PO<sub>4</sub>, 9 g/l NaCl, 795 mg/l Na<sub>2</sub>HPO<sub>4</sub> 2xH<sub>2</sub>O, pH 7.4) and twice with PBS buffer +2.5x Complete™ EDTA-free protease inhibitor (Sigma-Aldrich). The weight of pelleted cells was determined. Cells were transferred into a 10 ml syringe and pressed into liquid nitrogen to obtain “frozen spaghetti”. Cells were disrupted by grinding (Freezer/Mill 6870, SPEX CertiPrep, settings: 6 cycles, 2 min on, 2 min off, rate 14). Grinded cells were slowly dissolved in 1.3x volume of 3x buffer A (200 mM HEPES/KOH, 150 mM NaCl, 1.5 mM MgCl<sub>2</sub>, 0.5 mM EDTA, 15% glycerol, 1 mM DTT, 2.5x Complete™ EDTA-free protease inhibitor, pH 7.8). Cell extract was incubated at 4°C for at least 1 h under stirring and centrifuged (15 min, 4°C, 15000 g). The KCl concentration of the supernatant was adjusted to 200 mM KCl. After ultracentrifugation (30 min, 4 °C, 140000 g) the supernatant was flash frozen and stored at -80°C. 500 µl IgG bead slurry were used for 100 ml cell extract. IgG beads were washed twice with IgG buffer (10 mM Tris/HCl, 150 mM NaCl, pH 8.0). Cell extract was thawed at room temperature and incubated with washed IgG beads (GE Healthcare) for 1 h at 4°C on a rotating wheel. After incubation, the beads were washed 5x with 10x beads volume of IgG buffer +0.4 mM DTT, 10 mM PMSF, 1x Complete™ EDTA-free protease inhibitor, 2x with wash buffer (10 mM Tris/HCl, 300 mM NaCl, 0.5 mM EDTA, 0.05 % NP-40, 0.4 mM DTT, 1x Complete™ EDTA-free protease inhibitor, pH 8.0) and once with TEV buffer (10 mM Tris/HCl, 150 mM NaCl, 0.5 mM EDTA, 0.05 % NP-40, 0.4 mM DTT, 1x Complete™ EDTA-free protease inhibitor, pH 8.0) using Gravity Flow Columns (Biorad). Protein was eluted by adding 200 U TEV (AcTEV™ Protease, Life Technologies) for 1 h at 16°C on rotating wheel. After elution, buffer conditions were adjusted with glycerol to obtain 20% glycerol final concentration. Protein concentration was determined by Nanodrop (Thermo Scientific) at 280 nm using epsilon = 0.91 cm<sup>-1</sup> ml/mg. 100 µl aliquots of elution fractions were flash frozen and stored at -80°C.

### 4.2.5 FLAG-tag purification of endogenous Hrp1

Hrp1-Flag purification was performed as described in (Pointner *et al.*, 2012). Briefly, *S. pombe* cells (*h- hrp3::leu+ leu1-32 hrp1-2xFLAG::KanMX*) (Pointner *et al.*, 2012) were grown in 6x 2 l medium to a density of 25x10<sup>6</sup> cells/ml in YEA medium. Cells were harvested for 10 min at 4 °C and at 3000 g, washed once with ice-cold ddH<sub>2</sub>O and once with H-0.3 buffer (25 mM HEPES/KOH, 300 mM NaCl, 0.5 mM EGTA, 0.1 mM EDTA, 2 mM

MgCl<sub>2</sub>, 20 % glycerol, 0.02% NP-40, 1 mM β-mercaptoethanol, 8 mM PMSF, 1x Complete™ EDTA-free protease inhibitor, pH 7.8). Cells were disrupted as for the TAP-tag purification (chapter 4.2.4). Disrupted cell powder was mixed with 1.3 ml of H-0.3 buffer per gram cell powder and incubated for 1 h at 4°C. After ultracentrifugation (1 h, 4°C, 100000 g) supernatant was either flash frozen and stored at -80°C or directly used for purification. Anti-FLAG® M2 agarose beads (ANTI-FLAG® M2-agarose from mouse, 10 µl beads for 3 ml of cell extract, Sigma-Aldrich) were washed 3x with H-0.3 buffer +1x Complete™ EDTA-free protease inhibitor. Supernatant was added to equilibrated beads and incubated for 3 h at 4°C on a rotating wheel. The beads with bound proteins were washed 4x with H-0.3 buffer, 4x with H-0.5 buffer (as H-0.3 buffer but 500 mM NaCl) and 3x with H-0.1 buffer (as H-0.3 buffer but 100 mM NaCl). Flag-tagged proteins were eluted with same volume of 1 mg/ml FLAG® peptide (Sigma) in H-0.1 buffer for 1 h at 4°C under rotating. Elution was repeated 2x for 30 min at 4°C, once for 15 min at 4°C and once for 1 min at 4°C while rotating. Protein concentration was determined by Nanodrop (Thermo Scientific) at 280 nm using epsilon = 0.91 cm<sup>-1</sup> ml/mg. 100 µl aliquots of elution fractions were flash frozen and stored at -80°C.

#### 4.2.6 *In vitro* reconstitution of chromatin by salt gradient dialysis (SGD)

Salt gradient dialysis (SGD) was performed as previously described in (Krietenstein *et al.*, 2012). The genomic plasmid library pURSP1 was used for genome-wide reconstitution (kind gift of Jürg Stolz) (Barbet *et al.*, 1992). Briefly, in a total volume of 100 µl, 10 µg plasmid library DNA, variable amount of histone octamers, 20 µg BSA (Biorad, 500-0002) were mixed in high salt buffer (10 mM Tris/HCl pH 7.6, 2 M NaCl, 1 mM EDTA, pH 8.0, 0.05% Igepal) and transferred to a dialysis chamber (Dialysis membrane MWCO 3,500 kDa, Spectrum Laboratories). Dialysis was performed O/N at RT or 30°C by slowly diluting (15-16 h) 300 ml high salt buffer with 3 l low salt buffer (as high salt buffer but 50 mM NaCl) using a peristaltic pump. Dialysis was finished by incubating against 1 l low salt buffer for 1-1.5 h at RT or 30°C. The salt gradient dialyzed chromatin was stored at 4°C.

#### 4.2.7 *In vitro* reconstitution remodeling reaction and MNase digestion

For *in vitro* reconstitution remodeling reactions, different buffer conditions were tested. The buffers were reconstitution buffer (final buffer composition: 1 mM Tris/HCl, pH 7.6, 2 mM HEPES/KOH, pH 7.5, 19.6 mM HEPES/NaOH, pH 7.5, 13% glycerol, 2.7 mM DTT, 3 mM MgCl<sub>2</sub>, 0.6 mM EGTA, 0.1 mM EDTA, 85.5 mM NaCl, 8 mM KCl, 0.005% Tween, 0.1 mM Na<sub>2</sub>O<sub>5</sub>S<sub>2</sub>, 10 mM (NH<sub>4</sub>)<sub>2</sub>SO<sub>4</sub>, 3 mM ATP, 30 mM creatine phosphate (Sigma), 20 ng/µl creatine kinase (Roche Applied Science)) as described in (Krietenstein *et al.*, 2016) or Ekwall buffer (final buffer composition: 2 mM Tris/HCl, 50 mM NaCl, 0.12 mM EDTA, 0.01% NP-40, 0.2 mM DTT, 10% glycerol, 10 mM Na/HEPES, 0.1 mM EGTA, 5 mM MgCl<sub>2</sub>, 0.2 mM PMSF, 0.4 mM β-mercaptoethanol, 20 mM creatine phosphate, 3 mM ATP, 0.1 µg/µl BSA, 20 ng/µl creatine kinase (Roche Applied Science)) as described in (Pointner

*et al.*, 2012). Protein concentrations, tested in *in vitro* reconstitution remodeling reaction, were 4.3 nM for Hrp1 and Hrp3, or as indicated, and 20 nM for Sap1. Remodeling reaction mix had 100  $\mu$ l and was incubated for 4 h at 30°C. Subsequently, MNase digestion was performed by bringing to 2 mM CaCl<sub>2</sub> and adding 12  $\mu$ l of MNase stock solution (0.59 U/ml MNase (Sigma-Aldrich) in EX50 buffer) and incubation for 5 min at 30°C. Digestion was stopped by bringing to 10 mM EDTA and 1% SDS. 2 mg/ml Proteinase K (Bioline) was added and samples were incubated O/N at 55°C or for 1h at 37°C. DNA was prepared by phenol/chloroform extraction and isopropanol precipitation. DNA was dissolved in TE buffer.

### 4.2.8 MNase digestion for SGD chromatin

To digest SGD chromatin that was not used in a remodeling reaction, i.e., in the absence of ATP, the following reaction mix was prepared in 100  $\mu$ l volume (1  $\mu$ g SGD chromatin, 1 mM CaCl<sub>2</sub>, 12% glycerol, 2.5 mM DTT, 20 mM HEPES/KOH pH 7.5, 0.5 mM EGTA, 80 mM KCl, 10 mM ammonium sulfate). MNase stock solution (0.59 U/ml MNase (Sigma-Aldrich) in EX50 buffer) was diluted in MNase buffer (10 mM HEPES/KOH pH 7.5, 0.1 mg/ml BSA). MNase was titrated to obtain either a DNA laddering or mainly mononucleosomal band (e.g. 1:1000, 1:100, 1:10). Prior to MNase digestion 2mM CaCl<sub>2</sub> was added. MNase digestion and DNA preparation was as described in 4.2.7.

### 4.2.9 Restriction enzyme accessibility assay

Restriction enzyme accessibility assay was performed as described in (Lieleg *et al.*, 2015) using 601-25mer designer array plasmid in the *in vitro* reconstitution remodeling reaction. During remodeling reaction restriction enzyme KpnI was added (400 U or 800 U, NEB). After Proteinase K (Bioline) (final concentration 2 mg/ml) digestion and DNA purification using isopropanol precipitation, DNA was cleaved with XbaI and EcoRI (1 U, NEB) for 1 h at 37°C. Cleavage of 601-25mer designer array plasmid resulted either in fragments of 4937/2609 bp for XbaI/EcoRI cleavage or 3628/2659/1309 bp for XbaI/EcoRI/KpnI cleavage. Detection was performed by agarose gel electrophoresis with Ethidium bromide staining or Southern blotting (chapter 4.2.12).

### 4.2.10 Sequencing library preparation

The sequencing library preparation was adapted from NEBNext® ChIP-seq Library Prep Reagent Set for Illumina® protocol (NEB). End-repair of purified DNA (50  $\mu$ g) was performed by adding 3 U T4 DNA polymerase (E1201L, NEB), 10 U T4-PNK (M0201L), 1 U Klenow (M0212L) and 4 mM dNTPs in 50  $\mu$ l 1x T4 ligation buffer for 30 min at 20°C. DNA purification was performed using AMPure beads (Beckman Coulter). One volume AMPure beads and 1.5x volume NaCl/PEG solution (1,25M NaCl, 20% PEG8000) was added to the end-repair mix. The DNA bound to AMPure beads were separated using magnetic rack and washed 2x with 500  $\mu$ l 80% EtOH. DNA was resuspended in 50  $\mu$ l dA-tailing mix (5 U



Klenow Large Fragment (M0210L, NEB), 0.2 mM dATP and 1x NEB buffer 2) and incubated at 37°C for 30 min. The dA-tailed DNA bound to Ampure beads was washed as described above and eluted in ligation mix (12 U T4-Ligase (M0202L, NEB), 0.05 µM NEBNext® Adaptor and 1x T4 Ligase buffer). DNA was ligated to the NEBNext® Adaptor (E750L or E7335L) over night or for 30 min at 16°C. NEBNext® Adaptor was cleaved with 3 U User enzyme for 15 min at 37°C. The adaptor-ligated DNA was eluted in 36 µl 0.1x TE. The NEBNext® Multiplex Oligos (0.5 µM, Index primer Set 1 (E7335L) or Index Primer Set 2 (E750L), 2.5 mM dNTP solution mix and Phusion HF (1 U, M0530L, NEB) were added and PCR amplification was performed using following settings (1x 98° C for 30 s; 10-12x 98°C for 10 s, 65°C for 30 s and 72°C 15 s; 1x 72°C for 5 min, 4°C ∞). The adaptor-ligated and amplified DNA was separated by 1.5% agarose gel electrophoresis in TAE buffer and purified by Freeze'N'Squeeze DNA Gel Extraction Spin columns (Biorad) and precipitated by isopropanol precipitation. After resuspending in 15 µl 0.1x TE buffer DNA concentration was determined by Qubit dsDNA HS Assay Kit (Invitrogen). 10 nM DNA mix were combined depending on how many reads were needed for the corresponding sample. Fragment length and purity of DNA pool were checked by Agilent DNA 1000 Kit on BioAnalyzer (Agilent). The chromatogram should show a peak with a size of ca. 280 bp and no further peaks such as Adaptor dimers with a size of 120 bp.

#### 4.2.11 Sequencing

High-throughput sequencing of DNA sequencing library was performed at the Laboratory of Functional Genome Analysis (LAFUGA) in the Gene Center (Munich) by Dr. Stefan Krebs using either Illumina® Genome Analyzer IIx (single-end mode, 36 cycles) or a HiSeq 1500 (single-end mode, 50 cycles).

#### 4.2.12 Southern blot analysis

DNA was separated by 1-1.5% agarose gel electrophoresis in TAE buffer at 100 V for 2 h under stirring to avoid local overheating. The agarose gel was incubated for 20 min in denaturation buffer (0.5 M NaOH, 1.5 M NaCl). The blot membrane (Biodyne® B 0.45 µm, Pall Life Science) was washed first with ddH<sub>2</sub>O, and second in 20x SSC buffer (3 M NaCl, 0.3 M sodium citrate) for 10 min. Whatman paper was soaked shortly in 20x SSC buffer. The blot was assembled as following: two soaked Whatman papers (reaching into tray filled with 20x SSC), agarose gel, blotting membrane, two soaked Whatman paper, one dry Whatman paper, a stack of tissue paper and a glass plate on top with additional weight. Southern blotting was performed O/N. The membrane was baked for 2 h at 80°C and washed once with 500 ml 3x SSC buffer for 30 min at 68°C and 500 ml 3x SSC/1x Denhardt (10x Denhardt buffer 5% (w/v) SDS, 10 mM EDTA, pH 8.0, 0.2% (w/v) BSA, 0.2% (w/v) Ficoll, 0.2% (w/v) PVP40) for 2 h at 68°C. Prehybridisation was performed in 25 ml prehybridisation buffer (2 SSC, 1x Denhardt, 0.1 mg/ml heat denatured salmon sperm DNA) for 1 h at 68°C. The Prime-It II Random Primer Labeling Kit (Stratagene) was used to radioactively label DNA probes. 12 µl DNA (50 ng) was mixed with 5 µl random primer mix

and the reaction mix was denatured for 5 min at 95°C and subsequently cooled on ice. Reaction mix was incubated at 37°C for 10 min after addition of 5 µl dCTP buffer, 2.5 µl <sup>32</sup>P dCTP (3000 µCi/mmol) and 5 U Klenow large Fragment (MO210L, NEB). 100 µl STE buffer (0.1 M NaCl, 10 mM Tris/HCl, 1 mM EDTA, pH 8.0) was added to stop the reaction. Unbound radioactive labeled dCTP was removed by illustra MicroSpin S-300 HR Columns (VWR). The radioactive labeled DNA was denatured (5 min, 95°C), cooled on ice and half the volume of the radioactively labeled DNA was added to the membrane(s) in 5 ml prehybridisation buffer. Hybridization was performed O/N at 68°C on a rotating wheel. Membrane was rinsed 3x shortly with 2x SSC at RT and 3x with 2x SSC/1x Denhardt at 68°C for 30 min. In plastic foil wrapped membrane was exposed to Phosphorimager screen (Fujifilm imaging plate, BAS-MP) and detected by Phosphorimager (FLA3000, FUJIFILM). Quantification of DNA signal intensities was performed using AIDA software v.4.27 (Raytest). The percentage of DNA fragment was calculated using the ratio of total signal intensity in whole lane (= 100%) to the signal intensity of the corresponding DNA fragment (Figure 2.26 and Figure 2.27).

### 4.3 Bioinformatics

The bioinformatical analyses were established and conducted by Dr. Pawel Smialowski, if not stated otherwise, and are briefly summarized in the following.

#### 4.3.1 Data sets and genomic coordinates for TSS annotation

Sequencing reads of CAGEscan-seq and nanoCAGE-seq as delivered by DNAFORM (SourceBioScience) were uniquely mapped to *Schizosacharomyces pombe* genome release 20 from Ensembl (<https://www.ensembl.org/>) using STAR software (version 2.4.2a) (Dobin and Gingeras 2015). Integrated Genome Browser 9.0 (Robinson *et al.*, 2011) was used for visualization of mapped sequencing reads.

##### 4.3.1.1 TSS annotation and statistical analysis

TSS positions were determined by using CAGER 1.10 (Haberle *et al.*, 2015) and HOMER 4.8 (Heinz *et al.*, 2010). Initial G was removed from sequencing reads using CAGER 1.10. Putative TSSs were required to be spaced by at least 30 bp. Read signals that did not have any neighbors in range of +/-100 bp were marked as single signals (majority of cases). The remaining signals were marked as signal cluster TSS (= multiple TSSs). For comparative analysis identifying CSCTs, read signal intensities had to be 8x greater than any signal of the reference in a 30 bp window and 2x greater than the local background in a 100 bp window.

Similarities between data sets were ascertained by calculating the Pearson correlation, Jaccard statistics and relative distance distribution as described in Favorov *et al.*, 2012 (Favorov *et al.*, 2012).

#### 4.3.1.2 DNA feature analysis

Motif search analysis was performed by using WebLogo (Crooks *et al.*, 2004). DNA shape analysis was performed using GBshape database (Zhou *et al.*, 2013; Chiu *et al.*, 2015). GC skew analysis was defined using C and G content as  $(C - G) / (C + G)$  smoothed by moving average of 100 bp window. The GC skew was calculated for the same strand of the analyzed TSS. Position weight matrix (PWM) analysis was performed for Sap1 binding sites as described in (Stormo 2000) using consensus sequence as published in Tsankov *et al.*, 2011 (performed by Dr. Tobias Straub).

#### 4.3.2 MNase-seq analysis

Sequencing reads, generated by MNase-seq and MNase-ChIP-seq, were uniquely mapped to *Schizosaccharomyces pombe* genome release 20 from Ensembl (<https://www.ensembl.org/>) using Bowtie 1.2.2 (Langmead *et al.*, 2009). Nucleosome dyad positions were determined either as described in (Zhang *et al.*, 2011; Krietenstein *et al.*, 2016) (for chapter 2.2 and 2.3) or nucleosome positions were called using DANPOS (Chen *et al.*, 2013) and average values were normalized to 0-1 range (chapter 2.1). All composite plots were drawn using R version 3.1.2.

#### 4.3.3 ChIP-seq analysis

Sequencing reads of ChIP-seq were uniquely mapped to *Schizosaccharomyces pombe* genome release 20 from Ensembl (<https://www.ensembl.org/>) using STAR software version 2.4.2a with setup, which disallows intro (Dobin and Gingeras 2015). Peak detection for IP/Input fraction was performed by using HOMER 4.8 (Heinz *et al.*, 2010). Peaks were restricted to have a minimal distance of 280 bp. Peaks present in both biological replicates were used for further analysis. Motifs, which were most enriched around the Tbp1 binding sites, were extracted using HOMER 4.8 with motif length set to 8-12 and search area of 200 bp window. The genome was searched for the presence of given motifs using FIMO from MEME Suite version 4.11.1 (Bailey *et al.*, 2015).

#### 4.3.4 Simulation of nucleosome assembly

Simulation was done by Dr. Johannes Nuebler as described in (Osberg *et al.*, 2014; Osberg *et al.*, 2015).

---

## References

- Albert, I., Mavrich, T. N., Tomsho, L. P., Qi, J., Zanton, S. J., Schuster, S. C. and Pugh, B. F. (2007). "Translational and rotational settings of H2A.Z nucleosomes across the *Saccharomyces cerevisiae* genome." *Nature* **446**(7135): 572-576.
- Allshire, R. C. and Ekwall, K. (2015). "Epigenetic Regulation of Chromatin States in *Schizosaccharomyces pombe*." *Cold Spring Harb Perspect Biol* **7**(7): a018770.
- Almer, A., Rudolph, H., Hinnen, A. and Horz, W. (1986). "Removal of positioned nucleosomes from the yeast PHO5 promoter upon PHO5 induction releases additional upstream activating DNA elements." *Embo j* **5**(10): 2689-2696.
- Badis, G., Chan, E. T., van Bakel, H., Pena-Castillo, L., Tillo, D., Tsui, K., Carlson, C. D., Gossett, A. J., Hasiñoff, M. J., Warren, C. L., Gebbia, M., Talukder, S., Yang, A., Mnaimneh, S., Terterov, D., Coburn, D., Li Yeo, A., Yeo, Z. X., Clarke, N. D., Lieb, J. D., Ansari, A. Z., Nislow, C. and Hughes, T. R. (2008). "A library of yeast transcription factor motifs reveals a widespread function for Rsc3 in targeting nucleosome exclusion at promoters." *Mol Cell* **32**(6): 878-887.
- Bailey, T. L., Johnson, J., Grant, C. E. and Noble, W. S. (2015). "The MEME Suite." *Nucleic Acids Res* **43**(W1): W39-49.
- Bannister, A. J. and Kouzarides, T. (2011). "Regulation of chromatin by histone modifications." *Cell Res* **21**(3): 381-395.
- Barbet, N., Muriel, W. J. and Carr, A. M. (1992). "Versatile shuttle vectors and genomic libraries for use with *Schizosaccharomyces pombe*." *Gene* **114**(1): 59-66.
- Bartholomew, B. (2014). "Regulating the Chromatin Landscape: Structural and Mechanistic Perspectives." *Annual Review of Biochemistry* **83**(1): 671-696.
- Basehoar, A. D., Zanton, S. J. and Pugh, B. F. (2004). "Identification and distinct regulation of yeast TATA box-containing genes." *Cell* **116**(5): 699-709.
- Becker, P. B. and Wu, C. (1992). "Cell-free system for assembly of transcriptionally repressed chromatin from *Drosophila* embryos." *Mol Cell Biol* **12**(5): 2241-2249.
- Belotserkovskaya, R., Oh, S., Bondarenko, V. A., Orphanides, G., Studitsky, V. M. and Reinberg, D. (2003). "FACT facilitates transcription-dependent nucleosome alteration." *Science* **301**(5636): 1090-1093.
- Bernal, G. and Maldonado, E. (2007). "Isolation of a novel complex of the SWI/SNF family from *Schizosaccharomyces pombe* and its effects on in vitro transcription in nucleosome arrays." *Mol Cell Biochem* **303**(1-2): 131-139.
- Birney, E., Stamatoyannopoulos, J. A., Dutta, A., Guigo, R., Gingeras, T. R., Margulies, E. H., Weng, Z., Snyder, M., Dermitzakis, E. T., Thurman, R. E., Kuehn, M. S., Taylor, C. M., Neph, S., Koch, C. M., Asthana, S., Malhotra, A., Adzhubei, I., Greenbaum, J. A., Andrews, R. M., Flicek, P., Boyle, P. J., Cao, H., Carter, N. P., Clelland, G. K., Davis, S., Day, N., Dhami, P., Dillon, S. C., Dorschner, M. O., Fiegler, H., Giresi, P. G., Goldy, J., Hawrylycz, M., Haydock, A., Humbert, R., James, K. D., Johnson, B. E., Johnson, E. M., Frum, T. T., Rosenzweig, E. R., Karnani, N., Lee, K., Lefebvre, G. C., Navas, P. A., Neri, F., Parker, S. C., Sabo, P. J., Sandstrom, R., Shafer, A., Vetric, D., Weaver, M., Wilcox, S., Yu, M., Collins, F. S., Dekker, J., Lieb, J. D., Tullius, T. D., Crawford, G. E., Sunyaev, S., Noble, W. S., Dunham, I., Deneud, F., Reymond, A., Kapranov, P., Rozowsky, J., Zheng, D., Castelo, R., Frankish, A., Harrow, J., Ghosh, S., Sandelin, A., Hofacker, I. L., Baertsch, R., Keefe, D., Dike, S., Cheng, J., Hirsch, H. A., Sekinger, E. A., Lagarde, J., Abril, J. F., Shahab, A., Flamm, C., Fried, C., Hackermuller, J., Hertel, J., Lindemeyer, M., Missal, K., Tanzer, A., Washietl, S., Korbelt, J., Emanuelsson, O., Pedersen, J. S., Holroyd, N., Taylor, R., Swarbreck, D., Matthews, N., Dickson, M. C., Thomas, D. J., Weirauch, M. T., Gilbert, J., Drenkow, J., Bell, I., Zhao, X., Srinivasan, K. G., Sung, W. K., Ooi, H. S., Chiu, K. P., Foissac, S., Alioto, T., Brent, M., Pachter, L., Tress, M. L., Valencia, A., Choo, S. W., Choo, C. Y., Ucla, C., Manzano, C., Wyss, C., Cheung, E., Clark, T. G., Brown, J. B., Ganesh, M., Patel, S., Tammana, H., Chrast, J., Henrichsen, C. N., Kai, C., Kawai, J., Nagalakshmi, U., Wu, J., Lian, Z., Lian, J., Newburger, P., Zhang, X., Bickel, P., Mattick, J. S., Carninci, P., Hayashizaki, Y., Weissman, S., Hubbard, T., Myers, R. M., Rogers, J., Stadler, P. F., Lowe, T. M., Wei, C. L., Ruan, Y., Struhl, K., Gerstein, M., Antonarakis, S. E., Fu, Y., Green, E. D., Karaoz, U., Siepel, A., Taylor, J., Liefer, L. A., Wetterstrand, K. A., Good, P. J., Feingold, E. A., Guyer, M. S., Cooper, G. M., Asimeng, G., Dewey, C. N., Hou, M., Nikolaev, S., Montoya-Burgos, J. I., Loytynoja, A., Whelan, S., Pardi, F., Massingham, T., Huang, H., Zhang, N. R., Holmes, I., Mullikin, J. C., Ureta-Vidal, A., Paten, B., Sringhaus, M., Church, D., Rosenbloom, K., Kent, W. J., Stone, E. A., Batzoglou, S., Goldman, N., Hardison, R. C., Haussler, D., Miller, W., Sidow, A., Trinklein, N. D., Zhang, Z. D., Barrera, L., Stuart, R., King, D. C., Ameur, A., Enroth, S., Bieda, M. C., Kim, J., Bhinge, A. A., Jiang, N., Liu, J., Yao, F., Vega, V. B., Lee, C. W., Ng, P., Shahab, A., Yang, A., Moqtaderi, Z., Zhu, Z., Xu, X., Squazzo, S., Oberley, M. J., Inman, D., Singer, M. A., Richmond, T. A., Munn, K. J., Rada-Iglesias, A., Wallerman, O., Komorowski, J., Fowler, J. C., Couttet, P., Bruce, A. W., Dovey, O. M., Ellis, P. D., Langford, C. F., Nix, D. A., Euskirchen, G., Hartman, S.,

- Urban, A. E., Kraus, P., Van Calcar, S., Heintzman, N., Kim, T. H., Wang, K., Qu, C., Hon, G., Luna, R., Glass, C. K., Rosenfeld, M. G., Aldred, S. F., Cooper, S. J., Halees, A., Lin, J. M., Shulha, H. P., Zhang, X., Xu, M., Haidar, J. N., Yu, Y., Ruan, Y., Iyer, V. R., Green, R. D., Wadelius, C., Farnham, P. J., Ren, B., Harte, R. A., Hinrichs, A. S., Trumbower, H., Clawson, H., Hillman-Jackson, J., Zweig, A. S., Smith, K., Thakkapallayil, A., Barber, G., Kuhn, R. M., Karolchik, D., Armengol, L., Bird, C. P., de Bakker, P. I., Kern, A. D., Lopez-Bigas, N., Martin, J. D., Stranger, B. E., Woodroffe, A., Davydov, E., Dimas, A., Eyas, E., Hallgrimsdottir, I. B., Huppert, J., Zody, M. C., Abecasis, G. R., Estivill, X., Bouffard, G. G., Guan, X., Hansen, N. F., Idol, J. R., Maduro, V. V., Maskeri, B., McDowell, J. C., Park, M., Thomas, P. J., Young, A. C., Blakesley, R. W., Muzny, D. M., Sodergren, E., Wheeler, D. A., Worley, K. C., Jiang, H., Weinstock, G. M., Gibbs, R. A., Graves, T., Fulton, R., Mardis, E. R., Wilson, R. K., Clamp, M., Cuff, J., Gnerre, S., Jaffe, D. B., Chang, J. L., Lindblad-Toh, K., Lander, E. S., Koriabine, M., Nefedov, M., Osoegawa, K., Yoshinaga, Y., Zhu, B. and de Jong, P. J. (2007). "Identification and analysis of functional elements in 1% of the human genome by the ENCODE pilot project." *Nature* **447**(7146): 799-816.
- Booth, G. T., Wang, I. X., Cheung, V. G. and Lis, J. T. (2016). "Divergence of a conserved elongation factor and transcription regulation in budding and fission yeast." *Genome Res* **26**(6): 799-811.
- Bortvin, A. and Winston, F. (1996). "Evidence that Spt6p controls chromatin structure by a direct interaction with histones." *Science* **272**(5267): 1473-1476.
- Brocks, D., Schmidt, C. R., Daskalakis, M., Jang, H. S., Shah, N. M., Li, D., Li, J., Zhang, B., Hou, Y., Laudato, S., Lipka, D. B., Schott, J., Bierhoff, H., Assenov, Y., Helf, M., Ressenrova, A., Islam, M. S., Lindroth, A. M., Haas, S., Essers, M., Imbusch, C. D., Brors, B., Oehme, I., Witt, O., Lubbert, M., Mallm, J. P., Rippe, K., Will, R., Weichenhan, D., Stoecklin, G., Gerhauser, C., Oakes, C. C., Wang, T. and Plass, C. (2017). "DNMT and HDAC inhibitors induce cryptic transcription start sites encoded in long terminal repeats." *Nat Genet* **49**(7): 1052-1060.
- Brogaard, K., Xi, L., Wang, J. P. and Widom, J. (2012). "A map of nucleosome positions in yeast at base-pair resolution." *Nature* **486**(7404): 496-501.
- Buchanan, L., Durand-Dubief, M., Roguev, A., Sakalar, C., Wilhelm, B., Stralfors, A., Shevchenko, A., Aasland, R., Shevchenko, A., Ekwall, K. and Francis Stewart, A. (2009). "The Schizosaccharomyces pombe JmjC-protein, Msc1, prevents H2A.Z localization in centromeric and subtelomeric chromatin domains." *PLoS Genet* **5**(11): e1000726.
- Butler, J. E. and Kadonaga, J. T. (2002). "The RNA polymerase II core promoter: a key component in the regulation of gene expression." *Genes Dev* **16**(20): 2583-2592.
- Cairns, B. R. (2009). "The logic of chromatin architecture and remodelling at promoters." *Nature* **461**(7261): 193-198.
- Carninci, P. (2009). "Molecular biology: The long and short of RNAs." *Nature* **457**(7232): 974-975.
- Carninci, P., Nishiyama, Y., Westover, A., Itoh, M., Nagaoka, S., Sasaki, N., Okazaki, Y., Muramatsu, M. and Hayashizaki, Y. (1998). "Thermostabilization and thermoactivation of thermolabile enzymes by trehalose and its application for the synthesis of full length cDNA." *Proc Natl Acad Sci U S A* **95**(2): 520-524.
- Carninci, P., Sandelin, A., Lenhard, B., Katayama, S., Shimokawa, K., Ponjavic, J., Semple, C. A., Taylor, M. S., Engstrom, P. G., Frith, M. C., Forrest, A. R., Alkema, W. B., Tan, S. L., Plessy, C., Kodzius, R., Ravasi, T., Kasukawa, T., Fukuda, S., Kanamori-Katayama, M., Kitazume, Y., Kawaji, H., Kai, C., Nakamura, M., Konno, H., Nakano, K., Mottagui-Tabar, S., Arner, P., Chesi, A., Gustincich, S., Persichetti, F., Suzuki, H., Grimmond, S. M., Wells, C. A., Orlando, V., Wahlestedt, C., Liu, E. T., Harbers, M., Kawai, J., Bajic, V. B., Hume, D. A. and Hayashizaki, Y. (2006). "Genome-wide analysis of mammalian promoter architecture and evolution." *Nat Genet* **38**(6): 626-635.
- Celona, B., Weiner, A., Di Felice, F., Mancuso, F. M., Cesarini, E., Rossi, R. L., Gregory, L., Baban, D., Rossetti, G., Grianti, P., Pagani, M., Bonaldi, T., Ragoussis, J., Friedman, N., Camilloni, G., Bianchi, M. E. and Agresti, A. (2011). "Substantial histone reduction modulates genomewide nucleosomal occupancy and global transcriptional output." *PLoS Biol* **9**(6): e1001086.
- Chen, K., Xi, Y., Pan, X., Li, Z., Kaestner, K., Tyler, J., Dent, S., He, X. and Li, W. (2013). "DANPOS: dynamic analysis of nucleosome position and occupancy by sequencing." *Genome Res* **23**(2): 341-351.
- Chen, X. and Zhang, J. (2016). "The Genomic Landscape of Position Effects on Protein Expression Level and Noise in Yeast." *Cell Syst* **2**(5): 347-354.

## References

---

- Chereji, R. V., Kan, T. W., Grudniewska, M. K., Romashchenko, A. V., Berezikov, E., Zhimulev, I. F., Guryev, V., Morozov, A. V. and Moshkin, Y. M. (2016). "Genome-wide profiling of nucleosome sensitivity and chromatin accessibility in *Drosophila melanogaster*." *Nucleic Acids Res* **44**(3): 1036-1051.
- Chereji, R. V., Ocampo, J. and Clark, D. J. (2017). "MNase-Sensitive Complexes in Yeast: Nucleosomes and Non-histone Barriers." *Mol Cell* **65**(3): 565-577.e563.
- Chereji, R. V., Ramachandran, S., Bryson, T. D. and Henikoff, S. (2018). "Precise genome-wide mapping of single nucleosomes and linkers in vivo." *Genome Biol* **19**(1): 19.
- Cheung, V., Chua, G., Batada, N. N., Landry, C. R., Michnick, S. W., Hughes, T. R. and Winston, F. (2008). "Chromatin- and transcription-related factors repress transcription from within coding regions throughout the *Saccharomyces cerevisiae* genome." *PLoS Biol* **6**(11): e277.
- Chiu, T. P., Yang, L., Zhou, T., Main, B. J., Parker, S. C., Nuzhdin, S. V., Tullius, T. D. and Rohs, R. (2015). "GBshape: a genome browser database for DNA shape annotations." *Nucleic Acids Res* **43**(Database issue): D103-109.
- Chung, H. R., Dunkel, I., Heise, F., Linke, C., Krobitsch, S., Ehrenhofer-Murray, A. E., Sperling, S. R. and Vingron, M. (2010). "The effect of micrococcal nuclease digestion on nucleosome positioning data." *PLoS One* **5**(12): e15754.
- Clapier, C. R. and Cairns, B. R. (2009). "The biology of chromatin remodeling complexes." *Annu Rev Biochem* **78**: 273-304.
- Crooks, G. E., Hon, G., Chandonia, J. M. and Brenner, S. E. (2004). "WebLogo: a sequence logo generator." *Genome Res* **14**(6): 1188-1190.
- Dechassa, M. L., Sabri, A., Pondugula, S., Kassabov, S. R., Chatterjee, N., Kladde, M. P. and Bartholomew, B. (2010). "SWI/SNF has intrinsic nucleosome disassembly activity that is dependent on adjacent nucleosomes." *Mol Cell* **38**(4): 590-602.
- DeGennaro, C. M., Alver, B. H., Marguerat, S., Stepanova, E., Davis, C. P., Bahler, J., Park, P. J. and Winston, F. (2013). "Spt6 regulates intragenic and antisense transcription, nucleosome positioning, and histone modifications genome-wide in fission yeast." *Mol Cell Biol* **33**(24): 4779-4792.
- Dion, M. F., Kaplan, T., Kim, M., Buratowski, S., Friedman, N. and Rando, O. J. (2007). "Dynamics of replication-independent histone turnover in budding yeast." *Science* **315**(5817): 1405-1408.
- Dobin, A. and Gingeras, T. R. (2015). "Mapping RNA-seq Reads with STAR." *Curr Protoc Bioinformatics* **51**: 11.14.11-19.
- Dutrow, N., Nix, D. A., Holt, D., Milash, B., Dalley, B., Westbroek, E., Parnell, T. J. and Cairns, B. R. (2008). "Dynamic transcriptome of *Schizosaccharomyces pombe* shown by RNA-DNA hybrid mapping." *Nat Genet* **40**(8): 977-986.
- Engel, C., Gubbey, T., Neyer, S., Sainsbury, S., Oberthuer, C., Baejen, C., Bernecky, C. and Cramer, P. (2017). "Structural Basis of RNA Polymerase I Transcription Initiation." *Cell* **169**(1): 120-131.e122.
- Eser, P., Wachutka, L., Maier, K. C., Demel, C., Boroni, M., Iyer, S., Cramer, P. and Gagneur, J. (2016). "Determinants of RNA metabolism in the *Schizosaccharomyces pombe* genome." *Mol Syst Biol* **12**(2): 857.
- Farnung, L., Vos, S. M., Wigge, C. and Cramer, P. (2017). "Nucleosome-Chd1 structure and implications for chromatin remodelling." *Nature* **550**(7677): 539-542.
- Faulhaber, I. and Bernardi, G. (1967). "Chromatography of calf-thymus nucleoprotein on hydroxyapatite columns." *Biochim Biophys Acta* **140**(3): 561-564.
- Favorov, A., Mularoni, L., Cope, L. M., Medvedeva, Y., Mironov, A. A., Makeev, V. J. and Wheelan, S. J. (2012). "Exploring massive, genome scale datasets with the GenometriCorr package." *PLoS Comput Biol* **8**(5): e1002529.
- Finch, J. T. and Klug, A. (1976). "Solenoidal model for superstructure in chromatin." *Proc Natl Acad Sci U S A* **73**(6): 1897-1901.
- Flaus, A., Martin, D. M., Barton, G. J. and Owen-Hughes, T. (2006). "Identification of multiple distinct Snf2 subfamilies with conserved structural motifs." *Nucleic Acids Res* **34**(10): 2887-2905.

Flemming, W. (1878). Zur Kenntniss der Zelle und ihrer Theilungs-Erscheinungen. *Schr. Nat. Wiss. Ver. Schlesw.-Holst.* **3** (1): 23-27.

Floer, M., Wang, X., Prabhu, V., Berrozpe, G., Narayan, S., Spagna, D., Alvarez, D., Kendall, J., Krasnitz, A., Stepansky, A., Hicks, J., Bryant, G. O. and Ptashne, M. (2010). "A RSC/nucleosome complex determines chromatin architecture and facilitates activator binding." *Cell* **141**(3): 407-418.

Forrest, A. R., Kawaji, H., Rehli, M., Baillie, J. K., de Hoon, M. J., Haberle, V., Lassmann, T., Kulakovskiy, I. V., Lizio, M., Itoh, M., Andersson, R., Mungall, C. J., Meehan, T. F., Schmeier, S., Bertin, N., Jorgensen, M., Dimont, E., Arner, E., Schmidl, C., Schaefer, U., Medvedeva, Y. A., Plessy, C., Vitezic, M., Severin, J., Semple, C., Ishizu, Y., Young, R. S., Francescato, M., Alam, I., Albanese, D., Altschuler, G. M., Arakawa, T., Archer, J. A., Arner, P., Babina, M., Rennie, S., Balwierz, P. J., Beckhouse, A. G., Pradhan-Bhatt, S., Blake, J. A., Blumenthal, A., Bodega, B., Bonetti, A., Briggs, J., Brombacher, F., Burroughs, A. M., Califano, A., Cannistraci, C. V., Carbajo, D., Chen, Y., Chierici, M., Ciani, Y., Clevers, H. C., Dalla, E., Davis, C. A., Detmar, M., Diehl, A. D., Dohi, T., Drablos, F., Edge, A. S., Edinger, M., Ekwall, K., Endoh, M., Enomoto, H., Fagiolini, M., Fairbairn, L., Fang, H., Farach-Carson, M. C., Faulkner, G. J., Favorov, A. V., Fisher, M. E., Frith, M. C., Fujita, R., Fukuda, S., Furlanello, C., Furino, M., Furusawa, J., Geijtenbeek, T. B., Gibson, A. P., Gingeras, T., Goldowitz, D., Gough, J., Guhl, S., Guler, R., Gustincich, S., Ha, T. J., Hamaguchi, M., Hara, M., Harbers, M., Harshbarger, J., Hasegawa, A., Hasegawa, Y., Hashimoto, T., Herlyn, M., Hitchens, K. J., Ho Sui, S. J., Hofmann, O. M., Hoof, I., Hori, F., Huminiecki, L., Iida, K., Ikawa, T., Jankovic, B. R., Jia, H., Joshi, A., Jurman, G., Kaczkowski, B., Kai, C., Kaida, K., Kaiho, A., Kajiyama, K., Kanamori-Katayama, M., Kasianov, A. S., Kasukawa, T., Katayama, S., Kato, S., Kawaguchi, S., Kawamoto, H., Kawamura, Y. I., Kawashima, T., Kempfle, J. S., Kenna, T. J., Kere, J., Khachigian, L. M., Kitamura, T., Klinken, S. P., Knox, A. J., Kojima, M., Kojima, S., Kondo, N., Koseki, H., Koyasu, S., Krampitz, S., Kubosaki, A., Kwon, A. T., Laros, J. F., Lee, W., Lennartsson, A., Li, K., Lilje, B., Lipovich, L., Mackay-Sim, A., Manabe, R., Mar, J. C., Marchand, B., Mathelier, A., Mejhert, N., Meynert, A., Mizuno, Y., de Lima Morais, D. A., Morikawa, H., Morimoto, M., Moro, K., Motakis, E., Motohashi, H., Mummery, C. L., Murata, M., Nagao-Sato, S., Nakachi, Y., Nakahara, F., Nakamura, T., Nakamura, Y., Nakazato, K., van Nimwegen, E., Ninomiya, N., Nishiyori, H., Noma, S., Noma, S., Nozaki, T., Ogishima, S., Ohkura, N., Ohimiya, H., Ohno, H., Ohshima, M., Okada-Hatakeyama, M., Okazaki, Y., Orlando, V., Ovchinnikov, D. A., Pain, A., Passier, R., Patrikakis, M., Persson, H., Piazza, S., Prendergast, J. G., Rackham, O. J., Ramilowski, J. A., Rashid, M., Ravasi, T., Rizzu, P., Roncador, M., Roy, S., Rye, M. B., Saijyo, E., Sajantila, A., Saka, A., Sakaguchi, S., Sakai, M., Sato, H., Savvi, S., Saxena, A., Schneider, C., Schultes, E. A., Schulze-Tanzil, G. G., Schwegmann, A., Sengstag, T., Sheng, G., Shimoji, H., Shimon, Y., Shin, J. W., Simon, C., Sugiyama, D., Sugiyama, T., Suzuki, M., Suzuki, N., Swoboda, R. K., t Hoen, P. A., Tagami, M., Takahashi, N., Takai, J., Tanaka, H., Tatsukawa, H., Tatum, Z., Thompson, M., Toyodo, H., Toyoda, T., Valen, E., van de Wetering, M., van den Berg, L. M., Verado, R., Vijayan, D., Vorontsov, I. E., Wasserman, W. W., Watanabe, S., Wells, C. A., Winteringham, L. N., Wolvetang, E., Wood, E. J., Yamaguchi, Y., Yamamoto, M., Yoneda, M., Yonekura, Y., Yoshida, S., Zabierowski, S. E., Zhang, P. G., Zhao, X., Zucchelli, S., Summers, K. M., Suzuki, H., Daub, C. O., Kawai, J., Heutink, P., Hide, W., Freeman, T. C., Lenhard, B., Bajic, V. B., Taylor, M. S., Makeev, V. J., Sandelin, A., Hume, D. A., Carninci, P. and Hayashizaki, Y. (2014). "A promoter-level mammalian expression atlas." *Nature* **507**(7493): 462-470.

Forte, P., Leoni, L., Sampaolese, B. and Savino, M. (1989). "Cooperativity in nucleosomes assembly on supercoiled pBR322 DNA." *Nucleic Acids Res* **17**(21): 8683-8694.

Fujii, S., Kono, H., Takenaka, S., Go, N. and Sarai, A. (2007). "Sequence-dependent DNA deformability studied using molecular dynamics simulations." *Nucleic Acids Res* **35**(18): 6063-6074.

Funke, J. J., Ketterer, P., Lieleg, C., Schunter, S., Korber, P. and Dietz, H. (2016). "Uncovering the forces between nucleosomes using DNA origami." *Sci Adv* **2**(11): e1600974.

Gaillard, H. and Aguilera, A. (2016). "Transcription as a Threat to Genome Integrity." *Annu Rev Biochem* **85**: 291-317.

Gibson, D. G., Young, L., Chuang, R. Y., Venter, J. C., Hutchison, C. A., 3rd and Smith, H. O. (2009). "Enzymatic assembly of DNA molecules up to several hundred kilobases." *Nat Methods* **6**(5): 343-345.

Gilchrist, D. A., Dos Santos, G., Fargo, D. C., Xie, B., Gao, Y., Li, L. and Adelman, K. (2010). "Pausing of RNA polymerase II disrupts DNA-specified nucleosome organization to enable precise gene regulation." *Cell* **143**(4): 540-551.

Gkikopoulos, T., Schofield, P., Singh, V., Pinskaya, M., Mellor, J., Smolle, M., Workman, J. L., Barton, G. J. and Owen-Hughes, T. (2011). "A role for Snf2-related nucleosome-spacing enzymes in genome-wide nucleosome organization." *Science* **333**(6050): 1758-1760.

Godde, J. S. and Widom, J. (1992). "Chromatin structure of *Schizosaccharomyces pombe*. A nucleosome repeat length that is shorter than the chromatosomal DNA length." *J Mol Biol* **226**(4): 1009-1025.

## References

---

- Goffeau, A., Barrell, B. G., Bussey, H., Davis, R. W., Dujon, B., Feldmann, H., Galibert, F., Hoheisel, J. D., Jacq, C., Johnston, M., Louis, E. J., Mewes, H. W., Murakami, Y., Philippsen, P., Tettelin, H. and Oliver, S. G. (1996). "Life with 6000 genes." *Science* **274**(5287): 546, 563-547.
- Gossett, A. J. and Lieb, J. D. (2012). "In vivo effects of histone H3 depletion on nucleosome occupancy and position in *Saccharomyces cerevisiae*." *PLoS Genet* **8**(6): e1002771.
- Grune, T., Brzeski, J., Eberharter, A., Clapier, C. R., Corona, D. F., Becker, P. B. and Muller, C. W. (2003). "Crystal structure and functional analysis of a nucleosome recognition module of the remodeling factor ISWI." *Mol Cell* **12**(2): 449-460.
- Guillemette, B., Bataille, A. R., Gevry, N., Adam, M., Blanchette, M., Robert, F. and Gaudreau, L. (2005). "Variant histone H2A.Z is globally localized to the promoters of inactive yeast genes and regulates nucleosome positioning." *PLoS Biol* **3**(12): e384.
- Haberle, V., Forrest, A. R., Hayashizaki, Y., Carninci, P. and Lenhard, B. (2015). "CAGEr: precise TSS data retrieval and high-resolution promoterome mining for integrative analyses." *Nucleic Acids Res* **43**(8): e51.
- Haberle, V., Li, N., Hadzhiev, Y., Plessy, C., Previti, C., Nepal, C., Gehrig, J., Dong, X., Akalin, A., Suzuki, A. M., van, I. W. F. J., Armant, O., Ferg, M., Strahle, U., Carninci, P., Muller, F. and Lenhard, B. (2014). "Two independent transcription initiation codes overlap on vertebrate core promoters." *Nature* **507**(7492): 381-385.
- Hartley, P. D. and Madhani, H. D. (2009). "Mechanisms that specify promoter nucleosome location and identity." *Cell* **137**(3): 445-458.
- Heinz, S., Benner, C., Spann, N., Bertolino, E., Lin, Y. C., Laslo, P., Cheng, J. X., Murre, C., Singh, H. and Glass, C. K. (2010). "Simple combinations of lineage-determining transcription factors prime cis-regulatory elements required for macrophage and B cell identities." *Mol Cell* **38**(4): 576-589.
- Henikoff, S. and Ahmad, K. (2005). "Assembly of variant histones into chromatin." *Annu Rev Cell Dev Biol* **21**: 133-153.
- Hennig, B. P., Bendrin, K., Zhou, Y. and Fischer, T. (2012). "Chd1 chromatin remodelers maintain nucleosome organization and repress cryptic transcription." *EMBO Rep* **13**(11): 997-1003.
- Hirota, K., Miyoshi, T., Kugou, K., Hoffman, C. S., Shibata, T. and Ohta, K. (2008). "Stepwise chromatin remodelling by a cascade of transcription initiation of non-coding RNAs." *Nature* **456**(7218): 130-134.
- Hoffman, C. S., Wood, V. and Fantes, P. A. (2015). "An Ancient Yeast for Young Geneticists: A Primer on the *Schizosaccharomyces pombe* Model System." *Genetics* **201**(2): 403-423.
- Horz, W. and Altenburger, W. (1981). "Sequence specific cleavage of DNA by micrococcal nuclease." *Nucleic Acids Res* **9**(12): 2643-2658.
- Hoskins, R. A., Landolin, J. M., Brown, J. B., Sandler, J. E., Takahashi, H., Lassmann, T., Yu, C., Booth, B. W., Zhang, D., Wan, K. H., Yang, L., Boley, N., Andrews, J., Kaufman, T. C., Graveley, B. R., Bickel, P. J., Carninci, P., Carlson, J. W. and Celniker, S. E. (2011). "Genome-wide analysis of promoter architecture in *Drosophila melanogaster*." *Genome Res* **21**(2): 182-192.
- Hsieh, T. H., Weiner, A., Lajoie, B., Dekker, J., Friedman, N. and Rando, O. J. (2015). "Mapping Nucleosome Resolution Chromosome Folding in Yeast by Micro-C." *Cell* **162**(1): 108-119.
- Hu, Z., Chen, K., Xia, Z., Chavez, M., Pal, S., Seol, J. H., Chen, C. C., Li, W. and Tyler, J. K. (2014). "Nucleosome loss leads to global transcriptional up-regulation and genomic instability during yeast aging." *Genes Dev* **28**(4): 396-408.
- Hughes, A. L. and Rando, O. J. (2014). "Mechanisms underlying nucleosome positioning in vivo." *Annu Rev Biophys* **43**: 41-63.
- Hughes, A. L. and Rando, O. J. (2015). "Comparative Genomics Reveals Chd1 as a Determinant of Nucleosome Spacing in Vivo." *G3 (Bethesda)* **5**(9): 1889-1897.
- Ioshikhes, I. P., Albert, I., Zanton, S. J. and Pugh, B. F. (2006). "Nucleosome positions predicted through comparative genomics." *Nat Genet* **38**(10): 1210-1215.



- 
- Ivanovska, I., Jacques, P. E., Rando, O. J., Robert, F. and Winston, F. (2011). "Control of chromatin structure by spt6: different consequences in coding and regulatory regions." *Mol Cell Biol* **31**(3): 531-541.
- Jack, A. P. and Hake, S. B. (2014). "Getting down to the core of histone modifications." *Chromosoma* **123**(4): 355-371.
- Jaiswal, R., Singh, S. K., Bastia, D. and Escalante, C. R. (2015). "Crystallization and preliminary X-ray characterization of the eukaryotic replication terminator Reb1-Ter DNA complex." *Acta Crystallogr F Struct Biol Commun* **71**(Pt 4): 414-418.
- Jiang, C. and Pugh, B. F. (2009). "A compiled and systematic reference map of nucleosome positions across the *Saccharomyces cerevisiae* genome." *Genome Biol* **10**(10): R109.
- Johnson, D. S., Mortazavi, A., Myers, R. M. and Wold, B. (2007). "Genome-wide mapping of in vivo protein-DNA interactions." *Science* **316**(5830): 1497-1502.
- Juven-Gershon, T., Hsu, J. Y., Theisen, J. W. and Kadonaga, J. T. (2008). "The RNA polymerase II core promoter - the gateway to transcription." *Curr Opin Cell Biol* **20**(3): 253-259.
- Kadonaga, J. T. (2004). "Regulation of RNA polymerase II transcription by sequence-specific DNA binding factors." *Cell* **116**(2): 247-257.
- Kaplan, C. D., Laprade, L. and Winston, F. (2003). "Transcription elongation factors repress transcription initiation from cryptic sites." *Science* **301**(5636): 1096-1099.
- Kaplan, N., Moore, I., Fondufe-Mittendorf, Y., Gossett, A. J., Tillo, D., Field, Y., Hughes, T. R., Lieb, J. D., Widom, J. and Segal, E. (2010). "Nucleosome sequence preferences influence in vivo nucleosome organization." *Nat Struct Mol Biol* **17**(8): 918-920.
- Kaplan, N., Moore, I. K., Fondufe-Mittendorf, Y., Gossett, A. J., Tillo, D., Field, Y., LeProust, E. M., Hughes, T. R., Lieb, J. D., Widom, J. and Segal, E. (2009). "The DNA-encoded nucleosome organization of a eukaryotic genome." *Nature* **458**(7236): 362-366.
- Kaufner, N. F. and Potashkin, J. (2000). "Analysis of the splicing machinery in fission yeast: a comparison with budding yeast and mammals." *Nucleic Acids Res* **28**(16): 3003-3010.
- Kawaji, H., Lizio, M., Itoh, M., Kanamori-Katayama, M., Kaiho, A., Nishiyori-Sueki, H., Shin, J. W., Kojima-Ishiyama, M., Kawano, M., Murata, M., Ninomiya-Fukuda, N., Ishikawa-Kato, S., Nagao-Sato, S., Noma, S., Hayashizaki, Y., Forrest, A. R. and Carninci, P. (2014). "Comparison of CAGE and RNA-seq transcriptome profiling using clonally amplified and single-molecule next-generation sequencing." *Genome Res* **24**(4): 708-717.
- Korber, P. and Barbaric, S. (2014). "The yeast PHO5 promoter: from single locus to systems biology of a paradigm for gene regulation through chromatin." *Nucleic Acids Res* **42**(17): 10888-10902.
- Kornberg, R. D. and Lorch, Y. (1999). "Twenty-five years of the nucleosome, fundamental particle of the eukaryote chromosome." *Cell* **98**(3): 285-294.
- Kornberg, R. D. and Stryer, L. (1988). "Statistical distributions of nucleosomes: nonrandom locations by a stochastic mechanism." *Nucleic Acids Res* **16**(14a): 6677-6690.
- Korolev, N., Vorontsova, O. V. and Nordenskiold, L. (2007). "Physicochemical analysis of electrostatic foundation for DNA-protein interactions in chromatin transformations." *Prog Biophys Mol Biol* **95**(1-3): 23-49.
- Krietenstein, N., Wal, M., Watanabe, S., Park, B., Peterson, C. L., Pugh, B. F. and Korber, P. (2016). "Genomic Nucleosome Organization Reconstituted with Pure Proteins." *Cell* **167**(3): 709-721.e712.
- Krietenstein, N., Wippo, C. J., Lieleg, C. and Korber, P. (2012). "Genome-wide in vitro reconstitution of yeast chromatin with in vivo-like nucleosome positioning." *Methods Enzymol* **513**: 205-232.
- Krogan, N. J., Kim, M., Ahn, S. H., Zhong, G., Kobor, M. S., Cagney, G., Emili, A., Shilatifard, A., Buratowski, S. and Greenblatt, J. F. (2002). "RNA polymerase II elongation factors of *Saccharomyces cerevisiae*: a targeted proteomics approach." *Mol Cell Biol* **22**(20): 6979-6992.
- Kubik, S., Bruzzone, M. J., Albert, B. and Shore, D. (2017). "A Reply to "MNase-Sensitive Complexes in Yeast: Nucleosomes and Non-histone Barriers," by Chereji et al." *Mol Cell* **65**(3): 578-580.
-

## References

---

- Kubik, S., Bruzzone, M. J., Jacquet, P., Falcone, J. L., Rougemont, J. and Shore, D. (2015). "Nucleosome Stability Distinguishes Two Different Promoter Types at All Protein-Coding Genes in Yeast." *Mol Cell* **60**(3): 422-434.
- Kubik, S., Bruzzone, M. J. and Shore, D. (2017). "Establishing nucleosome architecture and stability at promoters: Roles of pioneer transcription factors and the RSC chromatin remodeler." *Bioessays* **39**(5).
- Kutach, A. K. and Kadonaga, J. T. (2000). "The downstream promoter element DPE appears to be as widely used as the TATA box in Drosophila core promoters." *Mol Cell Biol* **20**(13): 4754-4764.
- Lai, W. K. M. and Pugh, B. F. (2017). "Understanding nucleosome dynamics and their links to gene expression and DNA replication." *Nat Rev Mol Cell Biol* **18**(9): 548-562.
- Langmead, B., Trapnell, C., Pop, M. and Salzberg, S. L. (2009). "Ultrafast and memory-efficient alignment of short DNA sequences to the human genome." *Genome Biol* **10**(3): R25.
- Lantermann, A., Stralfors, A., Fagerstrom-Billai, F., Korber, P. and Ekwall, K. (2009). "Genome-wide mapping of nucleosome positions in Schizosaccharomyces pombe." *Methods* **48**(3): 218-225.
- Lantermann, A. B., Straub, T., Stralfors, A., Yuan, G. C., Ekwall, K. and Korber, P. (2010). "Schizosaccharomyces pombe genome-wide nucleosome mapping reveals positioning mechanisms distinct from those of Saccharomyces cerevisiae." *Nat Struct Mol Biol* **17**(2): 251-257.
- Lee, J., Choi, E. S., Seo, H. D., Kang, K., Gilmore, J. M., Florens, L., Washburn, M. P., Choe, J., Workman, J. L. and Lee, D. (2017). "Chromatin remodeller Fun30(Fft3) induces nucleosome disassembly to facilitate RNA polymerase II elongation." *Nat Commun* **8**: 14527.
- Lee, J. S., Garrett, A. S., Yen, K., Takahashi, Y. H., Hu, D., Jackson, J., Seidel, C., Pugh, B. F. and Shilatifard, A. (2012). "Codependency of H2B monoubiquitination and nucleosome reassembly on Chd1." *Genes Dev* **26**(9): 914-919.
- Lee, W., Tillo, D., Bray, N., Morse, R. H., Davis, R. W., Hughes, T. R. and Nislow, C. (2007). "A high-resolution atlas of nucleosome occupancy in yeast." *Nat Genet* **39**(10): 1235-1244.
- Lenhard, B., Sandelin, A. and Carninci, P. (2012). "Metazoan promoters: emerging characteristics and insights into transcriptional regulation." *Nat Rev Genet* **13**(4): 233-245.
- Li, H., Hou, J., Bai, L., Hu, C., Tong, P., Kang, Y., Zhao, X. and Shao, Z. (2015). "Genome-wide analysis of core promoter structures in Schizosaccharomyces pombe with DeepCAGE." *RNA Biol* **12**(5): 525-537.
- Lieleg, C., Ketterer, P., Nuebler, J., Ludwigsen, J., Gerland, U., Dietz, H., Mueller-Planitz, F. and Korber, P. (2015). "Nucleosome spacing generated by ISWI and CHD1 remodelers is constant regardless of nucleosome density." *Mol Cell Biol* **35**(9): 1588-1605.
- Lieleg, C., Krietenstein, N., Walker, M. and Korber, P. (2015). "Nucleosome positioning in yeasts: methods, maps, and mechanisms." *Chromosoma* **124**(2): 131-151.
- Lorch, Y., Maier-Davis, B. and Kornberg, R. D. (2014). "Role of DNA sequence in chromatin remodeling and the formation of nucleosome-free regions." *Genes Dev* **28**(22): 2492-2497.
- Lowary, P. T. and Widom, J. (1998). "New DNA sequence rules for high affinity binding to histone octamer and sequence-directed nucleosome positioning." *J Mol Biol* **276**(1): 19-42.
- Luger, K. (2003). "Structure and dynamic behavior of nucleosomes." *Curr Opin Genet Dev* **13**(2): 127-135.
- Luger, K., Dechassa, M. L. and Tremethick, D. J. (2012). "New insights into nucleosome and chromatin structure: an ordered state or a disordered affair?" *Nat Rev Mol Cell Biol* **13**(7): 436-447.
- Luger, K., Mader, A. W., Richmond, R. K., Sargent, D. F. and Richmond, T. J. (1997). "Crystal structure of the nucleosome core particle at 2.8 Å resolution." *Nature* **389**(6648): 251-260.
- Mahat, D. B., Kwak, H., Booth, G. T., Jonkers, I. H., Danko, C. G., Patel, R. K., Waters, C. T., Munson, K., Core, L. J. and Lis, J. T. (2016). "Base-pair-resolution genome-wide mapping of active RNA polymerases using precision nuclear run-on (PRO-seq)." *Nat Protoc* **11**(8): 1455-1476.

- Mavrich, T. N., Jiang, C., Ioshikhes, I. P., Li, X., Venters, B. J., Zanton, S. J., Tomsho, L. P., Qi, J., Glaser, R. L., Schuster, S. C., Gilmour, D. S., Albert, I. and Pugh, B. F. (2008). "Nucleosome organization in the Drosophila genome." *Nature* **453**(7193): 358-362.
- McManus, J., Perry, P., Sumner, A. T., Wright, D. M., Thomson, E. J., Allshire, R. C., Hastie, N. D. and Bickmore, W. A. (1994). "Unusual chromosome structure of fission yeast DNA in mouse cells." *J Cell Sci* **107 ( Pt 3)**: 469-486.
- Mellor, J., Woloszczuk, R. and Howe, F. S. (2016). "The Interleaved Genome." *Trends Genet* **32**(1): 57-71.
- Mobius, W. and Gerland, U. (2010). "Quantitative test of the barrier nucleosome model for statistical positioning of nucleosomes up- and downstream of transcription start sites." *PLoS Comput Biol* **6**(8).
- Monahan, B. J., Villen, J., Marguerat, S., Bahler, J., Gygi, S. P. and Winston, F. (2008). "Fission yeast SWI/SNF and RSC complexes show compositional and functional differences from budding yeast." *Nat Struct Mol Biol* **15**(8): 873-880.
- Moreno, M. B., Duran, A. and Ribas, J. C. (2000). "A family of multifunctional thiamine-repressible expression vectors for fission yeast." *Yeast* **16**(9): 861-872.
- Morse, R. H. (2009). "Analysis of DNA topology in yeast chromatin." *Methods Mol Biol* **523**: 93-108.
- Moyle-Heyrman, G., Zaichuk, T., Xi, L., Zhang, Q., Uhlenbeck, O. C., Holmgren, R., Widom, J. and Wang, J. P. (2013). "Chemical map of Schizosaccharomyces pombe reveals species-specific features in nucleosome positioning." *Proc Natl Acad Sci U S A* **110**(50): 20158-20163.
- Nagalakshmi, U., Wang, Z., Waern, K., Shou, C., Raha, D., Gerstein, M. and Snyder, M. (2008). "The transcriptional landscape of the yeast genome defined by RNA sequencing." *Science* **320**(5881): 1344-1349.
- Narlikar, G. J., Sundaramoorthy, R. and Owen-Hughes, T. (2013). "Mechanisms and functions of ATP-dependent chromatin-remodeling enzymes." *Cell* **154**(3): 490-503.
- Neil, H., Malabat, C., d'Aubenton-Carafa, Y., Xu, Z., Steinmetz, L. M. and Jacquier, A. (2009). "Widespread bidirectional promoters are the major source of cryptic transcripts in yeast." *Nature* **457**(7232): 1038-1042.
- Ni, T., Corcoran, D. L., Rach, E. A., Song, S., Spana, E. P., Gao, Y., Ohler, U. and Zhu, J. (2010). "A paired-end sequencing strategy to map the complex landscape of transcription initiation." *Nat Methods* **7**(7): 521-527.
- Ocampo, J., Chereji, R. V., Eriksson, P. R. and Clark, D. J. (2016). "The ISW1 and CHD1 ATP-dependent chromatin remodelers compete to set nucleosome spacing in vivo." *Nucleic Acids Res* **44**(10): 4625-4635.
- Olins, A. L., Carlson, R. D. and Olins, D. E. (1975). "Visualization of chromatin substructure: epsilon bodies." *J Cell Biol* **64**(3): 528-537.
- Osberg, B., Nuebler, J. and Gerland, U. (2015). "Adsorption-Desorption Kinetics of Soft Particles." *Phys Rev Lett* **115**(8): 088301.
- Osberg, B., Nuebler, J., Korber, P. and Gerland, U. (2014). "Replication-guided nucleosome packing and nucleosome breathing expedite the formation of dense arrays." *Nucleic Acids Res* **42**(22): 13633-13645.
- Papamichos-Chronakis, M. and Peterson, C. L. (2013). "Chromatin and the genome integrity network." *Nat Rev Genet* **14**(1): 62-75.
- Papamichos-Chronakis, M., Watanabe, S., Rando, O. J. and Peterson, C. L. (2011). "Global regulation of H2A.Z localization by the INO80 chromatin-remodeling enzyme is essential for genome integrity." *Cell* **144**(2): 200-213.
- Park, D., Shivram, H. and Iyer, V. R. (2014). "Chd1 co-localizes with early transcription elongation factors independently of H3K36 methylation and releases stalled RNA polymerase II at introns." *Epigenetics Chromatin* **7**(1): 32.
- Park, M. J., Jang, Y. K., Choi, E. S., Kim, H. S. and Park, S. D. (2002). "Fission yeast Rap1 homolog is a telomere-specific silencing factor and interacts with Taz1p." *Mol Cells* **13**(2): 327-333.
- Parnell, T. J., Huff, J. T. and Cairns, B. R. (2008). "RSC regulates nucleosome positioning at Pol II genes and density at Pol III genes." *Embo j* **27**(1): 100-110.

## References

---

- Patel, A., Chakravarthy, S., Morrone, S., Nodelman, I. M., McKnight, J. N. and Bowman, G. D. (2013). "Decoupling nucleosome recognition from DNA binding dramatically alters the properties of the Chd1 chromatin remodeler." *Nucleic Acids Res* **41**(3): 1637-1648.
- Pattenden, S. G., Gogol, M. M. and Workman, J. L. (2010). "Features of cryptic promoters and their varied reliance on bromodomain-containing factors." *PLoS One* **5**(9): e12927.
- Patterton, H. G. and von Holt, C. (1993). "Negative supercoiling and nucleosome cores. I. The effect of negative supercoiling on the efficiency of nucleosome core formation in vitro." *J Mol Biol* **229**(3): 623-636.
- Pelechano, V., Wei, W. and Steinmetz, L. M. (2013). "Extensive transcriptional heterogeneity revealed by isoform profiling." *Nature* **497**(7447): 127-131.
- Perales, R., Zhang, L. and Bentley, D. (2011). "Histone occupancy in vivo at the 601 nucleosome binding element is determined by transcriptional history." *Mol Cell Biol* **31**(16): 3485-3496.
- Pointner, J., Persson, J., Prasad, P., Norman-Axelsson, U., Stralfors, A., Khorosjutina, O., Krietenstein, N., Svensson, J. P., Ekwall, K. and Korber, P. (2012). "CHD1 remodelers regulate nucleosome spacing in vitro and align nucleosomal arrays over gene coding regions in *S. pombe*." *Embo j* **31**(23): 4388-4403.
- Pokholok, D. K., Harbison, C. T., Levine, S., Cole, M., Hannett, N. M., Lee, T. I., Bell, G. W., Walker, K., Rolfe, P. A., Herbolsheimer, E., Zeitlinger, J., Lewitter, F., Gifford, D. K. and Young, R. A. (2005). "Genome-wide map of nucleosome acetylation and methylation in yeast." *Cell* **122**(4): 517-527.
- Quinn, J. J. and Chang, H. Y. (2016). "Unique features of long non-coding RNA biogenesis and function." *Nat Rev Genet* **17**(1): 47-62.
- Rach, E. A., Winter, D. R., Benjamin, A. M., Corcoran, D. L., Ni, T., Zhu, J. and Ohler, U. (2011). "Transcription initiation patterns indicate divergent strategies for gene regulation at the chromatin level." *PLoS Genet* **7**(1): e1001274.
- Raisner, R. M., Hartley, P. D., Meneghini, M. D., Bao, M. Z., Liu, C. L., Schreiber, S. L., Rando, O. J. and Madhani, H. D. (2005). "Histone variant H2A.Z marks the 5' ends of both active and inactive genes in euchromatin." *Cell* **123**(2): 233-248.
- Rhee, H. S. and Pugh, B. F. (2012). "Genome-wide structure and organization of eukaryotic pre-initiation complexes." *Nature* **483**(7389): 295-301.
- Rhind, N., Chen, Z., Yassour, M., Thompson, D. A., Haas, B. J., Habib, N., Wapinski, I., Roy, S., Lin, M. F., Heiman, D. I., Young, S. K., Furuya, K., Guo, Y., Pidoux, A., Chen, H. M., Robbertse, B., Goldberg, J. M., Aoki, K., Bayne, E. H., Berlin, A. M., Desjardins, C. A., Dobbs, E., Dukaj, L., Fan, L., FitzGerald, M. G., French, C., Gujja, S., Hansen, K., Keifenheim, D., Levin, J. Z., Mosher, R. A., Muller, C. A., Pfiffner, J., Priest, M., Russ, C., Smialowska, A., Swoboda, P., Sykes, S. M., Vaughn, M., Vengrova, S., Yoder, R., Zeng, Q., Allshire, R., Baulcombe, D., Birren, B. W., Brown, W., Ekwall, K., Kellis, M., Leatherwood, J., Levin, H., Margalit, H., Martienssen, R., Nieduszynski, C. A., Spatafora, J. W., Friedman, N., Dalgaard, J. Z., Baumann, P., Niki, H., Regev, A. and Nusbaum, C. (2011). "Comparative functional genomics of the fission yeasts." *Science* **332**(6032): 930-936.
- Robinson, J. T., Thorvaldsdottir, H., Winckler, W., Guttman, M., Lander, E. S., Getz, G. and Mesirov, J. P. (2011). "Integrative genomics viewer." *Nat Biotechnol* **29**(1): 24-26.
- Rozpedowska, E., Hellborg, L., Ishchuk, O. P., Orhan, F., Galafassi, S., Merico, A., Woolfit, M., Compagno, C. and Piskur, J. (2011). "Parallel evolution of the make-accumulate-consume strategy in *Saccharomyces* and *Dekkera* yeasts." *Nat Commun* **2**: 302.
- Ryan, D. P. and Owen-Hughes, T. (2011). "Snf2-family proteins: chromatin remodellers for any occasion." *Curr Opin Chem Biol* **15**(5): 649-656.
- Sandelin, A., Carninci, P., Lenhard, B., Ponjavic, J., Hayashizaki, Y. and Hume, D. A. (2007). "Mammalian RNA polymerase II core promoters: insights from genome-wide studies." *Nat Rev Genet* **8**(6): 424-436.
- Schalch, T., Duda, S., Sargent, D. F. and Richmond, T. J. (2005). "X-ray structure of a tetranucleosome and its implications for the chromatin fibre." *Nature* **436**(7047): 138-141.

- Schones, D. E., Cui, K., Cuddapah, S., Roh, T. Y., Barski, A., Wang, Z., Wei, G. and Zhao, K. (2008). "Dynamic regulation of nucleosome positioning in the human genome." *Cell* **132**(5): 887-898.
- Segal, E., Fondufe-Mittendorf, Y., Chen, L., Thastrom, A., Field, Y., Moore, I. K., Wang, J. P. and Widom, J. (2006). "A genomic code for nucleosome positioning." *Nature* **442**(7104): 772-778.
- Sharma, V. M., Li, B. and Reese, J. C. (2003). "SWI/SNF-dependent chromatin remodeling of RNR3 requires TAF(II)s and the general transcription machinery." *Genes Dev* **17**(4): 502-515.
- Shen, C. H., Leblanc, B. P., Alfieri, J. A. and Clark, D. J. (2001). "Remodeling of yeast CUP1 chromatin involves activator-dependent repositioning of nucleosomes over the entire gene and flanking sequences." *Mol Cell Biol* **21**(2): 534-547.
- Shim, Y. S., Choi, Y., Kang, K., Cho, K., Oh, S., Lee, J., Grewal, S. I. and Lee, D. (2012). "Hrp3 controls nucleosome positioning to suppress non-coding transcription in eu- and heterochromatin." *Embo j* **31**(23): 4375-4387.
- Simic, R., Lindstrom, D. L., Tran, H. G., Roinick, K. L., Costa, P. J., Johnson, A. D., Hartzog, G. A. and Arndt, K. M. (2003). "Chromatin remodeling protein Chd1 interacts with transcription elongation factors and localizes to transcribed genes." *Embo j* **22**(8): 1846-1856.
- Simon, R. H. and Felsenfeld, G. (1979). "A new procedure for purifying histone pairs H2A + H2B and H3 + H4 from chromatin using hydroxylapatite." *Nucleic Acids Res* **6**(2): 689-696.
- Sipiczki, M. (2000). "Where does fission yeast sit on the tree of life?" *Genome Biol* **1**(2): Reviews1011.
- Smale, S. T. and Kadonaga, J. T. (2003). "The RNA polymerase II core promoter." *Annu Rev Biochem* **72**: 449-479.
- Smolle, M., Venkatesh, S., Gogol, M. M., Li, H., Zhang, Y., Florens, L., Washburn, M. P. and Workman, J. L. (2012). "Chromatin remodelers Isw1 and Chd1 maintain chromatin structure during transcription by preventing histone exchange." *Nat Struct Mol Biol* **19**(9): 884-892.
- Smolle, M. and Workman, J. L. (2013). "Transcription-associated histone modifications and cryptic transcription." *Biochim Biophys Acta* **1829**(1): 84-97.
- Sobel, R. E., Cook, R. G., Perry, C. A., Annunziato, A. T. and Allis, C. D. (1995). "Conservation of deposition-related acetylation sites in newly synthesized histones H3 and H4." *Proc Natl Acad Sci U S A* **92**(4): 1237-1241.
- Soriano, I., Quintales, L. and Antequera, F. (2013). "Clustered regulatory elements at nucleosome-depleted regions punctuate a constant nucleosomal landscape in *Schizosaccharomyces pombe*." *BMC Genomics* **14**: 813.
- Spadafora, C., Noviello, L. and Geraci, G. (1976). "Chromatin organization in nuclei of sea urchin embryos. Comparison with the chromatin organization of the sperm." *Cell Differ* **5**(4): 225-231.
- Stockdale, C., Flaus, A., Ferreira, H. and Owen-Hughes, T. (2006). "Analysis of nucleosome repositioning by yeast ISWI and Chd1 chromatin remodeling complexes." *J Biol Chem* **281**(24): 16279-16288.
- Stormo, G. D. (2000). "DNA binding sites: representation and discovery." *Bioinformatics* **16**(1): 16-23.
- Struhl, K. (1989). "Molecular mechanisms of transcriptional regulation in yeast." *Annu Rev Biochem* **58**: 1051-1077.
- Suto, R. K., Clarkson, M. J., Tremethick, D. J. and Luger, K. (2000). "Crystal structure of a nucleosome core particle containing the variant histone H2A.Z." *Nat Struct Biol* **7**(12): 1121-1124.
- Suzuki, H., Forrest, A. R., van Nimwegen, E., Daub, C. O., Balwiercz, P. J., Irvine, K. M., Lassmann, T., Ravasi, T., Hasegawa, Y., de Hoon, M. J., Katayama, S., Schroder, K., Carninci, P., Tomaru, Y., Kanamori-Katayama, M., Kubosaki, A., Akalin, A., Ando, Y., Arner, E., Asada, M., Asahara, H., Bailey, T., Bajic, V. B., Bauer, D., Beckhouse, A. G., Bertin, N., Bjorkegren, J., Brombacher, F., Bulger, E., Chalk, A. M., Chiba, J., Cloonan, N., Dawe, A., Dostie, J., Engstrom, P. G., Essack, M., Faulkner, G. J., Fink, J. L., Fredman, D., Fujimori, K., Furuno, M., Gojobori, T., Gough, J., Grimmond, S. M., Gustafsson, M., Hashimoto, M., Hashimoto, T., Hatakeyama, M., Heinzl, S., Hide, W., Hofmann, O., Hornquist, M., Huminiecki, L., Ikeo, K., Imamoto, N., Inoue, S., Inoue, Y., Ishihara, R., Iwayanagi, T., Jacobsen, A., Kaur, M., Kawaji, H., Kerr, M. C., Kimura, R., Kimura, S., Kimura, Y., Kitano, H., Koga, H., Kojima, T., Kondo, S., Konno, T., Krogh, A., Kruger, A., Kumar, A., Lenhard, B., Lennartsson, A., Lindow, M., Lizio, M., Macpherson, C., Maeda, N., Maher, C. A., Maqungo, M., Mar, J., Matigian, N. A., Matsuda, H., Mattick, J. S., Meier, S., Miyamoto, S., Miyamoto-Sato, E., Nakabayashi, K., Nakachi, Y., Nakano, M., Nygaard, S., Okayama, T., Okazaki, Y., Okuda-Yabukami, H., Orlando, V., Otomo, J., Pachkov, M., Petrovsky, N., Plessy,

## References

---

C., Quackenbush, J., Radovanovic, A., Rehli, M., Saito, R., Sandelin, A., Schmeier, S., Schonbach, C., Schwartz, A. S., Semple, C. A., Sera, M., Severin, J., Shirahige, K., Simons, C., St Laurent, G., Suzuki, M., Suzuki, T., Sweet, M. J., Taft, R. J., Takeda, S., Takenaka, Y., Tan, K., Taylor, M. S., Teasdale, R. D., Tegner, J., Teichmann, S., Valen, E., Wahlestedt, C., Waki, K., Waterhouse, A., Wells, C. A., Winther, O., Wu, L., Yamaguchi, K., Yanagawa, H., Yasuda, J., Zavolan, M., Hume, D. A., Arakawa, T., Fukuda, S., Imamura, K., Kai, C., Kaiho, A., Kawashima, T., Kawazu, C., Kitazume, Y., Kojima, M., Miura, H., Murakami, K., Murata, M., Ninomiya, N., Nishiyori, H., Noma, S., Ogawa, C., Sano, T., Simon, C., Tagami, M., Takahashi, Y., Kawai, J. and Hayashizaki, Y. (2009). "The transcriptional network that controls growth arrest and differentiation in a human myeloid leukemia cell line." *Nat Genet* **41**(5): 553-562.

Svejstrup, J. Q. (2010). "The interface between transcription and mechanisms maintaining genome integrity." *Trends Biochem Sci* **35**(6): 333-338.

Tachiwana, H., Kagawa, W. and Kurumizaka, H. (2012). "Comparison between the CENP-A and histone H3 structures in nucleosomes." *Nucleus* **3**(1): 6-11.

Tachiwana, H., Kagawa, W., Shiga, T., Osakabe, A., Miya, Y., Saito, K., Hayashi-Takanaka, Y., Oda, T., Sato, M., Park, S. Y., Kimura, H. and Kurumizaka, H. (2011). "Crystal structure of the human centromeric nucleosome containing CENP-A." *Nature* **476**(7359): 232-235.

Takahashi, H., Lassmann, T., Murata, M. and Carninci, P. (2012). "5' end-centered expression profiling using cap-analysis gene expression and next-generation sequencing." *Nat Protoc* **7**(3): 542-561.

Thomas, M. C. and Chiang, C. M. (2006). "The general transcription machinery and general cofactors." *Crit Rev Biochem Mol Biol* **41**(3): 105-178.

Tirosh, I. and Barkai, N. (2008). "Two strategies for gene regulation by promoter nucleosomes." *Genome Res* **18**(7): 1084-1091.

Tirosh, I., Berman, J. and Barkai, N. (2007). "The pattern and evolution of yeast promoter bendability." *Trends Genet* **23**(7): 318-321.

Trinklein, N. D., Aldred, S. F., Hartman, S. J., Schroeder, D. I., Otilar, R. P. and Myers, R. M. (2004). "An abundance of bidirectional promoters in the human genome." *Genome Res* **14**(1): 62-66.

Tsankov, A., Yanagisawa, Y., Rhind, N., Regev, A. and Rando, O. J. (2011). "Evolutionary divergence of intrinsic and trans-regulated nucleosome positioning sequences reveals plastic rules for chromatin organization." *Genome Res* **21**(11): 1851-1862.

Tsankov, A. M., Thompson, D. A., Socha, A., Regev, A. and Rando, O. J. (2010). "The role of nucleosome positioning in the evolution of gene regulation." *PLoS Biol* **8**(7): e1000414.

Tsukiyama, T., Palmer, J., Landel, C. C., Shiloach, J. and Wu, C. (1999). "Characterization of the imitation switch subfamily of ATP-dependent chromatin-remodeling factors in *Saccharomyces cerevisiae*." *Genes Dev* **13**(6): 686-697.

Uwimana, N., Collin, P., Jeronimo, C., Haibe-Kains, B. and Robert, F. (2017). "Bidirectional terminators in *Saccharomyces cerevisiae* prevent cryptic transcription from invading neighboring genes." *Nucleic Acids Res* **45**(11): 6417-6426.

van Bakel, H., Tsui, K., Gebbia, M., Mnaimneh, S., Hughes, T. R. and Nislow, C. (2013). "A compendium of nucleosome and transcript profiles reveals determinants of chromatin architecture and transcription." *PLoS Genet* **9**(5): e1003479.

Vary, J. C., Jr., Gangaraju, V. K., Qin, J., Landel, C. C., Kooperberg, C., Bartholomew, B. and Tsukiyama, T. (2003). "Yeast Isw1p forms two separable complexes in vivo." *Mol Cell Biol* **23**(1): 80-91.

Watanabe, S. and Peterson, C. L. (2016). "Response to Comment on "A histone acetylation switch regulates H2A.Z deposition by the SWR-C remodeling enzyme"." *Science* **353**(6297): 358.

Watson, A. T., Daigaku, Y., Mohebi, S., Etheridge, T. J., Chahwan, C., Murray, J. M. and Carr, A. M. (2013). "Optimisation of the *Schizosaccharomyces pombe* *urg1* expression system." *PLoS One* **8**(12): e83800.

Weber, C. M. and Henikoff, S. (2014). "Histone variants: dynamic punctuation in transcription." *Genes Dev* **28**(7): 672-682.

- Weiner, A., Hughes, A., Yassour, M., Rando, O. J. and Friedman, N. (2010). "High-resolution nucleosome mapping reveals transcription-dependent promoter packaging." *Genome Res* **20**(1): 90-100.
- Whitehouse, I., Rando, O. J., Delrow, J. and Tsukiyama, T. (2007). "Chromatin remodelling at promoters suppresses antisense transcription." *Nature* **450**(7172): 1031-1035.
- Wippo, C. J., Israel, L., Watanabe, S., Hochheimer, A., Peterson, C. L. and Korber, P. (2011). "The RSC chromatin remodelling enzyme has a unique role in directing the accurate positioning of nucleosomes." *Embo j* **30**(7): 1277-1288.
- Wippo, C. J. and Korber, P. (2012). "In vitro reconstitution of in vivo-like nucleosome positioning on yeast DNA." *Methods Mol Biol* **833**: 271-287.
- Wood, V., Gwilliam, R., Rajandream, M. A., Lyne, M., Lyne, R., Stewart, A., Sgouros, J., Peat, N., Hayles, J., Baker, S., Basham, D., Bowman, S., Brooks, K., Brown, D., Brown, S., Chillingworth, T., Churcher, C., Collins, M., Connor, R., Cronin, A., Davis, P., Feltwell, T., Fraser, A., Gentles, S., Goble, A., Hamlin, N., Harris, D., Hidalgo, J., Hodgson, G., Holroyd, S., Hornsby, T., Howarth, S., Huckle, E. J., Hunt, S., Jagels, K., James, K., Jones, L., Jones, M., Leather, S., McDonald, S., McLean, J., Mooney, P., Moule, S., Mungall, K., Murphy, L., Niblett, D., Odell, C., Oliver, K., O'Neil, S., Pearson, D., Quail, M. A., Rabinowitsch, E., Rutherford, K., Rutter, S., Saunders, D., Seeger, K., Sharp, S., Skelton, J., Simmonds, M., Squares, R., Squares, S., Stevens, K., Taylor, K., Taylor, R. G., Tivey, A., Walsh, S., Warren, T., Whitehead, S., Woodward, J., Volckaert, G., Aert, R., Robben, J., Grymonprez, B., Weltjens, I., Vanstreels, E., Rieger, M., Schafer, M., Muller-Auer, S., Gabel, C., Fuchs, M., Dusterhoft, A., Fritzc, C., Holzer, E., Moestl, D., Hilbert, H., Borzym, K., Langer, I., Beck, A., Lehrach, H., Reinhardt, R., Pohl, T. M., Eger, P., Zimmermann, W., Wedler, H., Wambutt, R., Purnelle, B., Goffeau, A., Cadieu, E., Dreano, S., Gloux, S., Lelaure, V., Mottier, S., Galibert, F., Aves, S. J., Xiang, Z., Hunt, C., Moore, K., Hurst, S. M., Lucas, M., Rochet, M., Gaillardin, C., Tallada, V. A., Garzon, A., Thode, G., Daga, R. R., Cruzado, L., Jimenez, J., Sanchez, M., del Rey, F., Benito, J., Dominguez, A., Revuelta, J. L., Moreno, S., Armstrong, J., Forsburg, S. L., Cerutti, L., Lowe, T., McCombie, W. R., Paulsen, I., Potashkin, J., Shpakovski, G. V., Ussery, D., Barrell, B. G. and Nurse, P. (2002). "The genome sequence of *Schizosaccharomyces pombe*." *Nature* **415**(6874): 871-880.
- Woodcock, C. L., Frado, L. L. and Rattner, J. B. (1984). "The higher-order structure of chromatin: evidence for a helical ribbon arrangement." *J Cell Biol* **99**(1 Pt 1): 42-52.
- Wyers, F., Rougemaille, M., Badis, G., Rousselle, J. C., Dufour, M. E., Boulay, J., Regnault, B., Devaux, F., Namane, A., Seraphin, B., Libri, D. and Jacquier, A. (2005). "Cryptic pol II transcripts are degraded by a nuclear quality control pathway involving a new poly(A) polymerase." *Cell* **121**(5): 725-737.
- Xi, Y., Yao, J., Chen, R., Li, W. and He, X. (2011). "Nucleosome fragility reveals novel functional states of chromatin and poises genes for activation." *Genome Res* **21**(5): 718-724.
- Xu, Z., Wei, W., Gagneur, J., Perocchi, F., Clauder-Munster, S., Camblong, J., Guffanti, E., Stutz, F., Huber, W. and Steinmetz, L. M. (2009). "Bidirectional promoters generate pervasive transcription in yeast." *Nature* **457**(7232): 1033-1037.
- Yen, K., Vinayachandran, V. and Pugh, B. F. (2013). "SWR-C and INO80 chromatin remodelers recognize nucleosome-free regions near +1 nucleosomes." *Cell* **154**(6): 1246-1256.
- Yuan, G. C., Liu, Y. J., Dion, M. F., Slack, M. D., Wu, L. F., Altschuler, S. J. and Rando, O. J. (2005). "Genome-scale identification of nucleosome positions in *S. cerevisiae*." *Science* **309**(5734): 626-630.
- Zentner, G. E. and Henikoff, S. (2013). "Regulation of nucleosome dynamics by histone modifications." *Nat Struct Mol Biol* **20**(3): 259-266.
- Zhang, Y., Moqtaderi, Z., Rattner, B. P., Euskirchen, G., Snyder, M., Kadonaga, J. T., Liu, X. S. and Struhl, K. (2009). "Intrinsic histone-DNA interactions are not the major determinant of nucleosome positions in vivo." *Nat Struct Mol Biol* **16**(8): 847-852.
- Zhang, Z., Wippo, C. J., Wal, M., Ward, E., Korber, P. and Pugh, B. F. (2011). "A packing mechanism for nucleosome organization reconstituted across a eukaryotic genome." *Science* **332**(6032): 977-980.
- Zhao, J., Herrera-Diaz, J. and Gross, D. S. (2005). "Domain-wide displacement of histones by activated heat shock factor occurs independently of Swi/Snf and is not correlated with RNA polymerase II density." *Mol Cell Biol* **25**(20): 8985-8999.

## References

---

Zhou, T., Yang, L., Lu, Y., Dror, I., Dantas Machado, A. C., Ghane, T., Di Felice, R. and Rohs, R. (2013). "DNASHape: a method for the high-throughput prediction of DNA structural features on a genomic scale." Nucleic Acids Res **41**(Web Server issue): W56-62.



## Abbreviations

<b>Abf1</b>	ARS-binding factor 1
<b>Arp5</b>	Actin-related protein 5
<b>bp</b>	Base pair
<b>BRE</b>	B recognition element
<b>CAGE</b>	Cap analysis gene expression
<b>CENP-A</b>	Centromere protein A
<b>CHD</b>	Chromodomain-helicase-DNA-binding
<b>ChIP</b>	Chromatin immunoprecipitation
<b>CSCT</b>	Chromatin suppressed cryptic transcript
<b>CUT</b>	Cryptic unstable transcript
<b>DBD</b>	DNA binding domain
<b>DCE</b>	Downstream core element
<b>DPE</b>	Downstream promoter element
<b><i>Drosophila</i></b>	<i>Drosophila melanogaster</i>
<b><i>E. coli</i></b>	<i>Escherichia coli</i>
<b>EMM</b>	Edinburgh minimal medium
<b>FACT</b>	Facilitates chromatin transcription
<b>fbp1</b>	Fructose-1,6-bisphosphatase 1
<b>FLO8</b>	Flocculation 8
<b>GRF</b>	General regulatory factor
<b>GTF</b>	General transcription factor
<b>HP1</b>	Heterochromatin protein 1
<b>Hrp1</b>	Helicase-related protein 1
<b>Hrp3</b>	Helicase-related protein 3
<b>HSA</b>	Helicase SANT
<b>HSS</b>	HAND-SANT-SLIDE
<b>INO80</b>	Inositol requiring 80
<b>Inr</b>	Initiator
<b>ISWI</b>	Imitation switch
<b>LB</b>	Lysogeny broth
<b>Mb</b>	Millions of base pair
<b>Micro-C</b>	Micrococcal nuclease capture
<b>MNase</b>	Micrococcal nuclease
<b>MNase-seq</b>	Micrococcal nuclease sequencing
<b>MTE</b>	Motif ten element
<b>NCP</b>	Nucleosome core particle
<b>ncRNA</b>	Noncoding RNA
<b>NDR</b>	Nucleosome-depleted region
<b>NFR</b>	Nucleosome free region
<b>NRL</b>	Nucleosome repeat length
<b>ORF</b>	Open reading frame
<b>PCR</b>	Polymerase chain reaction
<b>PEX</b>	Pombe whole cell extract ( <i>S. pombe</i> )
<b>PIC</b>	Pre-initiation complex
<b>Pro-cap-seq</b>	Precision nuclear run-on cap sequencing
<b>PTM</b>	Post-translational modification
<b>Rap1</b>	Ras-related protein 1
<b>Reb1</b>	RNA polymerase I enhancer binding protein 1
<b>RNA PolII</b>	RNA polymerase II
<b>RNAi</b>	RNA interference
<b>Rrp6</b>	Ribosomal RNA-processing protein 6
<b><i>S. cerevisiae</i></b>	<i>Saccharomyces cerevisiae</i>
<b><i>S. pombe</i></b>	<i>Schizosaccharomyces pombe</i>

## Abbreviations

---

<b>Sap1</b>	Switch-activating protein 1
<b>SGD</b>	Salt gradient dialysis
<b>SHL</b>	Superhelical location
<b>Snf2</b>	Sucrose non-fermenting 2
<b>Spt6</b>	Suppressor of Ty insertion 6
<b>STE11</b>	Sterile 11
<b>Sth1</b>	SNF two Homolog 1
<b>SUT</b>	Stable unannotated transcript
<b>SWI/SNF</b>	Switching defective/sucrose non-fermenting
<b>Swi6</b>	Switching defective 6
<b>SWR1</b>	SWi2/Snf2-related 1
<b>TBP</b>	TATA box binding protein
<b>TIF-seq</b>	Transcript isoform sequencing
<b>ts</b>	Temperature sensitive
<b>TSS</b>	Transcription start site
<b>U</b>	Unit
<b>UASp</b>	Upstream activation sequence for phosphate regulation
<b><i>Xenopus</i></b>	<i>Xenopus leavis</i>
<b>Xrn1</b>	5'-3' exoribonuclease 1
<b>XUT</b>	Xrn1-sensitive transcript
<b>YES</b>	Yeast extract with supplements
<b>YEX</b>	Yeast whole cell extract ( <i>S. cerevisiae</i> )

## Acknowledgements

First of all, I would like to especially thank PD Dr. Philipp Korber. Thank you not only for giving me the opportunity to work in your lab and for supervision of my PhD thesis, but also for strengthening my scientific and critical thinking, for a lot of helpful discussions to push the projects forward and many opportunities to go on great conferences, workshops and lab visits. And a great thank you for the critical reading of my PhD thesis.

A special thank goes to Prof. Dr. Peter B. Becker not only for the great scientific environment, but also for the great working atmosphere which enabled a collegial and friendly collaboration in his department.

Many thanks also to my collaborations partners for their support and advice for my projects:

- ... Prof. Dr. Jürg Bähler and Dr. Samuel Marguerat for collaborative work on the “CAGE project”.
- ... Dr. Pawel Smialowski for bioinformatical input, helpful discussions about our “CAGE project” and many many plots.
- ... Prof. Dr. Karl Ekwall for the possibility to work in his lab “Department of Biosciences and Nutrition” at the Karolinska Institut in Stockholm.
- ... Dr. Punit Prasad and Wenbo Dong for helping hands and helpful advices in protein purification and an unforgettable stay at the Karolinska Institut in Stockholm.
- ... Prof. Ulrich Gerland for collaborative work on the “601 project”.
- ... Dr. Johannes Nuebler for modeling and helpful discussion about our “601 project”.
- ... Dr. Tobias Straub for bioinformatical advice.
- ... Dr. Stefan Krebs and Dr. Helmut Blum for DNA sequencing.

Many thanks also to the former and present members of the “Molecular Biology Department” for sharing protocols and reagents, helping hands with instruments, all scientific and non-scientific activities...It was a pleasure to work with you!

I also would like to thank Dr. Elizabeth Schroeder-Reiter not only for being a great coordinator of the IRTG Program, but also for organizing all kind of activities and the support to participate in workshops and trainings.

Ein ganz herzliches Dankeschön an Edith Müller und Carolin Brieger bei der Unterstützung bei allen administrativen Angelegenheiten und für die unzähligen Bestellungen.

Vielen Dank auch an Silvia Härtel und Andrea Schmid bei der Unterstützung im Labor, vor allem Andrea für die Arbeit mit der Hefe, die immer alles etwas anders macht.

Eins der größten Dankeschöns gilt der „Northlab + Sarah“ alias NerdLab-Gruppe (Nils Krietenstein, Corinna Lieleg, Sebastian Pünzeler, Lisa-Maria Zink und Sarah Schunter) und

den neuen Korberlingen (Elisa Oberbeckmann und Iris Langstein), die das Doktorandenleben nicht nur durch die Hilfe im Labor erleichtert haben, sondern auch mit kulinarischen Highlights (Riesenschnitzel, vegetarischer Döner, Couscous-Salat etc.), entspannten Kaffeepausen und unzähligen Grillabenden versüßt haben. Vor allem ein ganz liebes Dankeschön an Nils und Corinna für eure Hilfe nicht nur während, sondern auch nach eurer Zeit im Labor, ich war sehr gerne euer Padawan!

Nicht zu vergessen möchte ich meiner Familie einen ganz besonderen Dank aussprechen, die mich immer dabei unterstützt haben diesen Weg einzuschlagen. Vor allem dir, Mama, dass du uns Kindern, zu denen gemacht hast, was wir heute sind! Auch möchte ich meiner Schwester Alesia danken, die mich immer wieder darin bestärkt hat diesen Weg zu gehen.

Auch dir, Sebastian, gilt ein liebes Dankeschön, in der intensivsten Phase der Doktorarbeit hast du mich bei allem unterstützt und mir immer wieder Mut zugesprochen. Danke, dass du für mich da bist!

---

---